The Standard Model and LHC Phenomenology

Notes of the *Standard Model and LHC phenomenology* course of the Oxford Master in Mathematical Physics and the Particle (MMathPhys) and the Particle Theory Graduate School. Course webpage: `http://mmathphys.physics.ox.ac.uk/`. The lectures will take place on **Tuesdays and Wednesdays** each week during Trinity Term 2015 **from 10.00 to 11.00**, at the **Fisher Room, Denys Wilkinson Building**.

These notes are intended to be used as support material for the course, rather than a proper set of lecture notes. They have not been cross-checked or proof-read, so use at your own risk. Hopefully they will at some point evolve into a proper set of lecture notes, in the meantime the bibliography provides detailed material to complement the lectures.

These notes are greatly indebted to the various excellent references in the bibliography, in particular to Paolo Nason's and Giulia Zanderighi's QCD lectures [9, 8] and to the *QCD and Collider Physics* textbook of Ellis, Stirling and Webber, from where a substantial part of this material has been borrowed.

Current version: May 10, 2016

Table of Contents

Syllabus

- The Standard Model: an historical introduction.
- The strong interaction. Motivation for QCD. The hadron spectrum. Evidence for a new quantum degree of freedom: color. Evidence for a new gauge boson: the gluon. Scaling in deep-inelastic scattering.
- The QCD Lagrangian. Similarities and differences with QED Feynman rules. Color algebra and color flow. Symmetries of QCD.
- Asymptotic freedom. QCD in electron-positron annihilation. Renormalization group equations. The running of the strong coupling constant. Sterman-Weinberg jets and radiative corrections. Soft and collinear singularities in NLO matrix elements. Infrared and collinear safe observables.
- Perturbative QCD in processes with hadrons in the initial state. QCD factorization and the parton model. Parton Distribution Functions. The parton model and radiative corrections. Factorization of initial state divergences and DGLAP evolution of parton distributions.
- State-of-the-art perturbative QCD at the LHC. Collider kinematics. Jet production at hadron colliders. Drell-Yan production and impact on PDFs. Theoretical uncertainties in perturbative QCD. Searches for New Physics at the LHC.
- Parton fragmentation in perturbative QCD. Parton evolution as a semi-classical branching process. Monte Carlo event generators and realistic simulation of hadronic final states. Jet reconstruction in hadronic collisions. Jet algorithms and jet substructure methods.
- Electroweak interactions. Historical introduction. Weak decays, Fermi theory, violations of unitarity. Symmetries of the weak interaction. Neutral and charged currents. Experimental evidence for the W and Z bosons.
- $SU(2) \times U_Y(1)$ gauge symmetry and spontaneous symmetry breaking. Mass generation for gauge bosons. The Higgs mechanism. Custodial symmetry and Yukawa masses. Anomaly cancellation. Feynman rules in electroweak theory.
- Higgs phenomenology at hadron colliders. Production channels and decay modes. Comparison with LHC measurements. Unitarization of vector-boson scattering. Higgs pair production. Prospects for Higgs physics at the LHC.

References

[1] M. E. Peskin and D. V. Schroeder, "An introduction to quantum field theory," Reading, USA: Addison-Wesley (1995).

[2] M. D. Schwartz, "Quantum Field Theory and the Standard Model," Cambridge University Press (2014).

[3] J. Collins, "Foundations of perturbative QCD," Cambridge monographs on particle physics, nuclear physics and cosmology (2014).

[4] C. P. Burgess and G. D. Moore, "The standard model: A primer," Cambridge, UK: Cambridge Univ. Press (2007).

[5] R. K. Ellis, W. J. Stirling and B. R. Webber, "QCD and collider physics," Camb. Monogr. Part. Phys. Nucl. Phys. Cosmol. **8**, 1 (1996).

[6] G. Dissertori, I. G. Knowles and M. Schmelling, "Quantum Chromodynamics: High energy experiments and theory," International series of monographs on physics, 115, Oxford Science Publications.

[7] J. Rojo, "The Strong Interactions and LHC phenomenology", lecture notes available online at `http://juanrojo.com/teaching`

[8] G. Zanderighi, "QCD and collider physics", lecture notes available online at `http://www2.physics.ox.ac.uk/sites/default/files/QCDLectures.pdf`

[9] P. Nason, "Introduction to QCD", lecture notes available online at `http://moby.mib.infn.it/~nason/misc/QCD-intro.ps.gz`

Introduction

These lecture notes contain some of the material covered by the **Standard Model and LHC phenomenology** course of the Oxford Master in Mathematical Physics and the Particle (MMathPhys) and of the the Particle Theory Graduate School. The aim is to provide a general overview of the basic framework of the Standard Model of particle physics with emphasis on its tests and applications at the Large Hadron Collider. Topics covered include perturbative Quantum Chromodynamics, Electroweak Theory and the Higgs sector, among others.

These notes are intended to be used as support material for the course, rather than a proper set of lecture notes. They have not been cross-checked or proof-read, so use at your own risk. Hopefully they will at some point evolve into a proper set of lecture notes, in the meantime the bibliography provides detailed material to complement the lectures.

The Standard Model: an introduction

Slides of this lecture available from

`http://pcteserver.mi.infn.it/~nnpdf/MMathPhys/SM-MMathPhys-JuanRojo-introduction.pdf`

Quantum Chromodynamics: historical evidence

Following this historical introduction to the Standard Model, let us now present in more detail one of its main building blocks: Quantum Chromodynamics, the theory of the strong interactions. First of all let us discuss the main pieces of evidence that historically were crucial to convince physicists of first of all the existence of a new quantum number (color) and second of the real existence of quarks as components of hadrons, the two basic ingredients of QCD.

$SU(3)$ symmetry and evidence for color

Historically, the color quantum number was introduced to explain some puzzling features of the hadron spectrum. In the 60s a large number of strongly interacting particles had been discovered: pions, kaons, baryons, etc, and the question was whether they were fundamental or composite by more fundamental degrees of freedom. Gell-Mann and Zweig introduced the quark model which allowed to organize hadrons in terms of quarks, hypothetical particles with following peculiar properties:

- Quarks are fermions with spin 1/2
- they have fractional electric charge: +2/3 or 1/3
- Quarks exists in three flavours, called *up*, *down* and *strange*, which lead to the observed hadron spectrum. Strange quarks in particular were needed to describe in this framework particles like *Kaons*.

However, to make sense of particles like Δ^{++}, composed by three up quarks with the same spin, a new property needs be introduced:

- Quark have a new internal degree of freedom, color, with $N_C = 3$

Electric Charge= $\frac{2}{3}e$	up	charm	top
$m =$	few MeV	$\approx$ 1.5 GeV	$\approx$170 GeV
Electric Charge= $-\frac{1}{3}e$	down	strange	bottom
$m =$	few MeV	few hundred MeV	$\approx$ 5 GeV

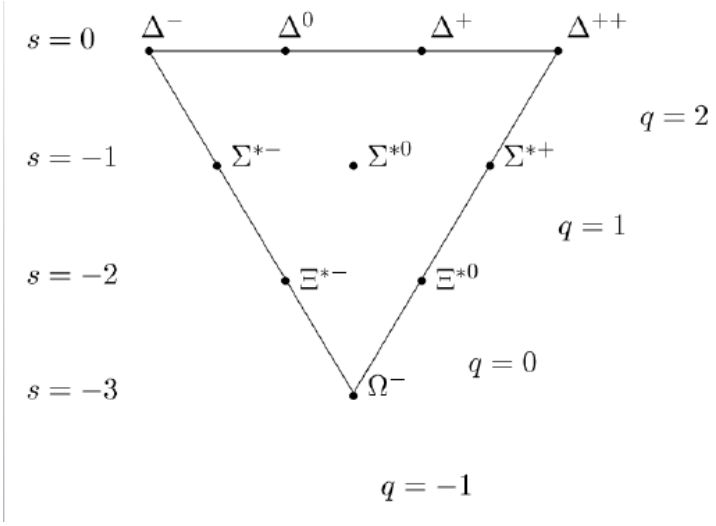

Figure 1: Upper plot: properties of quarks. Lower plot: the baryon decuplet with its various quantum numbers.

- Color is confined in Nature, so all observed hadrons should be color-singlet.

making possible to avoid Pauli's exclusion principle.

Q: Why the Δ^{++} baryon is not allowed from the Pauli exclusion principle in the absence of color?

In Fig. 1 we summarize the properties of known quarks, and illustrate the baryon decuplet with its various quantum numbers.

Q: Why three families of quarks exists? Could there be more? What are the implications?
A: We have no explanation of why three families, but the fact that we have ≥ 3 families of leptons has important implications. For example, three families are needed to have CP violation through the quark mixing matrix, which could be important for baryogenesis in the early universe.

Q: Why originally people doubted that a quantum field theory like QED could be used to describe the strong interaction?

Deep-inelastic scattering and the R ratio: evidence for quarks

QCD and the color quantum number appeared to be a nice mathematical trick to organize the structure of all known hadrons. The evidence for their existence of quarks as real particles, as constituents of hadrons, was provided only in the early 70s, by a series of experiments called Deep-Inelastic Scattering (DIS).

The structure of the proton from deep-inelastic structure functions. DIS is the scattering of a highly energetic proton off a proton target (see Fig. 2):

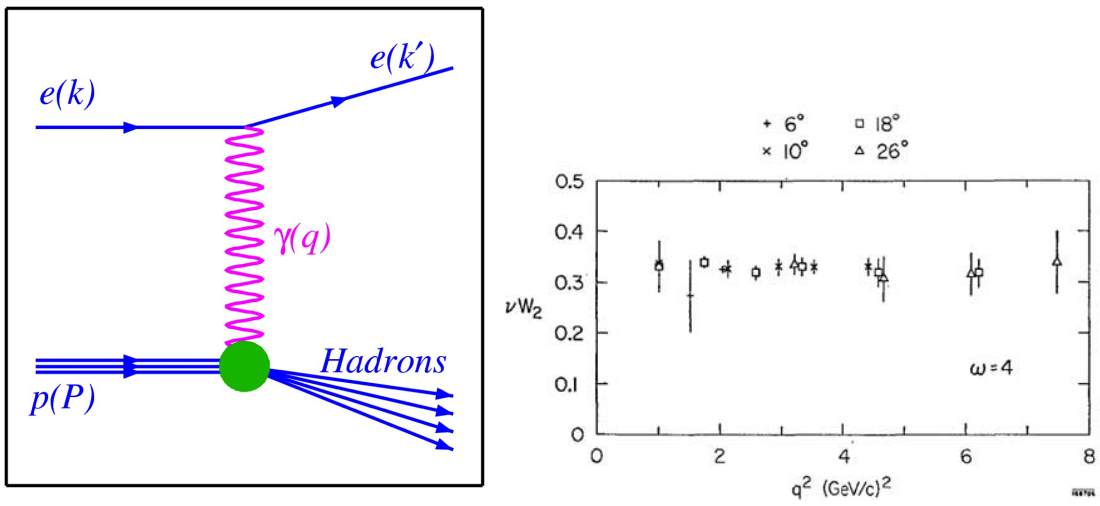

Figure 2: Left plot: the deep-inelastic scattering process. Right plot: the original SLAC DIS structure function measurements, as a function of the four-momentum transfer between the electron and the proton.

$$e^-(k) + p(P) \to e^-(k') + X\,, \tag{1}$$

where in general the proton will be destroyed by the collision (hence the name *inelastic*). The four momentum transfer between the lepton and the proton is

$$q \equiv k' - k\,. \tag{2}$$

The kinematics of the deep-inelastic scattering process are completely specified by the following variables

$$x_{\rm Bj} \equiv \frac{Q^2}{2\,P\cdot q}, \quad Q^2 \equiv -q^2\,, \quad y \equiv \frac{q\cdot p}{k\cdot p}\,. \tag{3}$$

As we will see below, the so-called Bjorken-x variable is related to the momentum fraction carried by quarks, but so far it is only defined a kinematic invariant.

To differentiate from *elastic scattering*, the condition must be that $Q^2 \gg M_p^2$, else the proton would not be destroyed. For instance, the center-of-mass energy of the proton-virtual photon collision will be

$$W^2 \equiv (P+q)^2 = M_p^2 + Q^2\frac{1-x}{x} \simeq Q^2\frac{1-x}{x}\,, \tag{4}$$

where the proton mass can typically be neglected in the calculation. The value $x = 1$ is known as the *elastic limit*. A nice property of DIS is that the complete kinematics of the process are fully specified by measuring the four-momenta of the outgoing lepton, which is experimentally much cleaner than reconstructing the hadronic remnants.

As in the case of the Rutherford experiment that lead to the discovery of the atomic nucleus, here the existence of quasi-free, point-like objects in the proton with fractional electric charge can be inferred from the angular deflection of leptons after the scattering with protons. In the parton model, which we will discuss in more detail later in the lectures, *scaling* is the statement that, after removing the trivial kinematic factors, the cross-section *does not depend* on the four-momentum transfer in the collision, Q^2, or in other words,

that the scattering centers in the proton are point-like objects, rather than some smooth charge distribution which would lead to a form factor instead.

In the parton model of QCD, the measured SLAC cross-sections can be written as

$$\nu W_2(Q^2,\nu) = \frac{Q^2}{Mx} W_2(Q^2,x) \equiv F_2(x,Q^2) = x\sum_i e_q^2 q_i(x)\,. \tag{5}$$

The cross-section for *DIS structure function* $F_2(x,Q^2)$ is proportional to the PDFs of the quarks $q_i(x)$, weighted by the quark charge. These PDFs represent the fraction of the proton's momentum being carried by each individual quark flavor. The scaling of the original SLAC data can be seen in Fig. 2. Perturbative QCD induces logarithmic corrections in Q^2 in Eq. (5), which have been observed by more recent DIS experiments. Eq. (5) is quite remarkable: it indicates that the proton can be treated as in *incoherent sum of non-interacting quarks*.

Q: Can we test if the proton contains a gluon in a deep-inelastic scattering experiment? What would be the corresponding Feynman diagram in this case?

Evidence of color in e^+e^- collisions. Another crucial piece of evidence for both color and quarks was provided by the measurement of the ratio of $\sigma(e^+e^- \to \text{hadrons})$ over $\sigma(e^+e^- \to \mu^+\mu^-)$, know as the R-ratio, defined as:

$$R(\sqrt{s}) \equiv \frac{e^+e^- \to \text{hadrons}}{e^+e^- \to \mu^+\mu^-} = N_c \sum_f Q_f^2 \tag{6}$$

where the RHS follows from the corresponding Feynmann diagrams with quarks on the final state in the quark parton model: as compared to leptons, we have N_c types of quarks of each flavor, and the $\gamma q\bar{q}$ vertex is weighted by the corresponding electric charge.

Q: Can you draw the Feynman diagrams that contribute to $R(\sqrt{s})$ for $\sqrt{s} \ll M_Z$? What happens as the center of mass energy becomes closer to the Z boson mass?

The dependence of the R ratio with $\sqrt{s}$ is also useful to determine the mass of the heavy quarks: only for $\sqrt{s} \geq 2m_h$ can heavy quarks be produced in e^+e^- annihilation and thus contribute to the R ratio. In Fig. 3 we show the R ratio as a function of $\sqrt{s}$. In addition to the resonances, for the continuum cross-section we see that the overall value is in good agreement with the QCD expectations based on the parton model, and indeed we see the change of value when crossing heavy quark thresholds, in particular charm and bottom thresholds. Above the bottom threshold the value of the R-ratio stabilizes to

$$R_5 = \frac{11}{3} = 3\left[2\left(\frac{2}{3}\right)^2 + 3\left(\frac{1}{3}\right)^2\right]\,, \tag{7}$$

As can be seen from Fig. 3, the data strongly disagrees with the possibility that quarks carry no color quantum number.

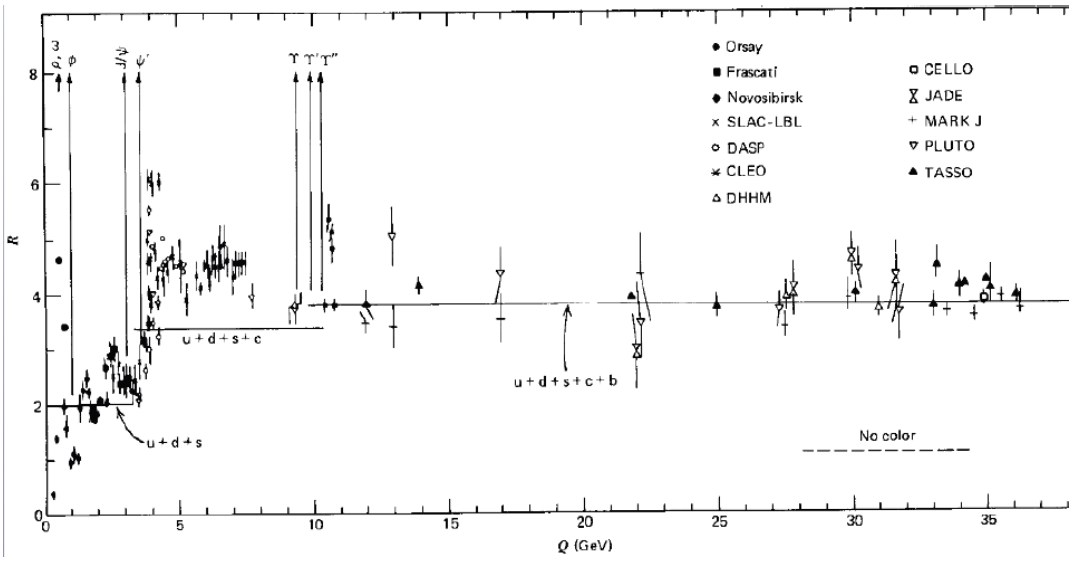

Figure 3: The ratio of hadron production in electron-positron annihilation over muon-antimuon pair, as a function of $\sqrt{s}$, the center-of-mass energy of the collision

Q: Why the formation of hadronic resonances lead to a large enhancement of the $\sigma(e^+e^- \to \text{hadrons})$ cross-section? What are the corresponding Feynman diagrams? What this is telling us about the strong interaction?

A: The quark pair constitute a bound state. The production cross-section is then enhanced due to strong interaction effects.

Q: Has the top quark ever been produced in e^+e^- annihilation? Why not? Why producing top quarks in e^+e^- annihilation could be interesting?

To summarize, by the end of the 70s several pieces of evidence had accumulated that confirmed the existence of the color quantum number and of the independent existence of quarks inside hadrons, that transform under the $\text{SU}(3)_c$ gauge group. Therefore, it is possible to describe the strong interactions by a Quantum Field Theory similar (but with crucial differences) as that of Quantum Electrodynamics.

The QCD Lagrangian

After this introduction to the basic motivation to QCD as a theory of the strong interactions, let us discuss its Lagrangian and its basic properties, in particular its symmetries.

Quantum Electrodynamics

The QED Lagrangian has the following form:

$$\mathcal{L}_{\rm QED} = \overline{\psi}\left(i\gamma^\mu D_\mu - m\right)\psi - \frac{1}{4}F_{\mu\nu}F^{\mu\nu}\,, \tag{8}$$

where for simplicity we have assumed a single fermion of mass m and electric charge e - the addition of more fermions with different masses and charges is trivial. In this Lagrangian, the covariant derivative is defined as

$$D_\mu \equiv \partial_\mu + ieA_\mu\,, \tag{9}$$

with e the electric charge of this fermion, and the field strength tensor is the usual definition from classical electrodynamics

$$F_{\mu\nu} = \partial_\mu A_\nu - \partial_\nu A_\mu\,, \tag{10}$$

The basic property of this Lagrangian is the invariance over local $U(1)$ transformation, where $U(1)$ is the abelian rotation group. This is know as the *gauge symmetry of the theory*. Under such rotation, fermions transform as

$$\psi(x) \to \psi'(x) = e^{i\phi(x)}\psi(x) \tag{11}$$

The vector potential can always be modified by an additive derivate of the form

$$A^\mu \to A^{'\mu} = A^\mu + \partial^\mu \chi(x) \tag{12}$$

It is easy to see that the field strength tensor is invariant under gauge transformations - this is a result from classical electrodynamics.

Q: Is this property specific of QED or already holds for classical electromagnetism?
A: The electromagnetic field is invariant if the vector potential is modified by a total derivative, as can be seen from Maxwell's equations.

Q: What other classical external symmetries does the QED Lagrangian have, Eq. (8)?
A: It is invariant under the Poincare group: translations, rotations and Lorentz boosts. There are also discrete symmetries like parity invariance.

It is also clear that the QED Lagrangian will be gauge invariant if the covariant derivative transforms in the same way as the fermion field, since by construction

$$D_\mu \to D'_\mu = e^{i\phi(x)}D_\mu \tag{13}$$

which as can be seen is achieved when we choose the gauge transformation of the four-vector potential to be

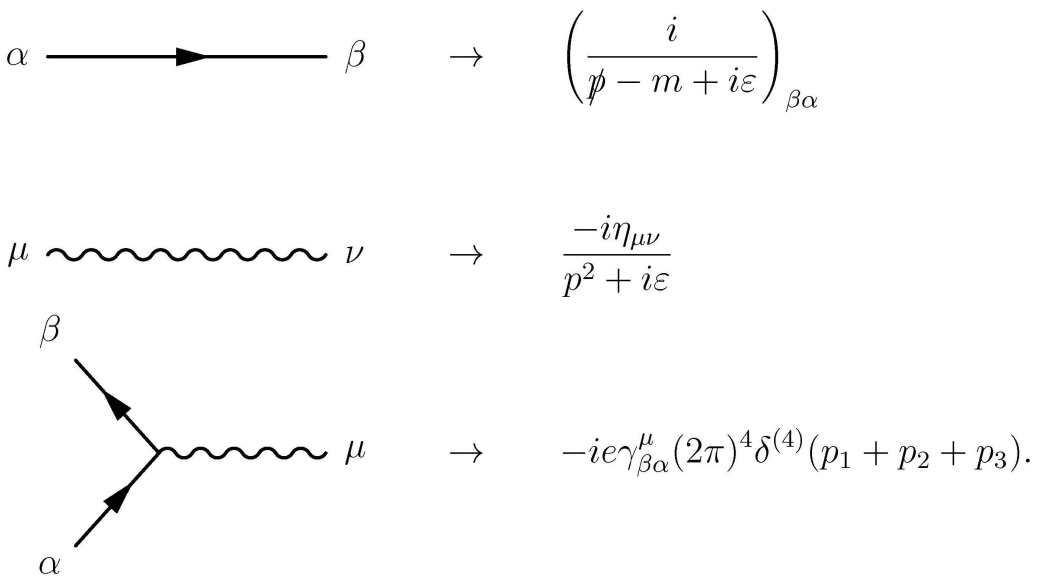

Figure 4: Feynman rules in Quantum Electrodynamics for the propagator of a fermion and a photon, and for the fermion-photon vertex. In these Feynman rules, α and β are Dirac spinor indices, and μ and ν are Lorentz indices.

the following:

$$\chi(x) = -\frac{\phi(x)}{e}\,, \tag{14}$$

Therefore, requiring *gauge invariance under U(1)* fixes the various terms of the QED Lagrangian.

Q: Can we add a mass term for the photon in the QED Lagrangian?

Q: In principle one can also add to the QED Lagrangian a term of the form $-(1/4)F_{\mu\nu}\widetilde{F}^{\mu\nu}$, with the dual tensor defined as $\widetilde{F}^{\mu\nu} \equiv \epsilon^{\mu\nu\rho\sigma}F_{\rho\sigma}$, which is gauge invariant. Why this term is absent in Eq. (8)?
Recall that in terms of the EM fields we have $F_{\mu\nu}\widetilde{F}^{\mu\nu} \sim \left(\vec{B}\cdot\vec{E}\right)$.

Using standard techniques, it is possible to derive the Feynman rules that allow the computation of amplitudes in QED. In Fig. 4 we show the Feynman rules in QED for the propagator of a fermion and a photon, and for the fermion-photon vertex, were α and β are Dirac spinor indices, and μ and ν are Lorentz indices. Using these relatively simple rules, it is possible to compute QED process at arbitrary orders in the perturbative expansion in the coupling $\alpha \sim g^2$.

The $SU(3)$ gauge group

As compared to QED, the main difference in the QCD case is the existence of new internal quantum number, color, which, in the language of gauge theory, leads to an invariance under a different non-abelian group. QED is an abelian gauge theory, where the relevant gauge group is the abelian $U(1)$. As opposed to it, the gauge group of QCD is $SU(3)$, the group of specially unitary transformations of degree $n = 3$. This group is defined by all $n \times n$ unitary matrices

$$U^T U = \mathbb{1} \tag{15}$$

$$\lambda_1 = \begin{pmatrix} 0 & 1 & 0 \\ 1 & 0 & 0 \\ 0 & 0 & 0 \end{pmatrix} \quad \lambda_2 = \begin{pmatrix} 0 & -i & 0 \\ i & 0 & 0 \\ 0 & 0 & 0 \end{pmatrix} \quad \lambda_3 = \begin{pmatrix} 1 & 0 & 0 \\ 0 & -1 & 0 \\ 0 & 0 & 0 \end{pmatrix},$$

$$\lambda_4 = \begin{pmatrix} 0 & 0 & 1 \\ 0 & 0 & 0 \\ 1 & 0 & 0 \end{pmatrix} \quad \lambda_5 = \begin{pmatrix} 0 & 0 & -i \\ 0 & 0 & 0 \\ i & 0 & 0 \end{pmatrix} \quad \lambda_6 = \begin{pmatrix} 0 & 0 & 0 \\ 0 & 0 & 1 \\ 0 & 1 & 0 \end{pmatrix},$$

$$\lambda_7 = \begin{pmatrix} 0 & 0 & 0 \\ 0 & 0 & -i \\ 0 & i & 0 \end{pmatrix} \quad \lambda_8 = \frac{1}{\sqrt{3}} \begin{pmatrix} 1 & 0 & 0 \\ 0 & 1 & 0 \\ 0 & 0 & -2 \end{pmatrix}.$$

Figure 5: The Gell-Mann matrices for the fundamental representation of $SU(3)$.

which have determinant equal to 1, det U = 1. The fact that the gauge invariance of QCD is under a non-abelian group has important consequences, as we will see now.

In the *fundamental representation*, a suitable choice of generators for $SU(3)$ are the Gell-Mann matrices, which are hermitian and traceless,

$$t^A \equiv \frac{1}{2}\lambda^A \,, \quad A = 1, \ldots, 8 \,, \tag{16}$$

and which obey the commutation relations of the group's Lie algebra

$$\left[t^A, t^B\right] = i f^{ABC} t^C \,, \quad A, B, C = 1, \ldots, 8 \,, \tag{17}$$

with f^{ABC} the structure constants of $SU(3)$, namely

$$f_{123} = 1 \,, \tag{18}$$

$$f_{147} = -f_{156} = f_{246} = f_{257} = f_{345} = -f_{367} = \frac{1}{2} \,, \tag{19}$$

$$f_{458} = f_{678} = \frac{\sqrt{3}}{2} \,, \tag{20}$$

and the corresponding permutations. All other structure constants are zero. The Gell-Mann matrices for the fundamental representation of $SU(3)$ are summarized in Fig. 5.

Hadron structure and SU(3). Let us now define the quark wave-function as follows:

$$\psi^{(f)\leftarrow \text{flavor}}_{i\leftarrow \text{color}} \,, \tag{21}$$

which has two indices: a flavor index (like in QED) and a color index (genuinely new feature of QCD). The color index was take any value up to N_c, the number of colors in the theory. In QCD, quarks transform in the fundamental representation of $SU(3)$

$$\psi_i^{(f)} \to \psi_i^{(f)'} = U_{ij}(x)\psi_j^{(f)} \tag{22}$$

which leaves the flavor degrees of freedom untouched. Note that the $SU(3)$ transformation are given by

$$U_{ij}(x) = \exp\left(i\theta^a(x)\, t^a_{ij}\right) \, . \tag{23}$$

Given that all observed strongly-interesting particles are color-singlet, the total color charge of physical states must be zero. To see this, consider the the wave function of a quark-antiquark bound state, known as *mesons*, constructed as

$$\sum_i^{N_c} \psi_i^{*(f)} \psi_i^{(f')} \, , \tag{24}$$

which can be shown to be invariant under a and under a $SU(3)$ transformation

$$\sum_i^{N_c} \left(\sum_j^{N_c} U^*_{ij} \psi_j^{*(f)} \right) \left(\sum_k^{N_c} U_{ik} \psi_k^{(f)} \right) = \sum_{kj} \left(\sum_i U^T_{ji} U_{ik} \right) \psi_j^{*(f)} \psi_k^{(f')} = \sum_k \psi_k^{*(f)} \psi_k^{(f')} \tag{25}$$

using the unitarity properties of the $SU(3)$ matrices.

On the other hand, this property must also hold for particles such as protons and neutrons, which are composed by three quarks (these hadrons are known as *baryons*). This can be achieved if the wave function of three-quark states is constructed as follows, using the antisymmetric tensor:

$$\sum_{ijk}^{N_c} \epsilon^{ijk} \psi_i^{(f)} \psi_j^{(f')} \psi_k^{(f'')} \, , \tag{26}$$

This can be shown to be color singlet using the relation

$$\sum_{ijk} \epsilon^{ijk} U_{ii'} U_{jj'} U_{kk'} = [\det \mathrm{U}] \; \epsilon^{i'j'k'} \, . \tag{27}$$

and the fact that the $SU(3)$ matrices are unitary. Therefore, baryons are also color singlet, in agreement with empirical observations. Note that the wave-function of the baryons Eq. (27) explains why hadrons like Δ^{++}, composed by three quarks, can still obey the Pauli exclusion principle: the exchange of any two of the identical quarks will change the sign of the wave function since $\epsilon^{ijk} = -\epsilon^{jik}$.

Q: Can we have more exotic hadrons, say tetraquarks or pentaquarks? Would they respect symmetries of QCD? Have they been observed experimentally?

Q: Do we understand from first principles why quarks and gluons are confined into hadrons?

The QCD Lagrangian and symmetries

Now, the QCD Lagrangian has formally a similar structure as compared to the QED one, Eq. (8), though now the invariance is with respect to the non-abelian group $SU(3)$, and this leads to a number of striking differences between the two theories. The QCD Lagrangian is thus the following:

$$\mathcal{L}_{\rm QCD} = \sum_f \overline{\psi}_i^{(f)} \left(i\gamma_\mu D_{ij}^\mu - m_f \delta_{ij} \right) \psi_j^{(f)} - \frac{1}{4} F_{\mu\nu}^a F_a^{\mu\nu} \,, \tag{28}$$

where a is now a color index that runs from 1 to $N_c - 1 = 8$, i, j are color indices from 1 to $N_c = 3$, since quarks transform in the fundamental representation of $SU(3)$, and we are assuming N_f massive fermions now. Unlike fermions, which transform in the *fundamental* representation of SU(3), gluons transform in the *adjoint* representation of SU(3).

Q: Why a gluon mass term of the form $m^2 A_a^\mu A_{\mu,a}$ is forbidden from the QCD Lagrangian? Do we have empirical evidence that $m = 0$?

In QCD, the covariant derivative is defined as follows:

$$D_{ij}^\mu = \partial^\mu \delta_{ij} + i g_s t_{ij}^a A_a^\mu \,. \tag{29}$$

where now g_s is the strong coupling constant, and the gluon field replaces the photon field that we had in QED. Now, note that in QCD the covariant derivative has a *matrix structure*: it is a matrix acting on fermions in the fundamental representation, unlike the case of QED. In particular, it mixes the color degrees of freedom. This has important physical consequences. In QCD, the field strength tensor is defined as

$$F_{\mu\nu}^a \equiv \partial_\mu A_\nu^a - \partial_\nu A_\mu^a - g_s f_{abc} A_\mu^b A_\nu^c \,, \tag{30}$$

with f_{abc} the structure constants of $SU(3)$ introduced above.

Q: What is the main difference between a theory of free photons and a theory of free gluons? Why the second is more interesting?

Now, the fermion sector of the Lagrangian must be independently gauge invariant, since in principle there are n_f fermion fields in the theory, each with a different mass. To achieve this, the covariant derivative must transform as the quark field itself

$$D_{ij}^\mu \psi_j \to \left(D_{ij}^\mu \psi_j \right)' = U_{ik}(x) D_{kj}^\mu \,, \psi_j \tag{31}$$

With this condition, one can check explicitly that the gauge transformation property of the gluon field is the

$$t^a A_a^\mu \to t^a A_a^{'\mu} = U(x) t^a A_a^\mu U^{-1}(x) + \frac{1}{g_s} \left(\partial^\mu U(x) \right) U^{-1}(x) \,. \tag{32}$$

where note that the SU(3) gauge transformation acts on the product $t^a A_a^\mu$, rather than on the gluon field itself.

Q: Is this the same transformation as in QED? What happens if the gauge group is Abelian?

An important difference between QED and QCD is that the field-strength tensor itself is **not** gauge

invariant. To show this, a useful relation is provided by the commutator between two covariant derivatives

$$[D_\mu,\, D_\nu] = i g_s\, t^a\, F^a_{\mu\nu}\,, \tag{33}$$

which can be derived from the definition of the covariant derivative acting on a fermion field. Now, transformation law of the field strength tensor under $SU(3)$ transformations will be given by

$$t^a F^a_{\mu\nu} \to t^a F^{'a}_{\mu\nu} = U(x)\, t^a F^a_{\mu\nu}\, U^{-1}(x)\,, \tag{34}$$

to is it in general not invariant under gauge transformations. However, the product $F^a_{\mu\nu}F^{\mu\nu}_a$ *is* invariant under $SU(3)$ transformations, and hence the gluon sector of the Lagrangian is also gauge invariant. We can use the following property of $SU(3)$

$$\text{Tr}\,\left[t^a t^b\right] = \frac{1}{2}\delta^{ab}\,, \tag{35}$$

and therefore we can have the following

$$-\frac{1}{4}F^a_{\mu\nu}F^{\mu\nu}_a = -\frac{1}{2}F^a_{\mu\nu}\,F^{\mu\nu,b}\text{Tr}\,\left[t^a t^b\right] = -\frac{1}{2}\text{Tr}\,\left[F^a_{\mu\nu}\,t^a\,F^{\mu\nu,b}\,t^b\right]\,, \tag{36}$$

which, using the transformation law Eq. (34), can be shown to be invariant under $SU(3)$ transformations due to the cyclic properties of the trace. Therefore, the purely gluonic piece of the QCD Lagrangian is gauge invariant, even if the individual field-strength tensor is not.

So we have seen that requiring invariance under SU(3) color transformations the form of the QCD Lagrangian is uniquely defined. As we will see below, a non-abelian gauge theory leads to the phenomenon of *asymptotic freedom*, which means that QCD looks similar to QED but only at high energies, while at low energies it looks like a very different kind of physical theory.

Chiral symmetry

In addition to the *exact* symmetries of the QCD Lagrangian, there is also an important *approximate* symmetry, which is chiral symmetry.

Strong interactions are found experimentally to behave very similar for particles, like protons and neutrons, that arise in the same *isospin multiplet*. Isospin is an approximate global $SU(2)$ symmetry which relates the up and the down content of hadrons, and that arises from the fact that $m_u \simeq m_d$. In the quark model, the isospin content of hadrons is defined as follows

$$I_3 = \frac{1}{2}\left[(n_u - n_{\bar{u}}) - (n_d - n_{\bar{d}})\right]\,, \tag{37}$$

so that we have that I_3 is 1/2 for protons and -1/2 for neutrons, members of the same isospin multiplet. Formally, an isospin transformation acts on the quark field as a unitary constant $SU(2)$ matrix

$$\psi^{(f)}_i \to \sum_{f'} U^{ff'}\,\psi^{(f')}_i\,, \tag{38}$$

which looks superficially similar to the color $SU(3)$ transformations, but they are completely different: this is a global transformation (not a local one as in the case of gauge symmetries) and it leaves the color indices

unchanged

We want to study under which conditions the fermion sector of the QCD Lagrangian is invariant under isospin transformations, so let us now separate the up and down fermions from all other fermions

$$\begin{aligned}\mathcal{L}_{\rm QCD} &= \overline{\psi}_i^{(u)}\left(i\gamma_\mu D_{ij}^\mu - m_u\delta_{ij}\right)\psi_j^{(u)} + \overline{\psi}_i^{(d)}\left(i\gamma_\mu D_{ij}^\mu - m_d\delta_{ij}\right)\psi_j^{(d)} \\ &+ \sum_{f,f\neq u,d}\overline{\psi}_i^{(f)}\left(i\gamma_\mu D_{ij}^\mu - m_f\delta_{ij}\right)\psi_j^{(f)} - \frac{1}{4}F_{\mu\nu}^a F_a^{\mu\nu}\,. \end{aligned} \tag{39}$$

Restricting the fermion sector to only up and down quarks, the isospin transformed QCD Lagrangian reads

$$\sum_{f',f''}\sum_f \left(U_{f'f}^T U_{ff''}\right)\overline{\psi}_i^{(f')}\left(i\gamma_\mu D_{ij}^\mu - m_f\delta_{ij}\right)\psi_j^{(f'')}\,. \tag{40}$$

Therefore, from this equation we see that the QCD Lagrangian will be invariant if $m_u = m_d$. As a particular case, this also includes the $m_d = m_u = 0$ scenario. Experimentally, we know that the up and down quark masses are much smaller than the typical scale of the QCD interactions

$$m_{u,d} \ll \Lambda_S\,, \tag{41}$$

and various techniques can be used to extract the values of the light quarks from data, using lattice calculations or other non-perturbative methods.

Chiral symmetry. In the limit of quark masses vanishing, we can separate left-handed and right-handed fermion chiralities and the Lagrangian will be separately invariant for the two components

$$\psi = \psi_R + \psi_L\,, \qquad \psi_L = \frac{1}{2}(1-\gamma_5)\psi\,, \qquad \psi_R = \frac{1}{2}(1+\gamma_5)\psi\,, \tag{42}$$

$$\sum_f\left(\overline{\psi}_R^{(f)}\left(i\gamma_\mu D^\mu\right)\psi_R^{(f)} + \overline{\psi}_L^{(f)}\left(i\gamma_\mu D^\mu\right)\psi_L^{(f)}\right)\,. \tag{43}$$

As a result of this invariance, chirality will be a conserved quantum number for massless fermions. In this case, the QCD Lagrangian would be chirally invariant. However, we know that QCD is not chirally invariant, and this arises because of the spontaneous breaking of chiral symmetry. Spontaneous breaking of a symmetry occurs when the symmetry group of the solutions of a theory is dynamically generated to be less than the symmetry of the original Lagrangian, as for example in the case of the Higgs mechanism. In the case of QCD, it is known that the vacuum has a non-zero expectation value of the light quark operator

$$\langle 0|\bar{q}q|0\rangle = \left\langle 0|\bar{u}u + \bar{d}d|0\right\rangle \simeq (250\text{ MeV})^3 \tag{44}$$

which breaks chiral symmetry, and is responsible for most of the hadron masses.

Q: What would be the pion masses in the case that the light quark masses vanished, $m_u = m_d = 0$?

Q: which is approximately the contribution of the Lagrangian quark masses to the hadrons masses? Can we then conclude that the Higgs mechanism is responsible for giving most of its mass to visible matter?

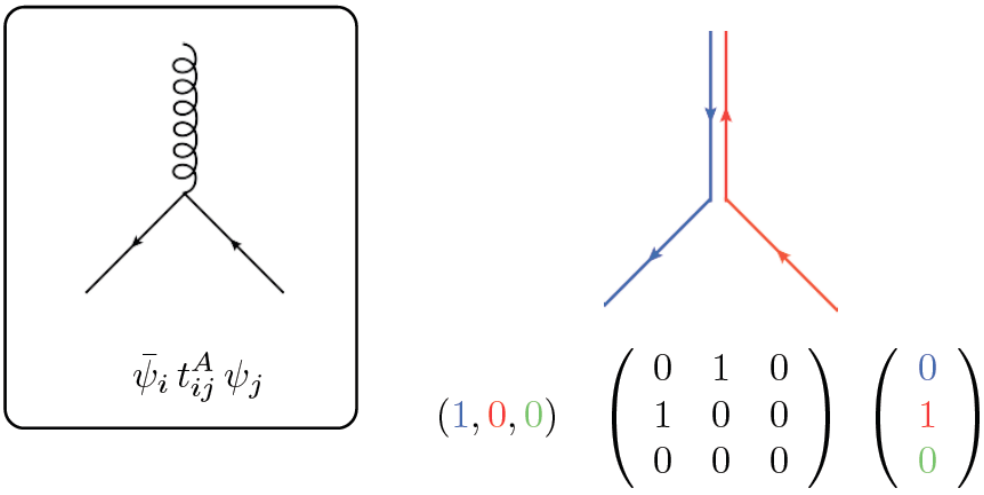

Figure 6: The emission of a gluon from a quark interpreted in terms of color flow, with the Gell-Mann matrix performing a rotation in color space.

Color flows and Feynman rules

The various contractions of color indices in the QCD Lagrangian can be interpreted as color flows between the different types of fields. In this specific example of Fig. 6, an incoming quark with red color emits a gluon and is transformed into an outgoing quark with blue color. Gluons carry both color and anti-color: they change the color charge of quarks and of other gluons. The allowed color flows are restricted by $SU(3)$ symmetry, as can be seen in this example with the Gell-Man matrix.

Following the same techniques as in the case of QED, it is possible to determine the Feynman rules that QCD must obey. These Feynman rules are summarized in Fig. 7. In the left part of the plot, we show the various propagators and vertices that are allowed in QCD, with the corresponding Feynman rules. Note the presence of three-gluon and four-gluon vertices, which are absent in QED: this is a genuine new feature of QCD, which arises from the non-abelian nature of $SU(3)$, and that has important consequences, like asymptotic freedom, which we will discuss below. In the three-gluon diagram of Fig. 7, p_i are the four momenta of each of the gluons, assuming they are incoming. When computing Feynman diagrams, all possible permutations of the three and four-gluon vertices need to be included.

In order to understand where the three- and four-gluon vertices come from, if we now expand the gluonic term of the QCD Lagrangian, keeping only the terms proportional to the strong coupling constant, we find the following terms

$$\begin{aligned} F_a^{\mu\nu} F^a_{\mu\nu} \quad &\rightarrow \quad \ldots + g_s^2 \, f_{abc} \, f_{ade} \, A^{\mu,b} \, A^{\nu,c} \, A^d_\mu \, A^e_\nu \\ &- \quad g_s \, f_{abc} \, A^{\mu,b} \, A^{\nu,c} \left[\partial_\mu \, A^a_\nu - \partial_\nu \, A^a_\mu \right] - g_s \, f_{abc} \, A^b_\mu \, A^c_\nu \left[\partial^\mu A^{\nu,a} - \partial^\nu A^{\mu,a} \right] \end{aligned} \tag{45}$$

which lead to the vertices shown in Fig. 7. The proportionality to p_i in the three-gluon vertex arises the derivatives in the second half of the equation above.

In Fig. 7, right part, we also show how the Feynman rules can be understood in terms of color flow. In all the diagrams, we can see that color is conserved, a basic property of $SU(3)$ symmetry. Therefore, in QCD

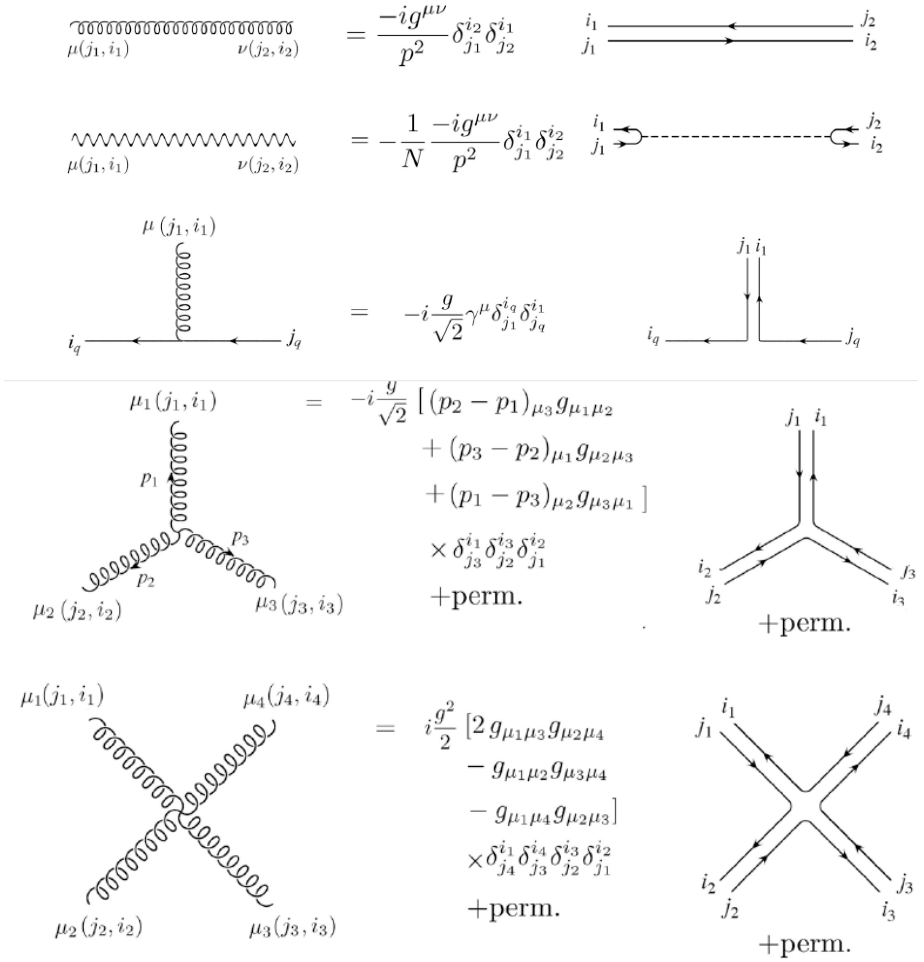

Figure 7: The Feynmann rules of QCD, for the propagation and interaction of quarks and gluons. In the right part of the plot, we show how the Feynman rules can be also interpreted in terms of color flow between quarks and gluons.

only diagrams which conserve color will be physically allowed.

Comparing the QCD Feynman rules in Fig. 7 with the corresponding QED Feynman rules of Fig. 4 we see that the main difference is the presence of self-interaction terms for gauge bosons: the three-gluon and four-gluon vertices. This is a direct consequence of the non-abelian nature of the gauge group of QCD, SU(3), and is the main reason of why at high energies the strong interaction can be described by the mathematical language of a perturbative quantum field theory.

Asymptotic freedom and confinement in QCD

Perhaps the most remarkable property of QCD is that of asymptotic freedom: the strength of the QCD interaction decreases when the momentum transfers involved in the interaction increase. This allows to use the basic tools of perturbative QFT to deal with hard QCD interactions. On the other hand, it also implies that at low scales QCD becomes non-perturbative, since the QCD coupling diverges, and the perturbative interpretation is not valid anymore. While this suggests confinement, since the strength of the interaction between two quarks would increase the more we try to separate them (larger distances corresponds to smaller energy scales), confinement has never been formally derived from the QCD Lagrangian, and only partial numerical evidence from lattice simulations has been obtained.

The running of the coupling constants in Quantum Field Theories like QED or QCD can be understood neatly from renormalization group arguments. Let us consider a given observable G in a generic QFT (for instance, a cross-section) with (bare) dimensionless coupling constant α, and a number of kinematical invariants $s_1 \ldots s_n$. In quantum field theories we encounter ultraviolet (UV) divergences, which in renormalizable theories can be removed by a suitable redefinition of the couplings and fields. If we denote by M the UV cut-off,[1] after renormalization the observable G will be given as follows

$$G = G(\alpha,\, M,\, s_1, \ldots, s_n)\ . \tag{46}$$

Now, the dependence on M can be eliminated by a suitable redefinition of the bare coupling (which does not depend on any scale) in terms of the renormalized coupling, order by order in the perturbative expansion

$$\alpha_{\rm ren} = \alpha + \sum_{l=2} c_l\,(M/\mu)\,\alpha^l\,, \tag{47}$$

where the coefficients c_l are dimensionless, and the arbitrary scale μ has been introduced for dimensional reasons.

We can now use a basic principle of renormalizable QFTs, namely,

Any physical quantity can be expressed in terms of the renormalized coupling $\alpha_{\rm ren}$, the scale μ and other kinematical invariants, without the need anymore of the UV cutoff.

Therefore, we can write

$$G\left(\alpha\left(\alpha_{\rm ren}, M/\mu\right),\, M,\, s_1, \ldots, s_n\right) = \widetilde{G}\left(\alpha_{\rm ren}, \mu, s_1, \ldots, s_n\right)\ , \tag{48}$$

In renormalizable QFTs, a single redefinition of the coupling makes finite **all** physical observables. The price to pay is the dependence of our results on the arbitrary *renormalization scale* μ, which could be eliminated only by computing the theory to all perturbative orders.

The renormalization group equations (RGE) arise from the condition that if we vary $\alpha_{\rm ren}$ and μ, keeping α and M fixed, cross-sections should be invariant (since before renormalization, physical observables depend

[1] Similar arguments can be derived with other renormalization techniques, such as dimensional regularization.

only on M and α, and we have done here only a change of variables). This leads to the conditions

$$\frac{\partial \widetilde{G}\left(\alpha_{\rm ren},\mu,s_1,\ldots,s_n\right)}{\partial \alpha_{\rm ren}} d\alpha_{\rm ren} + \frac{\partial \widetilde{G}\left(\alpha_{\rm ren},\mu,s_1,\ldots,s_n\right)}{\partial \mu} d\mu = 0 \tag{49}$$

$$\frac{\partial \alpha\left(\alpha_{\rm ren},M/\mu\right)}{\partial \alpha_{\rm ren}} d\alpha_{\rm ren} + \frac{\partial \alpha\left(\alpha_{\rm ren},M/\mu\right)}{\partial \mu^2} d\mu^2 = 0 \tag{50}$$

and from these expressions it is possible to determine that the dependence of the renormalized coupling $\alpha_{\rm ren}$ with the scale μ is given by:

$$\mu^2 \frac{d\alpha_{\rm ren}}{d\mu^2} = \beta(\alpha_{\rm ren}) \,. \tag{51}$$

This is so because putting together the various equations above we find

$$\mu^2 \frac{d\alpha_{\rm ren}}{d\mu^2} = -\frac{\mu^2 \partial \alpha\left(\alpha_{\rm ren},M/\mu\right)/\partial \mu^2}{\partial \alpha\left(\alpha_{\rm ren},M/\mu\right)/\partial \alpha_{\rm ren}} = -\frac{\mu^2 \partial \widetilde{G}\left(\alpha_{\rm ren},\mu,s_1,\ldots,s_n\right)/\partial \mu^2}{\partial \widetilde{G}\left(\alpha_{\rm ren},\mu,s_1,\ldots,s_n\right)/\partial \alpha_{\rm ren}} \tag{52}$$

and therefore the functional dependence of the renormalized coupling with the scale μ is fixed by the following conditions:

- It cannot depend on M, since RHS does not
- It cannot depend on the kinematical invariants, since LHS does not
- It cannot depend on μ, since we dont have other dimensionful variables available and the coupling is dimensionless

Therefore, at the first non-trivial order, the RGE equation Eq. (51) must read

$$\boxed{\frac{d}{d\,\log \mu^2} \alpha_{\rm ren}(\mu^2) = -b_0 \alpha_{\rm ren}^2 \,,} \tag{53}$$

Eq. (53) holds for any perturbative renormalizable QFT: the renormalized coupling *runs*, that is, it depends on the typical physical scale that enters each specific scattering amplitude. This equation can be easily solved to give

$$\alpha_{\rm ren}(\mu^2) = \frac{1}{b_0 \log \mu^2/\Lambda^2} \,, \tag{54}$$

Now, so far everything holds for a generic theory. In the case of QCD, the coefficient b_0 can be determined by computing the Feynman diagrams for the $\mathcal{O}\left(\alpha_s^2\right)$ corrections to the gluon propagator, summarized in Fig. 8.[2] The leading order term for the QCD beta function is given by

$$b_0 = \frac{33 - 2n_f}{12\pi} \tag{55}$$

The result that b_0 is positive arises from the gluon self-interactions, that is from the non-abelian nature of QCD (to see this, note that the diagram with quarks in the loop leads to the N_f-proportional piece). In other words, even a pure gluonic version of QCD would exhibit this property. Looking at Eq. (54), we see that $b_0 > 0$ implies that the theory becomes free (non-interacting) in the ultra-violet, hence the name

[2]The calculation was performed independently by Gross and Wilczek [1] and by Politzer [2] in 1973. It was the first assignment of Gross to Wilczek, who had then just started his Ph. D.

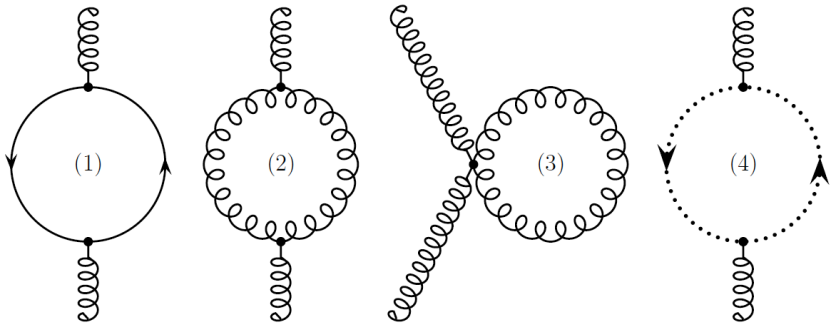

Figure 8: Feynman diagrams which contribute to the renormalization of the gluon propagator in QCD, which determine the leading order coefficient of the RGE equations for the running of $\alpha_{\rm ren}(\mu)$ in Eq. (53).

asymptotically free. In Fig. 9 we summarize recent experimental determinations of the QCD running coupling $\alpha_S(Q)$ for different scales, together with the four-loops QCD prediction. Asymptotic freedom can be seen by the fact that $\alpha_s(Q)$ decreases when Q is increased.

Q: How can we exploit a measurement of the strong coupling at high-scales to look for new physics beyond the Standard Model? Which scales can/should we probe to make this measurement constraining?

The situation is remarkably different in the case of QED. There, the first term of the beta function is negative, due to the absence of photon self-interactions in the QED Lagrangian:

$$b_0^{\rm QED} = -\frac{4n_f}{12\pi} \tag{56}$$

As opposed to QCD, QED becomes strongly interacting (non-perturbative) in the ultraviolet, that is, at very small distances and large scales. The scale where QED stops being weakly coupled is determined by the position of the Landau pole in QED, which is

$$\Lambda = m_e \exp\left(-\frac{1}{2b_0\alpha_{\rm ren}(m_e)}\right) \sim 10^{90}\,{\rm GeV} \gg M_{Pl} \tag{57}$$

much larger than any sensible scale, even the Plank scale where quantum gravity effects become important. For this reason non-perturbative effects are not relevant for Quantum Electrodynamics.

In summary, asymptotic freedom is one of the central properties in QCD: it becomes a free theory at very large energies. The renormalization group equations allows to determine the dependence of the running coupling on the scale, in terms of $\alpha_S(q_{\rm ref})$ at some reference scale, which needs to be extracted from experimental data. On the other hand, we still dont understand what are the dynamics that lead to confinement. The QCD coupling is large at low scales, but there perturbation theory breaks down. Confinement is an experimental observation (hadrons are always color singlets) but it is a purely non-perturbative phenomenon, thus non-perturbative methods are required, like lattice QCD. In Fig. 9 we show how in a lattice QCD calculation the quark-antiquark potential increases linearly with the with the separation between the quark and the antiquark, as expected in a confining theory, but still the relevant degrees of freedom are quarks and gluons, not hadrons. The mechanism that leads to the realization of confinement remains still elusive.

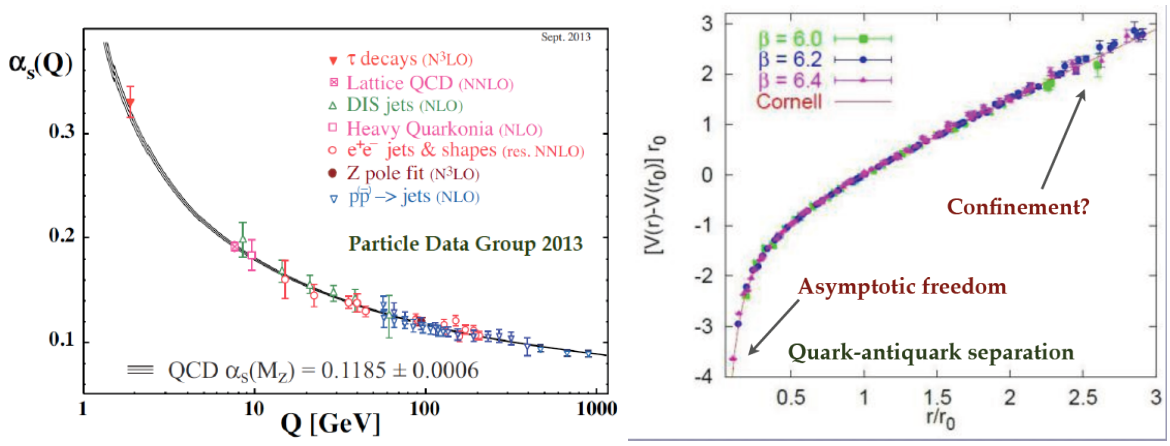

Figure 9: Left plot: summary of recent determinations of the QCD running coupling $\alpha_S(Q)$ for different scales, together with the four-loops QCD prediction. Asymptotic freedom can be seen by the fact that $\alpha_s(Q)$ decreases when Q is increased. Right plot: calculation of the potential between a quark-antiquark pair as a function of their separation, in lattice QCD.

Q: Why the lattice calculation for $\alpha_s(Q)$ cannot be considered as a direct demonstration of confinement? What are the degrees of freedom in a lattice calculation?

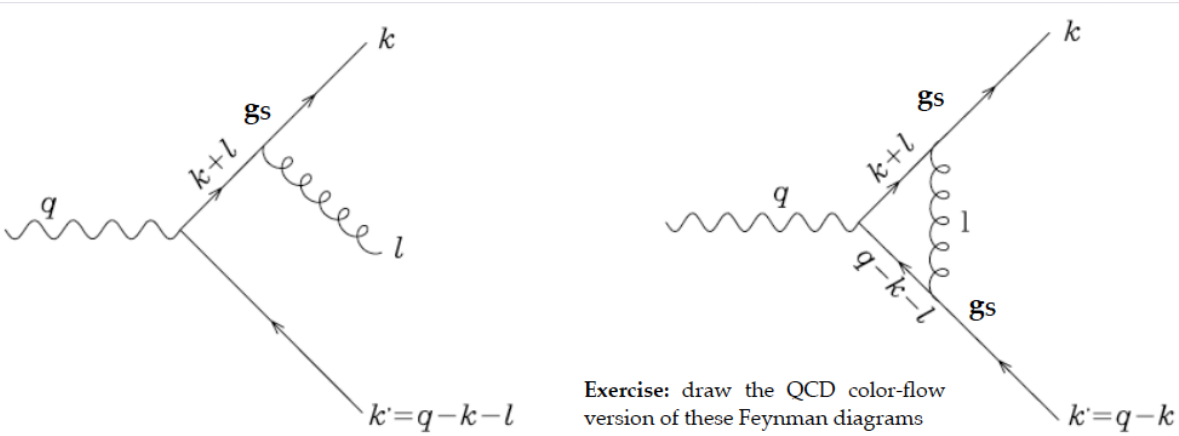

Figure 10: QCD corrections to quark-antiquark production in electron-positron annihilation. **Exercise**: draw the color-flow version of these diagrams.

Perturbative QCD in electron-positron annihilation

After this introduction to QCD, we turn out to explore its implications for a variety of high-energy reactions: we begin with electron-positron annihilation, then lepton-proton scattering and finally hadron-hadron collisions. We begin here with electron-positron annihilation, and study the consequences of radiative corrections in QCD. We already considered this process in Fig. 3, when we introduced the R ratio of hadron to lepton production in e^+e^- collisions. The calculation of the Born diagrams involved only QED interactions, and now we want to study what happens when we consider the first non-trivial QCD corrections.

The Born-level matrix element for this process follows from the QED Feynman rules:

$$\mathcal{M} = ie\bar{u}(k)\,\epsilon^{\mu}(q)\,\gamma_{\mu}\,v(k')\,. \tag{58}$$

The real emission and virtual correction to the Born diagram are illustrated in Fig. 10, which also sets the notation for the various four-momenta that will be used in the following. For the diagram with real radiation out of the outgoing quark (there is a similar contribution from the outgoing quark), and neglecting all fermion masses since this is a high energy processes, we find that the corresponding matrix element is given by

$$\mathcal{M}_1 = -ieg_s\,\bar{u}(k)t^a\epsilon_a^{\nu}(l)\,\gamma^{\nu}\,\frac{1}{\not{k}+\not{l}}\,\epsilon^{\mu}(q)\,\gamma_{\mu}\,v(k')\,, \tag{59}$$

where the appearance of g_s indicates that now we have activated QCD corrections.

To isolate the regions where the matrix element is enhanced, we can use a number of well-known properties of the Dirac algebra

$$\frac{1}{\not{k}+\not{l}} = \frac{\not{k}+\not{l}}{(k+l)^2}\,, \qquad \{\gamma^{\mu},\gamma^{\nu}\} = 2\eta^{\mu\nu}\mathbb{1}_4\,, \qquad \bar{u}(k)\not{k} = 0 \tag{60}$$

and be able to write Eq. (59) as follows

$$\mathcal{M}_1 = -ieg_s\,\bar{u}(k)\not{\epsilon}(q)\,v(k')\cdot\left[\frac{t^a\epsilon_a(l)\cdot k}{k\cdot l} - \frac{t^a\epsilon_a(l)\cdot k'}{k'\cdot l}\right]\,, \tag{61}$$

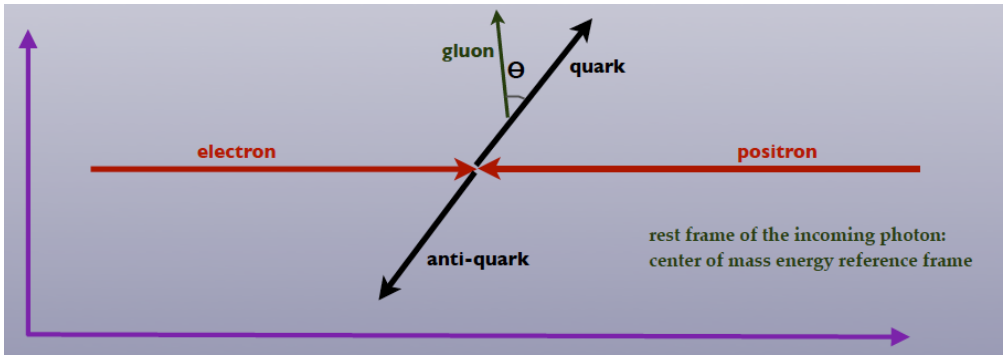

Figure 11: Kinematics of real gluon emission in quark-antiquark production via electron-positron annihilation.

In the above equation, and in the remaining of this lecture, we work in the *soft approximation*, which is $l \ll k, k'$, that is, the gluon is much softer than any of the two quarks. This is useful since this approximation isolates the kinematic region where the matrix element becomes divergent.

If now we square the matrix element, we note that it can be written as a factorized product of the Born matrix element squared and a term that depends on the kinematics of the three final state particles

$$|\mathcal{M}_1|^2 = |\mathcal{M}|^2 \, g_s^2 C_F \frac{2k \cdot k'}{(k \cdot l)\,(k' \cdot l)} \, . \tag{62}$$

To compute the cross-section for the real emission contribution, we need to add the corresponding phase space factor and integrate over all the relevant phase space, in order to obtain:

$$\sigma_1 = C_F \, g_s^2 \, \sigma_{\rm born} \cdot \int \frac{d^3 l}{2 l^0 \, (2\pi)^3} \frac{2k \cdot k'}{(k \cdot l)\,(k' \cdot l)} \, . \tag{63}$$

In order to interpret this result, it is useful to express the various Lorentz invariants in the laboratory frame, and denoting by θ the angle between the radiated gluon and the quark (see Fig. 11), we obtain the following expression

$$\sigma_1 = C_F \, \frac{g_s^2}{4\pi^2} \, \sigma_{\rm born} \int \frac{dl_0}{l_0} \, \frac{d\cos\theta}{(1+\cos\theta)\,(1-\cos\theta)} \tag{64}$$

so the real emission cross-section is the Born times the QCD coupling times an integral over the energy and the angle of the radiated gluon in the laboratory frame. The integral over energies is clearly divergent when the gluon becomes very soft, $l_0 \to 0$. The angular integral is also divergent, as one can see by using

$$\int \frac{x}{1-x^2} = -\frac{1}{2} \log\left(1-x^2\right) \, , \tag{65}$$

so the angular integral diverges when the gluon becomes collinear to the quark ($\theta = 0$) or to the anti-quark ($\theta = \pi$). Therefore, the real emission cross-section is now *divergent* due to *soft* and *collinear* emission of gluons. These soft and collinear divergences are a generic feature of massless gauge boson emission in QFTs, which are only canceled in inclusive enough observables.

It is also possible to compute the virtual diagrams in the same soft approximation. Putting everything

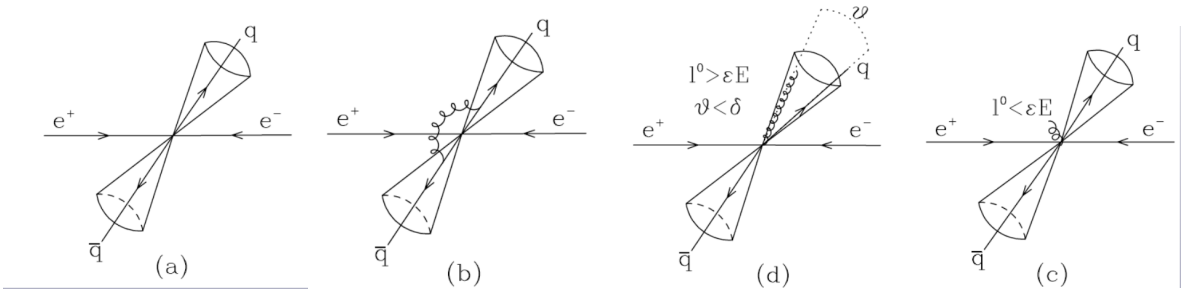

Figure 12: Diagrams for the various contributions to the QCD α_S corrections to the calculation for the cross-section for the production of Sterman-Weinberg jets. From left to right we have the Born diagram, the virtual correction, and real emission falling both inside and outside the jet cone.

together, we find that the QCD corrections to e^+e^- annihilation into hadrons are given by:

$$\begin{aligned} \sigma_0 &= \sigma_{\rm born} \\ \sigma_{1,\,\rm real} &= C_F\,\frac{g_s^2}{\pi^2}\,\sigma_{\rm born}\int\frac{dl_0}{l_0}\,\frac{d\cos\theta}{1-\cos^2\theta} \\ \sigma_{1,\,\rm virt} &= -C_F\,\frac{g_s^2}{\pi^2}\,\sigma_{\rm born}\int\frac{dl_0}{l_0}\,\frac{d\cos\theta}{1-\cos^2\theta}\,, \end{aligned} \tag{66}$$

where we see that in the soft limit the virtual corrections have the same structure, but different sign, as the real emission corrections. Therefore, if we integrate Eq. 66 without any phase space restriction, we find a finite result, with infrared and collinear singularities canceling between real and virtual terms. For example, doing the full calculation, it is possible to evaluate the $\mathcal{O}\left(\alpha_s\right)$ correction to the R-ratio, namely

$$R = R_{\rm born}\cdot\left(1+\frac{\alpha_s}{\pi}\right)\,. \tag{67}$$

The situation is however different if we try to compute the QCD corrections to less inclusive observables, such as jets. The first definition of a QCD jet, by Sterman and Weinberg, stated that

- an event contributes to the jet cross-section if we can find two cones, with opening angle δ, that contain a fraction $1-\epsilon$ of the total energy.

Note that in e^+e^- collisions the total energy of the event is fixed by the energy of the lepton beams, unlike in an hadronic collision. As opposed to the inclusive calculation above, for the jet cross-section the phase space for gluon emission is now limited, and this will have important consequences. In Fig. 12 we show the diagrams for the various contributions to the QCD α_S corrections to the calculation for the cross-section for the production of Sterman-Weinberg jets. From left to right we have the Born diagram, the virtual correction, and real emission falling both inside and outside the jet cone.

Let's compute the contributions to the various diagrams in Fig. 12 to the Sterman-Weinberg jet cross-section. The Born is unchanged by the jet definition. To see this, note that if the two partons as back to back all the energy of the event will fall into the two cones. For the real emission, we need to start from Eq. (64), but now with the integration restricted to the in-jet or out-jet phase space. In the case of radiation

inside the jet cone, we have

$$\sigma_1^{\rm jet,real,d} = C_F \, \frac{g_s^2}{\pi^2} \, \sigma_{\rm born} \int_{\epsilon E}^{E} \frac{dl_0}{l_0} \left[\int_0^{\delta} \frac{d\cos\theta}{1-\cos^2\theta} + \int_{\pi-\delta}^{\pi} \frac{d\cos\theta}{1-\cos^2\theta} \right] , \tag{68}$$

where the lower limit of the integration in the gluon energy arises because soft gluons, with $l_0 \leq \epsilon E$, do not contribute to the jet definition. In the case of soft-gluon emission, irrespective of whether or not radiation falls in the jet cone, the cross-section will be

$$\sigma_1^{\rm jet,real,c} = C_F \, \frac{g_s^2}{\pi^2} \, \sigma_{\rm born} \int_{0}^{\epsilon E} \frac{dl_0}{l_0} \left[\int_0^{\pi} \frac{d\cos\theta}{1-\cos^2\theta} \right] . \tag{69}$$

In order to make the jet cross-section finite, we need to compute the virtual correction. This reads

$$\sigma_1^{\rm jet,virt} = -C_F \frac{g_s^2}{\pi^2} \sigma_{\rm born} \int_0^{E} \frac{dl_0}{l_0} \int_0^{\pi} \frac{d\cos\theta}{1-\cos^2\theta} \tag{70}$$

since for virtual corrections there is no restriction on the kinematics of the gluon. Adding together the Born cross-section, the different real emission terms, and the virtual correction, we find that the jet cross-section is now *finite*:

$$\sigma^{\rm jet} = \sigma_{\rm born} \left(1 - \frac{g_s^2}{\pi^2} \int_{\epsilon E}^{E} \frac{dl_0}{l_0} \int_{\delta}^{\pi-\delta} \frac{d\cos\theta}{1-\cos^2\theta} \right) \tag{71}$$

$$= \sigma_{\rm born} \left(1 - \frac{4g_s^2}{4\pi^2} \log\epsilon \, \log\frac{1+\cos\delta}{1-\cos\delta} \right) . \tag{72}$$

and that it depends on the jet definition parameters ϵ and δ. The logarithmic dependence of the cross-section with these parameters is a remnant of the cancellation of soft and collinear divergences. The QCD correction becomes unreliable when either ϵ is too small (trying to resolve soft gluons) or the cone is too narrow (trying to resolve collinear gluons). Using similar techniques we can compute a number of phenomenologically relevant processes. An important example is the ratio of 3 over two jet events

$$R_{3/2} \equiv \frac{\sigma^{3\,\rm jets}}{\sigma^{2\,\rm jets}} = \frac{\sigma^{\rm tot} - \sigma^{\rm jet}}{\sigma^{\rm jet}} = \frac{\alpha_s}{\pi} \left(1 + 8 \, \log\epsilon \, \log\frac{1+\cos\delta}{1-\cos\delta} \right) \tag{73}$$

Note that any jet observables such as Eq. (73) depend by construction on the precise jet definition used.

Jets are a fundamental aspect of QCD at colliders. QCD jets were discovered in the late 70s in electron-positron colliders, and in the 80s and 90s they provided stringent tests of the validity of QCD at the Large Electron-Positron collider (LEP). Now at the LHC, jets not meant to be used as QCD tests anymore, but as essential tools for precision Standard Model measurements and for New Physics searches. Progress in the experimental measurement of QCD jets is illustrated in Fig. 13, where we compare in the left plot the discovery of the gluon in three-jet events from e^+e^- collisions at PETRA, in the late 70s with the right plot, a high energy dijet event as measured by the CMS experiment at the LHC, for a center of mass energy of $\sqrt{s} = 7$ TeV. We will discuss modern techniques for jet reconstruction and substructure later in these lectures, but before let's discuss the important topic of when a given observable can be computed reliably in QCD to all orders, so that infrared and collinear divergences always cancel.

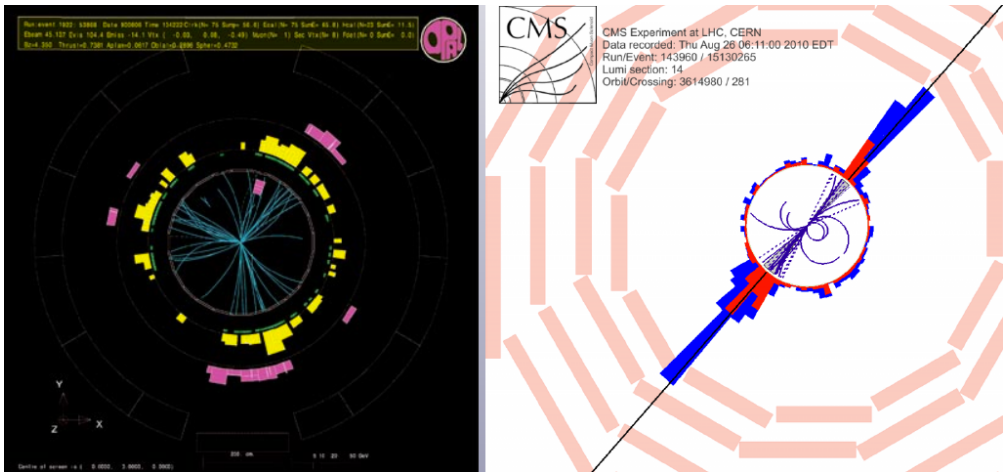

Figure 13: Left plot: discovery of the gluon in three-jet events from e^+e^- collisions at PETRA, in the late 70s. Right plot: high energy dijet event as measured by the CMS experiment at the LHC, for a center of mass energy of $\sqrt{s} = 7$ TeV.

Infrared and collinear safety

The formal definition of an infrared and collinear safe observable in QCD, that is, an observable insensitive to the long distance, infrared dynamics determined by non-perturbative physics, is

$$\mathcal{O}_{n+1}\left(k_1, k_2, \ldots, k_i, k_j, \ldots, k_n\right) \to \mathcal{O}_n\left(k_1, k_2, \ldots, k_i + k_j, \ldots, k_n\right) \tag{74}$$

when either k_i or k_j become soft, or when k_i becomes collinear to k_j. In order words, QCD infrared observables should be invariant wrt soft and collinear radiation both in the initial and in the final state. Only for infrared safe observables the comparison of data and theory is well defined to all orders in perturbation theory. We will come back to this important issue when discussing jets.

It is interesting to check which quantities are IRC safe

- Energy distribution of hardest particle in a event? No
- Jet cross-sections? Depends on the jet definition? Depends
- Multiplicity of gluons? No
- Cross-section for producing an additional quark or gluon with E ¿ Emin? No

For example, using the Sterman-Weinberg definition, the jet cross-section is not infrared and collinear safe to all orders. It is finite at $\mathcal{O}\left(\alpha_s\right)$, but starting from $\mathcal{O}\left(\alpha_s^2\right)$ divergences do not cancel anymore. This can be seen from the sketch in Fig. 14: a gluon that is just outside the SW cone, upon a collinear splitting can contribute to enough energy so that this event now is part of the jet cross-section. Since IRC safe observables cannot depend on collinear or soft splittings, this shows that the Sterman-Weinberg is not a good jet definition. Any sensible jet definition should be IRC safe, in other words, it would be insensitive to non-perturbative, long distance QCD dynamics.

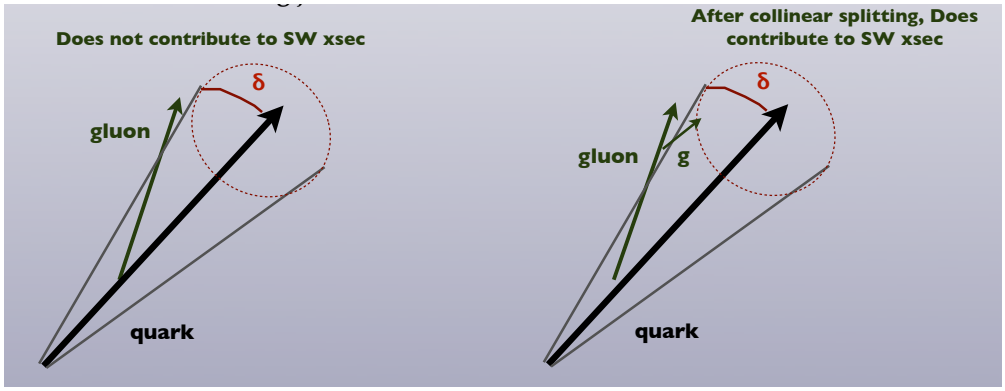

Figure 14: Origin of the IRC unsafety of the Sterman-Weinberg jets starting at at $\mathcal{O}(\alpha_s)$.

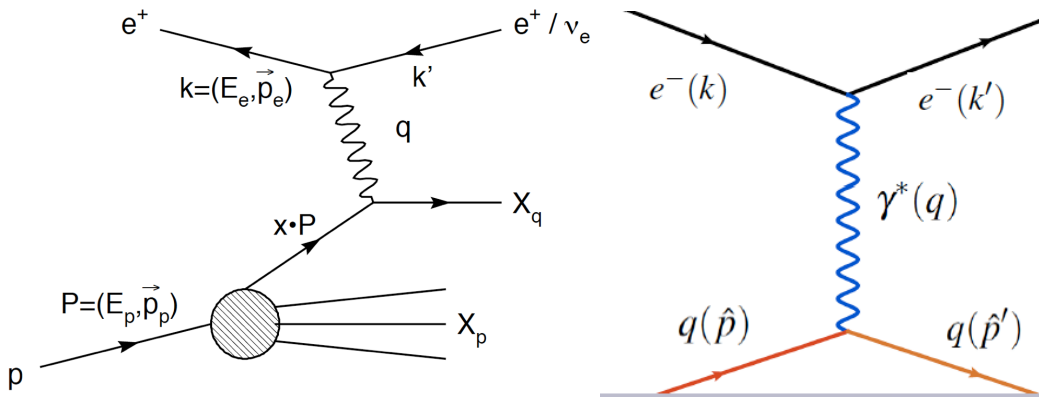

Figure 15: Left plot: the deep-inelastic scattering process. Right plot: the Born contribution to the lepton-quark scattering.

QCD in deep-inelastic scattering

After the study of the $\mathcal{O}(\alpha_S)$ corrections to electron-positron annihilation, and to the concept of jets, we now move to the study of the QCD corrections to the deep-inelastic scattering (DIS). This processes was already discussed in order to historically motivate the existence of quarks, see Fig. 2. Now we revisit it in more detail, and study the consequence that the QCD radiative corrections have in the naive parton model.

The QCD parton model

In the parton model, the DIS process is understood as the scattering of a virtual photon off one of the quarks in the proton, see Fig. 15. The probability to find a given quark in the proton with a fraction x of the total proton momentum is given by the quark parton distribution function (PDF), $q(x)$. Let's recall that DIS is the scattering of a highly energetic proton off a proton target,

$$e^-(k) + p(p) \to e^-(k') + X\,, \tag{75}$$

where in general the proton will be destroyed by the collision (hence the name *inelastic*). The four momentum transfer between the lepton and the proton is

$$q \equiv k' - k\,. \tag{76}$$

The kinematics of the deep-inelastic scattering process are completely specified by the following variables

$$x_{\rm Bj} \equiv \frac{Q^2}{2\,p\cdot q}, \quad Q^2 \equiv -q^2\,, \quad y \equiv \frac{q\cdot p}{k\cdot p}\,. \tag{77}$$

To differentiate from *elastic scattering*, the condition must be that $Q^2 \gg M_p^2$, else the proton would not be destroyed. For instance, the center-of-mass energy of the proton-virtual photon collision will be

$$W^2 \equiv (p+q)^2 = M_p^2 + Q^2\frac{1-x}{x} \simeq Q^2\frac{1-x}{x}\,, \tag{78}$$

where the proton mass can typically be neglected in the calculation. The value $x = 1$ is known as the elastic limit. A nice property of DIS is that the complete kinematics of the process are fully specified by measuring the four-momenta of the outgoing lepton.

Removing trivial kinematic factors, the DIS lepton-proton cross-section can be written in terms of a structure function $F_2(x)$, as a convolution between the $\gamma^* q \to X$ partonic cross-section and the PDFs of the proton,

$$\frac{Q^4 x}{2\pi\alpha^2_{\rm QED}\left(1+(1-y)^2\right)}\frac{d^2\sigma^{\rm DIS}}{dxdQ^2} = F_2(x) = \sum_{\rm q,\bar{q}}\int_x^1 \frac{dz}{z} f_q(z)\widehat{\sigma}_{q\gamma^*\to X}\left(\frac{x}{z}\right) . \tag{79}$$

Note that Eq. (79) is so far a *model*, not a consequence of QCD: we take the partonic QED quark-photon cross-section $\widehat{\sigma}_{q\gamma^*\to X}$ and convolute with the quark PDF $f_q(z)$. It is possible to formally derive the same expression in perturbative QCD to all orders using the *Factorization Theorem*.

In the naive parton model, the dependence of the PDFs with the momentum fraction x is a priory unknown (since it is determined by non-perturbative QCD dynamics). However, PDFs have still to satisfy a number of important sum rules, in particular the momentum sum rule,

$$\sum_{\rm q,\bar{q}}\int_0^1 dx\, x\, f_q(x) = 1\,, \tag{80}$$

which translates the fact that the total momentum of the proton is distributed among all the quarks, and the valence sum rules

$$\int_0^1 dx\, \left(f_u(x) - f_{\bar{u}}\right) = 2\,, \tag{81}$$

$$\int_0^1 dx\, \left(f_d(x) - f_{\bar{d}}\right) = 1\,, \tag{82}$$

$$\int_0^1 dx\, \left(f_s(x) - f_{\bar{s}}\right) = 0 \tag{83}$$

which ensure that the proton has the correct flavor quantum numbers. As we will show below, these sum rules are also satisfied in perturbative QCD, and will be valid for all scales Q^2: this is a direct consequence of the symmetries of the QCD Lagrangian. In the case of the momentum sum rule, Eq. (80), the contribution from the gluon will also be needed.

In the naive parton model, the gluon is absent since, being neutral, it does not couple directly to the virtual photon: in the DIS process, it can thus appear only at the level of $\mathcal{O}\left(\alpha_S\right)$ corrections.

Let's us take a closer look at the expressions for the DIS parton model. The first ingredient is the computation of the lepton-quark scattering, see right plot of Fig. 15. Since this is a Born calculation, no QCD corrections will be needed so far, When computing cross-sections in QCD and in QED, it is important to remember that one needs to average over all initial colors and polarizations and helicities, and sum over all final colors, polarizations and helicities. In this sense, there are a number useful spin sum relations of

Dirac spinors that help us in our task. In particular we have that

$$\sum_s u(p,s)\bar{u}(p,s) = \not{p} + m\,, \tag{84}$$

$$\sum_s v(p,s)\bar{v}(p,s) = \not{p} - m\,, \tag{85}$$

$$\sum_s u(p,s)\bar{v}(p',s) = \sum_s \bar{u}(p,s)\, v(p',s) = 0\,. \tag{86}$$

Note that the outer product of Dirac spinors always yields a matrix. We will also need to use the inner product between Dirac spinors which reads

$$\bar{u}(p,s)u(p,s') = 2\,m\,\delta_{ss'} \tag{87}$$

There are also analogous expressions when summing over helicities that we can use to simplify scattering amplitudes.

Now, the lepton-quark Born matrix element will be given by the following expression

$$\mathcal{M} = \frac{iee_q}{q^2}\,\bar{u}(\hat{p}')\gamma^\mu u(\hat{p})\,\bar{u}(k')\gamma_\mu u(k)\,, \tag{88}$$

which after squaring, summing over helicities and polarizations and using the various properties of the Dirac algebra yields

$$\frac{1}{4}\sum_{\rm pol}|\mathcal{M}|^2 = \frac{e^4e_q^2}{4q^4}\,{\rm tr}\left[\not{p}'\gamma^\mu\not{p}\gamma^\nu\right]\,{\rm tr}\left[\not{k}'\gamma_\mu\not{k}\gamma_\nu\right] \tag{89}$$

which using the expressions for the traces of the Dirac matrices can be simplified to

$$\frac{1}{4}\sum_{\rm pol}|\mathcal{M}|^2 = \frac{8e_q^2e^4}{q^4}\,\left[(k\cdot p)\,(k'\cdot p') + (k'\cdot p)\,(k\cdot p')\right]\,. \tag{90}$$

Note that the squared amplitude falls like $1/q^2$, due to the virtual photon propagator.

It is always useful to express the matrix element in terms of the Mandelstam variables, which are Lorentz invariants, rather than in terms of the four-momenta in some fixed reference frame. The s, t and u Mandelstam variables are defined as

$$\hat{s} \equiv (k+\hat{p})^2\,, \qquad \hat{t} \equiv (k-k')^2\,, \qquad \hat{u} \equiv (\hat{p}-k')^2\,, \tag{91}$$

Note that we use the notation $\hat{p}$ for partonic momenta, and p instead for the hadronic momenta. Note also that with these definitions $\hat{t} = -Q^2$.

In terms of the Mandelstam invariants, the squared amplitude reads

$$\frac{1}{4}\sum_{\rm pol}|\mathcal{M}|^2 = 8e_q^2e^4\,\frac{\hat{s}^2+\hat{u}^2}{\hat{t}^2}\,, \tag{92}$$

and including the appropriate phase space factors, we obtain the the partonic differential cross-section for

lepton-quark scattering is

$$\frac{d\hat{\sigma}}{d\hat{t}} = \frac{1}{16\pi\hat{s}^2}\frac{1}{4}\sum_{\text{pol}}|\mathcal{M}|^2 = m\frac{2\pi\alpha^2 e_q^2}{\hat{t}^2}\left(1+\frac{\hat{u}^2}{\hat{s}^2}\right) = \frac{2\pi\alpha^2 e_q^2}{Q^4}\left(1+(1-y)^2\right) . \tag{93}$$

where in the final equation we have used the expressions of the the DIS variables in terms of the Mandelstam invariants

$$Q^2 = -q^2 = -(k-k')^2 \qquad \hat{y} = y = \frac{q\cdot\hat{p}}{k\cdot\hat{p}} = 1-\frac{\hat{u}}{\hat{s}} \tag{94}$$

Now, the central *assumption* of the quark parton model is

The quark carries a fraction ξ of the total momentum of the proton, that is, $p \equiv \xi\,\hat{p}$.

Now recalling the definition of Bjorken-x, Eq. (77), which is a kinematical invariant, we find

$$\text{Momentum Conservation} \quad \rightarrow \quad \left(\hat{p}'\right)^2 = 0 = (\hat{p}+q)^2 \tag{95}$$

$$Q^2 = 2\hat{p}\cdot q = 2\xi p\cdot q = Q^2\xi/x_{\text{Bj}} \tag{96}$$

and therefore we obtain a very important result:

In the parton model, the Bjorken-x_{Bj} variable, which is determined purely from the lepton kinematics, can be identified with ξ, the momentum fraction that the struck quark carries in the proton.

This property also holds true for other processes: at Born level, we can relate final state kinematics to the momentum fraction carried by the struck partons. However, as we will see, when perturbative QCD corrections are introduced, the picture is different.

Combining all this ingredients, we can finally write the DIS parton-level cross-section

$$\frac{d\hat{\sigma}}{dQ^2dx} = \frac{4\pi\alpha^2}{Q^4}\left(1+(1-y)^2\right)\frac{1}{2}e_q^2\delta(x-\xi)\,, \tag{97}$$

where the $\delta(x-\xi)$ implements the condition that $x=\xi$ at Born level, and allows us to write the cross-section as a function of both x and Q^2. To obtain the corresponding hadron level cross-section, we use the parton model prescription and convolute with the quark PDF, as specified in Eq. (79).

$$\frac{d\sigma}{dQ^2dx} \equiv \int_0^1 dz f_q(z)\frac{d\hat{\sigma}}{dQ^2dx}(x,z) = \frac{4\pi\alpha^2}{Q^4}\left(1+(1-y)^2\right)\frac{1}{2}e_q^2 f_q(x)\,. \tag{98}$$

Again, at this level this is a model assumption, rather than a robust consequence of pQCD.

If we compare with the most general parametrisation of the hadronic DIS cross-section in terms of structure functions, constructed requiring only kinematics and Lorentz invariance, which is

$$\frac{d^2\sigma}{dxdQ^2} = \frac{4\pi\alpha^2}{Q^4}\left[\left(1+(1-y^2)\right)\,F_1(x,Q^2)+\frac{1-y}{x}(F_2(x,Q^2)-2xF_1(x,Q^2))\right] \tag{99}$$

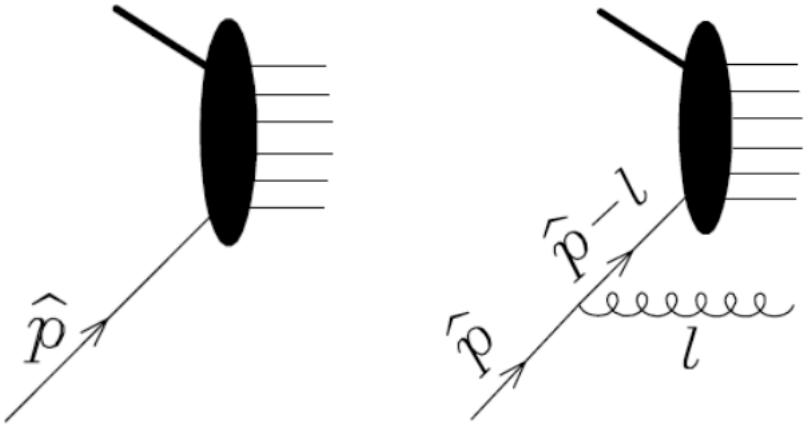

Figure 16: Left plot: the DIS matrix element calculation at Born level. Right plot: same as before but now accounting for the radiation of an additional gluon from the initial state quark.

we find that in the parton model, the structure functions will be given by

$$\begin{aligned} F_1(x,Q^2) &= \frac{1}{2}e_q^2\, f_q(x) \\ F_2(x,Q^2) &= 2x\, F_1(x,Q^2) \end{aligned} \tag{100}$$

Eqns. (100) are the central result of the parton model: it allow to relate observable structure functions with the parton distribution functions of the proton. At the Born level this relation is very simple.

Note that $F_i(x,Q^2)$, which in principle can depend both on x and Q^2, in the parton model depend only on x. This is the scaling property measured by the SLAC experiments, and is a consequence that partons are quasi-free, point-like objects within the proton.

Up to here we have ignored QCD corrections, so that PDFs and structure functions are scale-independent quantities. As we will now how, once QCD corrections are included, we will find collinear divergences, which will not cancel even for inclusive observables, as happened in e^+e^- annihilation. Fortunately, these singularities can be absorbed into the PDFs, inducing a scale dependence but otherwise leaving the DIS cross-sections nicely finite.

QCD radiative corrections in DIS

The calculation in the previous section neglects the effects of QCD radiative corrections. We will now compute, in a simplified way, what are the effects of QCD radiation on the DIS cross-section, finding some remarkable consequences, the most important one the evolution with the scale of the parton distribution functions.

The calculation will be performed as follows. The matrix element at the Born level can be written (see Fig. 16) as follows

$$\mathcal{M}(\hat{p})u(\hat{p})\,, \tag{101}$$

where $\mathcal{M}(\hat{p})$ represents the rest of the hard scattering, which is not relevant here. The Born cross-sections

will now be written as

$$\sigma^{\rm born} = \frac{N}{\hat{p}^0}\frac{1}{2}\sum \mathcal{M}(\hat{p})u(\hat{p})\bar{u}(\hat{p})\mathcal{M}^\dagger(\hat{p}) = \frac{N}{\hat{p}^0}\mathcal{M}(\hat{p})\frac{\not{\hat{p}}}{2}\mathcal{M}^\dagger(\hat{p})\,. \tag{102}$$

using the sum over massless quark helicities

$$\sum_s u(p,s)\bar{u}(p,s) = \not{p}\,. \tag{103}$$

Now, let's consider the effect of the radiation of a gluon off the quark leg, as illustrated in the right plot in Fig. 16. The corresponding matrix element is

$$g_s\,\mathcal{M}(\hat{p}-l)\,\frac{\not{\hat{p}}-\not{l}}{(\hat{p}-l)^2}\,t^a\epsilon_a^\mu(l)\gamma_\mu\,u(\hat{p})\,, \tag{104}$$

where now the momentum that flows into $\mathcal{M}$ is affected by the gluon emission. We know from the case of e^+e^- annihilation that when the gluon is collinear to the quark leg there will be a collinear singularity. Therefore it is useful to choose a parameterization of the four-momentum of the gluon that isolates the relevant regions where the matrix element becomes enhanced

$$l = (1-z)\hat{p} + l_\perp + \xi\eta\,, \tag{105}$$

so $l_\perp$ is the component of the gluon momentum transverse to the quark one. In this parametrisation, we can write the phase space factor for the gluon is

$$\frac{d^3l}{2l^0(2\pi)^3} = \frac{d^2l_\perp}{2\,(2\pi)^3}\frac{dz}{1-z}\,, \tag{106}$$

As before, we work in the soft and collinear limit, where the matrix elements are enhanced, and neglect all terms that are regular in this limit. With some manipulations, we find for the matrix element squared for real emission becomes

$$|\mathcal{M}_1|^2 = g_s^2\frac{2}{|l_\perp^2|}(1+z^2)\mathcal{M}(\hat{p}-l)\frac{\not{\hat{p}}}{2}\mathcal{M}^\dagger(\hat{p}-l)\,, \tag{107}$$

where the factor $|l_\perp^2|$ is a consequence of the gluon collinear divergence. Adding now the flux factor and integrating over all phase space, we end up with the real emission cross-section for the DIS process at the parton level is

$$\hat{\sigma}^{(1)} = \frac{\alpha_S C_F}{2\pi}\int \hat{\sigma}^{(0)}(zp)\frac{1+z^2}{1-z}\,\frac{dl_\perp^2}{l_\perp^2}\,dz\,, \tag{108}$$

where again we emphasize that here we are working in the collinear limit, where the transverse momentum of l is small. A remarkable property of QCD, which holds in many other processes, can be see from Eq. (108), which is the same observation that was made in the case of e^+e^- annihilation:

The real emission corrections, in the soft and collinear limits, factorize into the Born cross-section and a universal term which governs the QCD emission in this limit and that is process independent.

Note that now the argument of the Born cross-section is modified in Eq. (108) by the gluon emission: as

opposed to e^+e^- annihilation, in DIS QCD corrections modify the initial state kinematics. Including now also the NLO virtual corrections, the total cross-section for DIS at $\mathcal{O}(\alpha_S)$ will be given by:

$$\hat{\sigma}^{(1)} = \frac{\alpha_S C_F}{2\pi} \int \left[\sigma^{(0)}(z\hat{p}) - \sigma^{(0)}(\hat{p})\right] \frac{1+z^2}{1-z} \frac{dl_\perp^2}{l_\perp^2} dz \,, \tag{109}$$

From Eq. (109) we can derive two very important consequences:

- In the limit where the radiated gluon is *soft*, $z \to 0$, the real emission term has a soft singularity, which is however canceled by the virtual correction,
- however, the *collinear* singularity of the real emission term is *not* canceled by virtual corrections

This result, that collinear divergences do not cancel for initial state QCD radiation, indicate the failure of the naive parton model.

We now discuss how it is possible to improve the naive parton model and cancel the collinear divergences, obtaining a finite cross-section for DIS at $\mathcal{O}(\alpha_S)$. To do this, we introduce the so called *splitting function*:

$$\hat{\sigma}^{(1)} = \frac{\alpha_S C_F}{2\pi} \int \left[\sigma^{(0)}(z\hat{p}) - \sigma^{(0)}(\hat{p})\right] \frac{1+z^2}{1-z} \frac{dl_\perp^2}{l_\perp^2} dz \equiv \frac{\alpha_S C_F}{2\pi} \int P_{qq}(z)\sigma^{(0)}(z\hat{p}) \frac{dl_\perp^2}{l_\perp^2} dz \tag{110}$$

where, despite its name, the splitting function $P_{qq}(z)$ is a distribution, rather than a function

$$P_{qq}(z) \equiv \left(\frac{1+z^2}{1-z}\right)_+ , \tag{111}$$

with the following definition when acting on test functions:

$$\int_0^1 \left(\frac{1+z^2}{1-z}\right)_+ f(z) \equiv \int_0^1 \left(\frac{1+z^2}{1-z}\right) (f(z) - f(1)) \,. \tag{112}$$

The universal nature of collinear splittings in QCD leads to the appearance of these splitting functions in any process where a collinear splitting occurs. It will also be useful to introduce the following notation for convolutions

$$\left(f_1(x) \otimes f_2(x) \otimes \ldots \otimes f_n(x)\right) \sigma(p) \equiv \int \prod_{i=1}^{n} \left(dx_i \, f(x_i)\right) \sigma\left(x_1 \ldots x_n p\right) \tag{113}$$

where it can be shown that convolutions are commutative and that the identity operator is $\delta(x-1)$.

Let's discuss now what the the physical mechanism for the cancellation of initial-state collinear divergences. In previous lectures we showed that QCD becomes non-perturbative in the infrared, for scales $Q \lesssim \Lambda_{\rm QCD}$. This means that a collinear splitting corresponds to a kinematic region where perturbative QCD, sensu strictu, does not apply. Physically, this means that the initial-state singularity will be regulated by low-energy, non-perturbative effects (such as quark masses for example). To account for this cancellation, we can

Absorb the initial-state collinear divergence into a redefinition of the parton distributions functions, which are themselves determined by non-perturbative physics.

This can be achieved as follows. First of all, we can regulate the collinear singularity with a parameter λ, which in principle is determined by non-perturbative physics, and then write Eq. (110) as

$$\hat{\sigma}^{\rm NLO} = \left(\mathbb{1} + \frac{\alpha_s C_F}{2\pi} \ln \frac{Q^2}{\lambda^2} P_{qq} \right) \sigma^{(0)}(\hat{p}) \,, \tag{114}$$

Now we can introduce a new scale, the *factorization scale*, and expand the NLO cross-section, throwing away NNLO terms, as follows

$$\hat{\sigma}^{\rm NLO} = \left(\mathbb{1} + \frac{\alpha_s C_F}{2\pi} \ln \frac{\mu^2}{\lambda^2} P_{qq} \right) \otimes \left(\mathbb{1} + \frac{\alpha_s C_F}{2\pi} \ln \frac{Q^2}{\mu^2} P_{qq} \right) \sigma^{(0)}(\hat{p}) \,. \tag{115}$$

Next I need to convolute the partonic cross-section $\hat{\sigma}^{\rm NLO}$ with the quark PDFs to obtain the hadronic cross-section

$$\sigma^{\rm DIS}(p) = f_q \, \hat{\sigma}^{\rm NLO}(\hat{p}) \tag{116}$$

and now I can *redefine* the parton distributions, after absorbing the collinear divergence, as follows

$$\sigma^{\rm DIS}(p) = f_q \, \hat{\sigma}^{\rm NLO}(\hat{p}) \equiv \tilde{f}_q(\mu) \tilde{\sigma}(p,\mu) \,, \tag{117}$$

where we have defined the (now scale-dependent) PDF as

$$\tilde{f}(\mu) \equiv f \otimes \left(\mathbb{1} + \frac{\alpha_s C_F}{2\pi} \ln \frac{\mu^2}{\lambda^2} P_{qq} \right) \,, \tag{118}$$

and the partonic cross-section has been corrected as follows:

$$\tilde{\sigma}(p,\mu) \equiv \left(\mathbb{1} + \frac{\alpha_s C_F}{2\pi} \ln \frac{Q^2}{\mu^2} P_{qq} \right) \hat{\sigma}^{(0)}(\hat{p}) \,. \tag{119}$$

So that now we have achieved that:

The partonic DIS cross-section Eq. (119) is now finite, since it does not depend on the IR cutoff λ anymore. The price to pay is the introduction of a new, non-physical scale, the *factorization scale*.

There are some other important consequences of this derivation:

- The PDFs become now scale-dependent, due to μ, the factorization scale
- The partonic cross-section now also depends on this factorization scale
- PDFs are still determined by non-perturbative physics (and need to be fitted from data, hence the dependence in λ has no physical consequences), but as we wills how now, the dependence of $q(x,\mu)$ with μ is determined by perturbative QCD

It is important not to mix the *renormalization scale*, which arises from the subtraction of ultraviolet divergences, and the *factorization scale*, from the regulation of collinear singularities in processes with initial state hadrons. The two scales are unphysical and led to an inherent *theoretical uncertainty* in any pQCD calculation.

The redefinition of the PDFs in Eq. (118) is universal, process-independent, and holds to all orders in perturbation theory.

PDF evolution equations

The original PDFs, as introduced in the parton model, are non-perturbative objects. In perturbative QCD, Eq. (118), the dependence on the momentum fraction x is still determined by non-perturbative dynamics, but the dependence on the factorization scale μ is purely perturbative.

Let us thus now study the scale dependence of the newly defined PDFs. If now we differentiate the DIS cross-section Eq. (117) with respect to the factorization scale μ, we find, using the fact that before the redefinitions the cross-section was independent of μ,

$$\mu^2 \frac{\partial}{\partial \mu^2} \sigma^{\rm DIS}(p) = 0 = \left[\mu^2 \frac{\partial}{\partial \mu^2} \tilde{f}_q(\mu) \right] \tilde{\sigma}(p,\mu) + \tilde{f}_q(\mu) \left[\mu^2 \frac{\partial}{\partial \mu^2} \tilde{\sigma}(p,\mu) \right] , \tag{120}$$

and using the fact that the PDFs are universal, so the above equation holds for any partonic process, we find the following equation, using the definitions Eq. (118) and Eq. (119),

$$\mu^2 \frac{\partial}{\partial \mu^2} \tilde{f}_q(\mu) = \frac{\alpha_s C_F}{2\pi} \tilde{f}_q(\mu) \otimes P_{qq} \, , \tag{121}$$

where we have used that

$$\mu^2 \frac{\partial}{\partial \mu^2} \tilde{\sigma}(p,\mu) = -\frac{\alpha_s C_F}{2\pi} P_{qq} \tilde{\sigma}^{(0)}(p) \simeq -\frac{\alpha_s C_F}{2\pi} P_{qq} \tilde{\sigma}(p,\mu) + \mathcal{O}\left(\alpha_S^2\right) . \tag{122}$$

Eq. (121) is known as the DGLAP evolution equations for the PDFs.[3] These equations are an essential ingredient for LHC phenomenology: once PDFs are extracted from data at some scale, say 1 GeV, the evolution equations like Eq. 121 can be used to determine PDFs say at 5 TeV. Using the complete set of DGLAP equations and splitting functions (see for example Ellis-Stirling-Webber [5]) one can check that the valence and momentum sum rules are also satisfied in perturbative QCD, to all orders in perturbation theory. In Fig. 17 we show the NNPDF2.3NNLO set of parton distribution functions, at low scales $\mu^2 = 10$ GeV^2, and at a typical LHC scale $\mu^2 = 10^4$ GeV^2. This PDF evolution is completely determined by the perturbative DGLAP evolution equations.

A nice and illustrative exercise is to show that the integral of the difference between the PDFs of the up and anti-up quark (valence sum rule) is scale independent. To do this, start from the DGLAP non-singlet evolution equation:

$$\mu^2 \frac{\partial f_q(x,\mu^2)}{\partial \mu^2} = \frac{\alpha_s(\mu^2)}{2\pi} \int_x^1 \frac{dz}{z} P_{qq}(z) f_q\left(\frac{x}{z},\mu^2\right) , \tag{123}$$

and differentiate the sum rule with respect to the factorization scale μ,

$$\mu^2 \frac{\partial}{\partial \, \mu^2} \int_0^1 dx \left(f_u(x,\mu^2) - f_{\bar{u}}(x,\mu^2) \right) = \frac{\alpha_s(\mu^2)}{2\pi} \int_0^1 dx \int_x^1 \frac{dz}{z} P_{qq}(z) \left[f_u\left(\frac{x}{z},\mu^2\right) - f_{\bar{u}}\left(\frac{x}{z},\mu^2\right) \right] \tag{124}$$

[3] Actually, this is only part of the complete system of equations, in particular we are not considering the effects of gluons here. This is called as a *non-singlet* evolution equation.

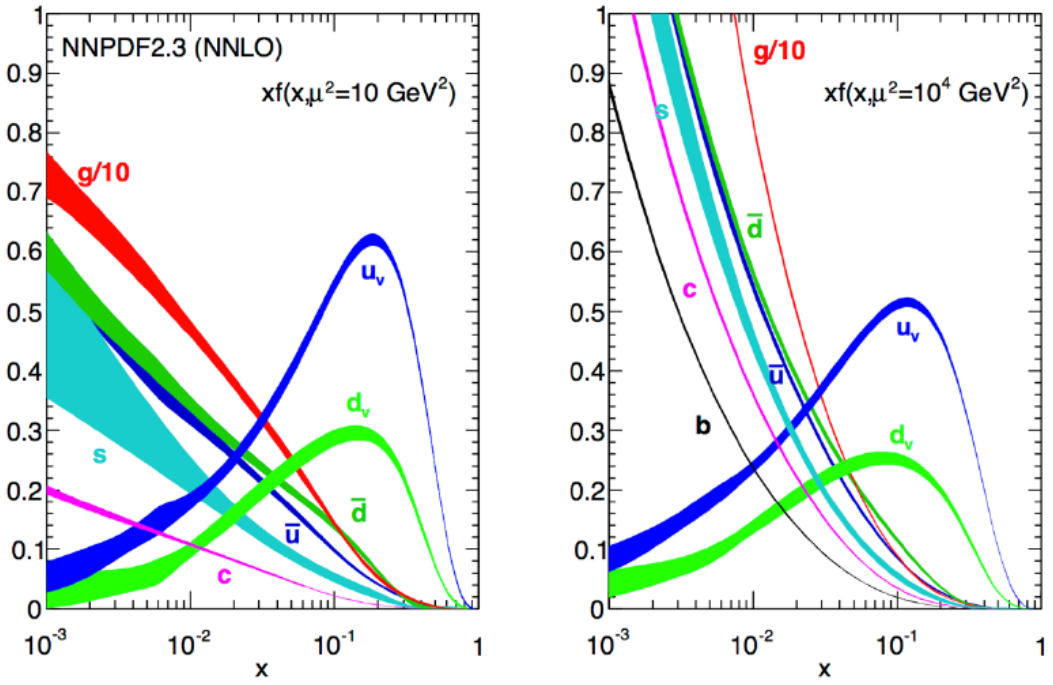

Figure 17: The NNPDF2.3NNLO set of parton distribution functions, at low scales $\mu^2 = 10$ GeV^2 (left plot) and at a typical LHC scale $\mu^2 = 10^4$ GeV^2 (right plot). The PDF evolution is completely determined by the perturbative DGLAP evolution equations. Note that the gluon PDF has been divided by 10 to be able to plot it using the same scale.

$$= \frac{\alpha_s(\mu^2)}{2\pi} \int_0^1 dz \int_0^1 dy\, P_{qq}(z) \left[f_u\left(y,\mu^2\right) - f_{\bar{u}}\left(y,\mu^2\right) \right] = 0 \tag{125}$$

where we have made the following change of variable

$$\int_0^1 dx \int_x^1 dz = \int_0^1 dz \int_0^z dx \qquad y \equiv \frac{x}{z} \tag{126}$$

and the following property of the splitting functions:

$$\int_0^1 dz P_{qq}(z) = 0 \tag{127}$$

Therefore, we conclude that the up quark valence sum Eq. (124) must be the same at all scales, and is thus a constant (in this case the integral should give a value 2, which is the up quark valence quantum number of the proton). Similar properties of the splitting functions ensure that the momentum and valence sum rules hold at any order in the pQCD expansion. Actually, the splitting function for quarks needs to be completed by its endpoint value, which gives

$$P_{qq}^{(}0)(x) = C_F \left[\frac{1+x^2}{(1-x)_+} + \frac{3}{2}\delta(1-x) \right] , \tag{128}$$

This is the final result at Born level.

QCD in hadronic collisions

In the two previous lectures we have discussed the consequences of perturbative QCD corrections for two different processes:

- electron-positron annihilation (no hadrons in the initial state): soft and collinear singularities cancel in inclusive enough observables (like a IRC-safe jet cross-section), and
- lepton-proton deep-inelastic scattering (one hadron in the initial state): initial-state collinear singularities do not cancel even for inclusive observables, but they can be absorbed into a redefinition of the PDFs, inducing a scale dependence determined by the DGLAP evolution equations.

Now we consider a more complicated process: hadron-hadron collisions, with two protons in the initial state. First of all we discuss which kinematic variables are more sensible to hadron-hadron collisions. A key difference as compared to e^+e^- annihilation is that

in hadronic collisions, the total longitudinal momentum of the partonic collision is unknown (determined by the PDFs) and is different for each event.

This implies that in general, the hadronic center of mass frame will be different to the partonic center of mass frame, and these two frames will only coincide when the colliding partons carry the same momentum fraction, $x_1 = x_2$. Therefore, in hadronic collisions, the most suitable event description is provided by quantities that are either invariant or that transform in a simple way under longitudinal boosts (to decrease sensitivity to this unknown initial state longitudinal momentum).

A suitable parameterization for four-momenta in hadronic collisions is can be constructed as follows. We begin by

$$p = (E, p_x, p_y, p_z) = \left(\sqrt{\vec{p}^2 + m^2}, |\vec{p}| \sin\theta \, \cos\phi, |\vec{p}| \sin\theta \, \sin\phi, |\vec{p}| \cos\theta\right) \tag{129}$$

where θ is the polar angle with respect to the hadron beam and ϕ is the azimuthal angle with respect also to the hadron beam axis, as shown in Fig. 18. It is customary to express the four-momentum p in terms of the rapidity y and the transverse mass m_T, defined as,

$$y \equiv \frac{1}{2} \ln \frac{E + p_z}{E - p_z} \,, \qquad m_T \equiv \sqrt{p_T^2 + m^2} \,, \tag{130}$$

so that the parametrisation Eq. (129) can be written as follows

$$p = (E, p_x, p_y, p_z) = (m_T \cosh \, y, |p_T| \cos\phi, |p_T| \sin\phi, m_T \sinh \, y) \,, \tag{131}$$

In Eq. (131), the transverse mass and the p_T are obviously invariant under longitudinal boosts, while the rapidity transforms additively, facilitating going from the partonic center-of-mass the hadronic center-of-mass. To derive Eq. (131) from Eq. (129), note that

$$\cosh y = 0.5 \left(\left(\frac{E + p_z}{E - p_z} \right)^{1/2} + \left(\frac{E - p_z}{E + p_z} \right)^{1/2} \right) = \frac{E}{\sqrt{m^2 + p_T^2}} = \frac{E}{m_T} \,, \tag{132}$$

and likewise for the other component of the four-momentum.

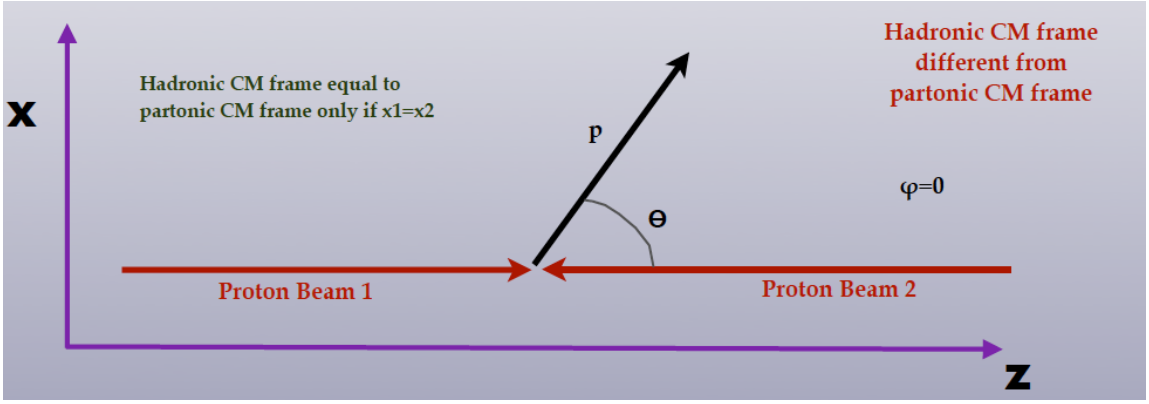

Figure 18: Kinematics of an hadron-hadron collision for an azimuthal angle of $\phi = 0$. In general, the hadronic center of mass frame will be different to the partonic center of mass frame.

It is easy to show that the rapidity y transforms additively under longitudinal boosts. To prove this, recall that under a longitudinal boost (that is, a boost in the z direction, the beam direction), a four-momentum transforms as

$$p \quad \rightarrow \quad p' = \gamma \left(E - \beta \, p_z, \, p_x \, , p_y \, , -\beta \, E + p_z \right) \, , \tag{133}$$

in terms of the usual Lorentz boost parameters

$$\beta \, = \, v \, , \qquad \gamma \, = \, \frac{1}{\sqrt{1-v^2}} \, , \tag{134}$$

so one can check that the rapidity transforms as

$$y \quad \rightarrow \quad y' \, = \, y + \frac{1}{2} \log \frac{1-\beta}{1+\beta} \, , \tag{135}$$

which has the important consequence that the difference between rapidities is boost invariant:

$$\Delta \, y' \equiv y'_1 - y'_2 \, = \, \Delta \, y \equiv y_1 - y_2 \, , \tag{136}$$

and thus should be less sensitive to the details of the PDFs than other kinematic variables. This explains the use of transverse variables and of the rapidity y to describe the kinematics of hadronic collisions. Given that that partonic center of mass frame is uniquely defined while the hadronic center of mass frame depend on the PDFs, this has the consequence that

perturbative calculations in hadron collisions are typically performed in the partonic center of mass frame, and then boosted to the laboratory frame.

In the limit of massless particles (defined as the limit in which $m \ll p_T$), the rapidity becomes the so-called *pseudo-rapidity*,

$$y \simeq \eta \equiv - \log \tan \frac{\theta}{2} \, , \tag{137}$$

which is often used in experimental analyses since it can be directly related to the geometrical acceptance of the detector. To check this property, note that when $m \ll p_T$, then $m_T \simeq p_T$, and therefore the four

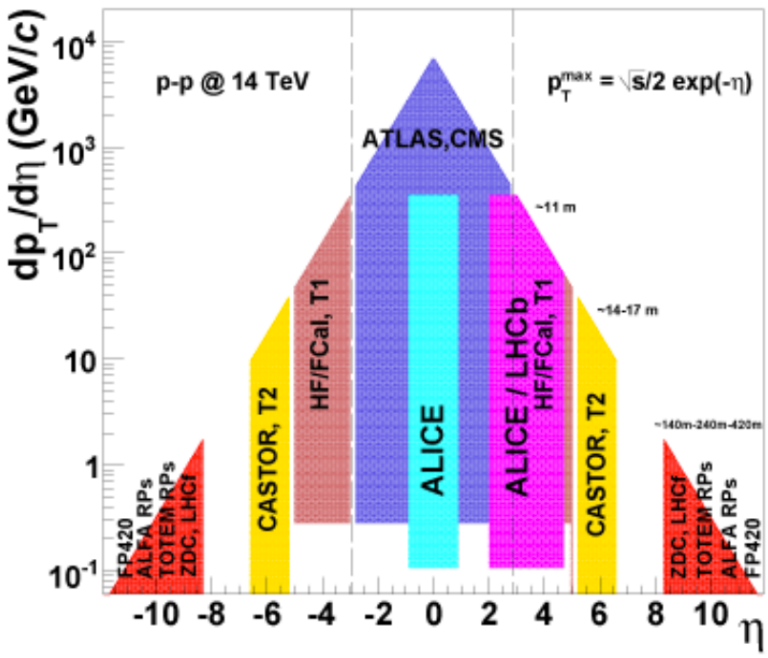

Figure 19: Approximate coverage in transverse momentum p_T and pseudo-rapidity η of current and future LHC detectors. For a given $\sqrt{s}$ and pseudo-rapidity η, the kinematically maximum available p_T is $p_T^{\rm max} \simeq \sqrt{s}e^{-y}/2$, as will be shown below.

momentum of a massless particle becomes

$$p \simeq p_T \left(\cosh y, \cos\phi, \sin\phi, \sinh y\right) \, , \tag{138}$$

and therefore we can write the rapidity as

$$y \simeq \frac{1}{2} \ln \frac{1+\cos\theta}{1-\cos\theta} = -\ln\tan\frac{\theta}{2} = \eta \tag{139}$$

where we have used $p_z \simeq E\cos\theta$ for massless particles.

Achieving the maximum possible coverage in pseudo-rapidity is a very important feature of a detector for hadron colliders, since this way one can access processes in the forward region. In Fig. 19 we show the approximate coverage in transverse momentum p_T and pseudo-rapidity η of current (and proposed) LHC detectors. The two main purpose detectors, ATLAS and CMS, can cover up to $\eta \sim 2.5$, extended to $\eta \sim 4$ with the forward calorimeters, while LHCb is a forward experiment with acceptance $2.0 \leq \eta \leq 4.5$. Other, smaller experiments like TOTEM increase the coverage of the forward region, and are important for a variety of analysis like the total pp cross-section or the validation of predictions for high-energy cosmic ray production.

Q: Explain why do you think that at the LHC the forward region is relevant for measurements of properties of high-energy cosmic rays.

As we will show below, the maximum partonic center of mass energy is achieved for central collisions $y = 0$, therefore the central region is crucial for searches of new BSM massive particles, while the forward

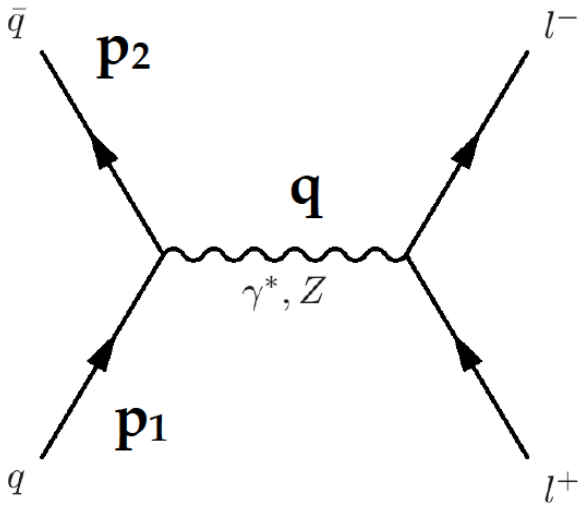

Figure 20: Feynman diagram for the hadroproduction of a neutral gauge boson, followed by the decay into two leptons, in the Born approximation. The four-momenta of the incoming quarks are labeled as p_1 and p_2.

region is very important to keep full kinematical coverage for lighted states, in particular the Higgs boson.

Another useful relation is provided by the phase space in these new coordinates, which reads

$$\frac{d^3p}{2E(2\pi)^2} = \frac{1}{2(2\pi)^3}\, d^2p_T\, dy\,, \tag{140}$$

as can be checked from the Jacobian of the change of variables

$$dp_x\, dp_y\, dp_z = \left|\left(\frac{\partial(p_x,p_y,p_z)}{\partial(p_T,y,\phi)}\right)\right| dp_T\, dy\, d\phi \tag{141}$$

$$d^3p = \left|\begin{pmatrix} p_T\cosh y & 0 & \sinh y \\ 0 & -p_T\sin\phi & \cos\phi \\ 0 & p_T\cos\phi & \sin\phi \end{pmatrix}\right| dp_T\, dy\, d\phi \tag{142}$$

which is the expression that is used in calculations of hadronic processes. This is another useful property of the parametrization Eq. (131) in terms of p_T and y:

In terms of p_T and y, the phase space factor is constant in both variables, no region is weighted more than any other.

In the following, we explore two of the most representative processes that can take place in hadron-hadron collisions: the Drell-Yan process, and inclusive jet production.

Drell-Yan production in hadronic collisions

Let us consider now the hadroproduction of massive vector bosons. Here we will work at the Born level only.[4] The corresponding Feynman diagram can be seem in Fig. 20. Using the Feynman rules for the production

[4]Including radiative corrections should be easy following the techniques of the previous lectures.

of a massive vector boson (assuming for simplicity a generic value of the electroweak coupling g), we obtain

$$\mathcal{M} = g\,\hat{v}(p_2)\,\gamma^\mu\,u(p_1)\,, \tag{143}$$

and the partonic cross-section reads, including the phase space factor,

$$\hat{\sigma} = \frac{1}{2\hat{s}}\frac{1}{4}\frac{1}{9}\int d\phi_1 \sum_{\text{spin,col}} |\mathcal{M}|^2 \tag{144}$$

where we have added the flux factor $1/2\hat{s}$, the average over initial state polarizations $1/4$ and the average over initial state colors $1/N_c^2$. Using the properties of the Dirac algebra, we find that the spin averaged matrix element squared is

$$\sum_{\text{spin,col}} |\mathcal{M}|^2 \,=\, 3g^2 \text{Tr}\left[\not{p}_1\,\gamma^\mu\,(-\not{p}_2)\,\gamma_\mu\right] = 12\,g^2\,\hat{s}\,, \tag{145}$$

where we have used that

$$\text{Tr}\left[\not{p}_1\,\gamma^\mu\,(-\not{p}_2)\,\gamma_\mu\right] = 8p_1\cdot p_2 \simeq 4\,(p_1+p_2)^2 = 4\hat{s}\,, \tag{146}$$

neglecting the masses of the incoming quarks. Doing the calculation, we find that that total partonic cross-section is

$$\hat{\sigma} = \frac{4\pi^2}{3}\frac{g^2}{4\pi}\,\delta(\hat{s}-M_V^2) \tag{147}$$

where we have used that the one-particle Lorentz-Invariant Phase Space factor reduces to the energy conservation delta function:

$$d\phi_1 \,=\, \int \frac{d^3q}{2q^0(2\pi)^3}(2\pi)^4\delta^{(4)}(p_1+p_2-q) \,=\, 2\pi\,\delta((p_1+p_2)^2-M_V^2)\,, \tag{148}$$

as expected in the case of a $2\to 1$ process (the phase space is trivial).

For the case of W^+ production, in the parton model, and keeping only the contribution from the first two generations of quarks and anti-quarks for simplicity, assuming a diagonal CKM mixing matrix, we get that the hadronic cross-section is given by the usual convolution over the PDFs:

$$\sigma_{W^+} \,=\, \int dx_1\,dx_2\,\left[\,f_u(x_1)f_{\bar{d}}(x_2)\,+\,f_{\bar{d}}(x_1)f_u(x_2)\right]\,\times\,\frac{\pi^2}{3}\frac{\alpha_{\text{QED}}}{\sin^2\theta_W}\,\delta(sx_1x_2-M_W^2) \tag{149}$$

so in this case the partonic matrix element is trivial and the production cross-section is determined directly by a certain convolution of PDFs, with a suitable flavor combination. Note that we select the scattering $u\bar{d}$ and $\bar{d}u$, where the first quark corresponds to the first proton and son on.

Let us take a closer look at the kinematics of this process. The kinematics of vector-boson production in hadronic collisions can be written as follows:

$$p_1 \;=\; (x_1E_{\text{beam}}/2, 0, 0, x_1E_{\text{beam}}/2) \tag{150}$$

$$p_2 \;=\; (x_2E_{\text{beam}}/2, 0, 0, -x_2E_{\text{beam}}/2) \tag{151}$$

$$q \;=\; ((x_1+x_2)E_{\text{beam}}/2, 0, 0, (x_1-x_2)E_{\text{beam}}/2) \tag{152}$$

with q the four-momentum of the gauge boson. In this process, the kinematics are fixed once the gauge boson rapidity is specified. Indeed, it is easy to check, using the definition of y, that

$$y = \frac{1}{2}\log\frac{q_0+q_z}{q_0-q_z} = \frac{1}{2}\log\frac{x_1}{x_2}\,, \tag{153}$$

$$x_1\,x_2\,s = M_W^2\,, \tag{154}$$

with no other variables, since this is a $2\to 1$ process. Therefore the values of the PDF Bjorken-x probed in this process are fixed once the vector-boson rapidity is specified.

$$x_1 = \frac{M_W}{\sqrt{s}}e^{y}\,, \qquad x_2 = \frac{M_W}{\sqrt{s}}e^{-y}\,, \tag{155}$$

so one parton will carry a larger momentum fraction than the other.

Using Eq. (155) it is possible to determine the coverage in (x_1, x_2) that a given collider has access to. For instance, at the LHC 14 TeV, for ATLAS and CMS, that have $y \leq 2.5$, we find that $x_1(x_2) = 0.07(0.0005)$, while for the LHCb detector, whose acceptance goes up to $y \leq 4.5$, we find instead $x_1(x_2) = 0.5(6\,10^{-5})$. Therefore, the measurements at forward rapidity cover a wider range of Bjorken-x, which is very useful for PDF studies.

Note also that at the Born level the W bosons are produced with vanishing transverse momentum, so it would be impossible to detect them (they would disappear through the beam pipe). The p_T of W bosons is generated by QCD radiative corrections (emission of a hard gluon) as well as by soft QCD dynamics (multiple emissions of soft and collinear gluons) for the small p_T tail.

The p_T spectrum of electroweak bosons is a central observable at hadron colliders from many points of view, like the *tuning* of MC event generators.

Doing the delta function integral in Eq. (149), we end up with the following result for the total cross-section

$$\begin{aligned}\sigma_{W^+} &= \int dx_1\,dx_2\,\left[f_u(x_1)f_{\bar{d}}(x_2) + f_{\bar{d}}(x_1)f_u(x_2)\right]\times\frac{\pi^2}{3}\frac{\alpha_{\rm QED}}{\sin^2\theta_W}\,\delta(sx_1x_2-M_W^2)\\ &= \frac{\pi^2}{3}\frac{\alpha_{\rm QED}}{\sin^2\theta_W}\frac{1}{s}\int_0^1\frac{dx_1}{x_1}\left[f_u(x_1)f_{\bar{d}}\left(\frac{M_W^2}{x_1 s}\right) + f_{\bar{d}}(x_1)f_u\left(\frac{M_W^2}{x_1 s}\right)\right]\,,\end{aligned} \tag{156}$$

and differentiating over the rapidity of the W boson, using $dx_1 = x_1\,dy$, as can be seen from Eq. (155), we obtain our first differential cross-section for an hadron collider process:

$$\frac{d\,\sigma_{W^+}}{d\,y_{W^+}} = \frac{\pi^2}{3}\frac{\alpha_{\rm QED}}{\sin^2\theta_W\,s}\left[f_u(x_1)f_{\bar{d}}\,(x_2) + f_{\bar{d}}(x_1)f_u\,(x_2)\right] \tag{157}$$

Interestingly, this differential cross-section is determined entirely for the shape of the PDFs at the values of $x_{1,2}$ fixed by the kinematics, Eq. (155).

The above derivation is an oversimplification of the whole picture, to begin with because the have considered only $u\bar{d}$ scattering. In Fig. 21 we show the contribution of different partonic initial states to the

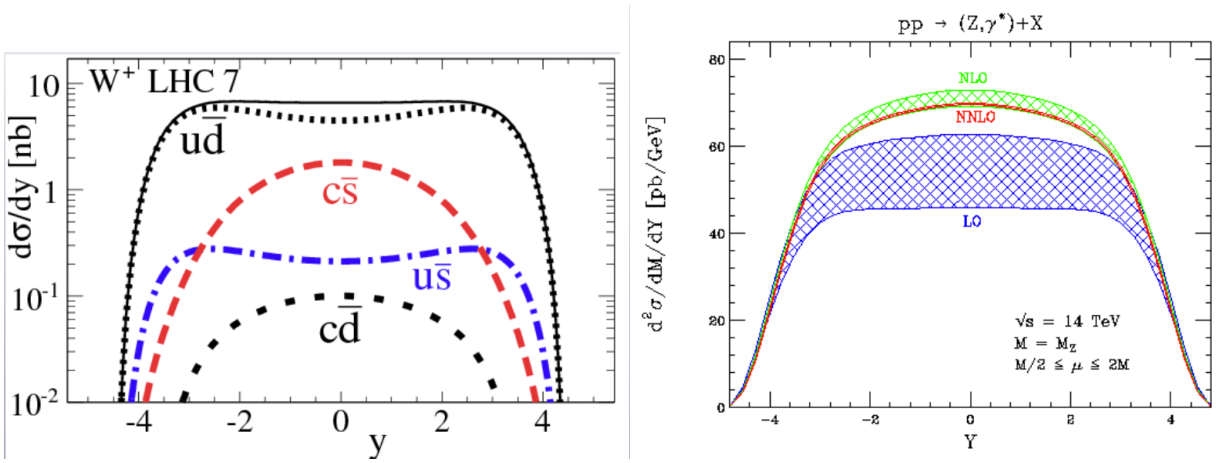

Figure 21: Left plot: the contribution of different partonic initial states to the rapidity distribution of W^+ bosons at the LHC 7 TeV. Right plot: the calculation of the rapidity distribution of Z bosons at the LHC 14 TeV, computed at LO, NLO and NNLO accuracy. The bands represent the theoretical uncertainty in the calculation arising from higher orders.

rapidity distribution of W^+ bosons at the LHC 7 TeV. Is clear that the effects of the second generation are important and cannot be neglected.

The accuracy in the theoretical prediction of the W boson kinematic distribution is important to extract fundamental parameters of the SM, like the W mass, that might provide indirect constraints on New Physics beyond the SM. A permille precision in a number of distributions is required to be able to perform a competitive measurement. See Fig. 22 for the results of the impact of the direct W mass measurement in the global electroweak fit.

Q: Why a precision measurement of the W mass can constrain new physics? More in general, what can we learn from radiative corrections? In the past, which information on new physics has been uncovered by this type of precision measurements?

Another implication is that Eq. (157) includes only the Born term. Using similar techniques as in the vase of e^+e^- and DIS it can be shown that soft and collinear final state divergences are canceled between real and virtual diagrams in inclusive enough distributions, and that the initial state collinear singularity subtraction can be performed exactly in the same was as in the vase of DIS. In the right plot of Fig. 21 we also show the calculation of the rapidity distribution of Z bosons at the LHC 14 TeV, computed at LO, NLO and NNLO accuracy. The bands represent the theoretical uncertainty in the calculation arising from higher orders, estimated by varying the renormalization and factorization scales with respect to the central scale.

In hadron collider calculations, scale variations of the type $0.5 \leq \mu/mu_F \leq 2$ and $0.5 \leq \mu/mu_R \leq 2$ are used to estimate higher-order uncertainties. The basic idea is that since in the full calculation (resuming all orders), there is no dependence on this scales, we can estimate missing higher orders with a suitable scale variation. This procedure is know to work reasonable well for a number of cases, but there are also important exceptions.

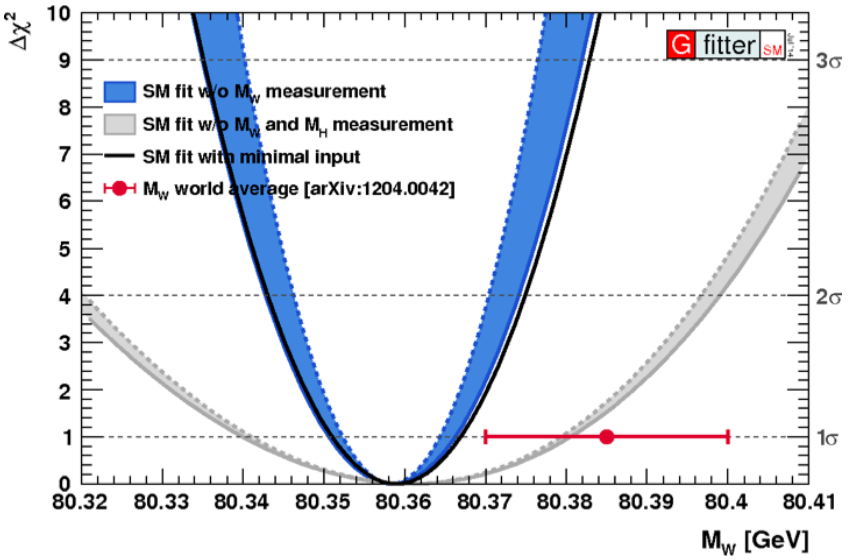

Figure 22: The impact of the direct W mass measurement in the global electroweak fit.

Jet production

Another central process of hadron collider phenomenology is the production of jets. This is the simplest hadroproduction $2 \to 2$ process, with two colored parton in the initial state and two in the final state. To construct the jet cross-section at the Born level, we need to convolute all possible partonic cross-sections for the scattering of quarks and gluons with the corresponding parton distributions. The fully differential jet cross-section will be given by

$$d\sigma^{\rm jet} = \sum_{ijkl} dx_1\, dx_2\, f_i(x_1)\, f_j(x_2)\, \frac{d\hat{\sigma}_{ij\to kl}}{d\Phi_2}\, d\Phi_2\,, \tag{158}$$

where the partonic cross-section $d\hat{\sigma}_{ij\to kl}/d\Phi_2$ can be computed using the QCD Feynmann rules. In Fig. 23 we show some representative diagrams for the quark and gluon scattering processes that contribute to the jet cross-section. Note the presence of genuine QCD vertices like three and four gluon vertices. In Fig. 23 we also show the results for the calculation of all the various partonic cross-sections for different initial and final state combinations. The results are expressed in terms of $\hat{s}$, $\hat{t}$ and $\hat{u}$, the Mandelstam variables of the partonic scattering.

Though here we will work in the Born approximation, final and initial state soft singularities can be dealt as usual in pQCD, either absorbing them in PDF redefinitions or with a suitable jet algorithm.

Let us take a closer look at the kinematics of jet production. For a $2 \to 2$ scattering of massless particles the kinematics are fully specified by the p_T of the back-to-back particles and by their rapidities y_1 and y_2. So we can write the four-momentum of the two final-state quarks or gluons as

$$\begin{aligned} p_1 &= (p_T \cosh\, y_1, p_T \cos\phi, p_T \sin\phi, p_T \sinh\, y_1) \\ p_2 &= (p_T \cosh\, y_2, -p_T \cos\phi, -p_T \sin\phi, p_T \sinh\, y_2) \end{aligned} \tag{159}$$

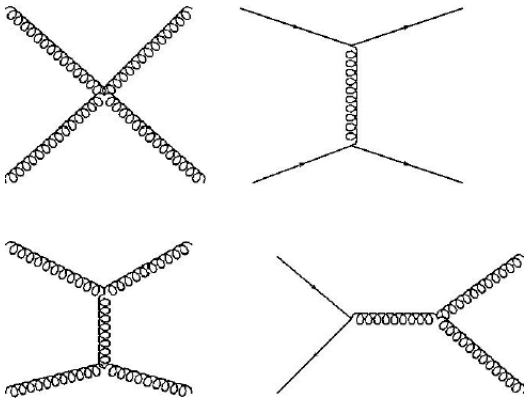

Process	$\frac{d\hat{\sigma}}{d\hat{\Phi}_2}$
$qq' \to qq'$	$\frac{1}{2\hat{s}}\frac{4}{9}\frac{\hat{s}^2+\hat{u}^2}{\hat{t}^2}$
$qq \to qq$	$\frac{1}{2}\frac{1}{2\hat{s}}\left[\frac{4}{9}\left(\frac{\hat{s}^2+\hat{u}^2}{\hat{t}^2}+\frac{\hat{s}^2+\hat{t}^2}{\hat{u}^2}\right)-\frac{8}{27}\frac{\hat{s}^2}{\hat{u}\hat{t}}\right]$
$q\bar{q} \to q'\bar{q}'$	$\frac{1}{2\hat{s}}\frac{4}{9}\frac{\hat{t}^2+\hat{u}^2}{\hat{s}^2}$
$q\bar{q} \to q\bar{q}$	$\frac{1}{2\hat{s}}\left[\frac{4}{9}\left(\frac{\hat{s}^2+\hat{u}^2}{\hat{t}^2}+\frac{\hat{t}^2+\hat{u}^2}{\hat{s}^2}\right)-\frac{8}{27}\frac{\hat{u}^2}{\hat{s}\hat{t}}\right]$
$q\bar{q} \to gg$	$\frac{1}{2}\frac{1}{2\hat{s}}\left[\frac{32}{27}\frac{\hat{t}^2+\hat{u}^2}{\hat{t}\hat{u}}-\frac{8}{3}\frac{\hat{t}^2+\hat{u}^2}{\hat{s}^2}\right]$
$gg \to q\bar{q}$	$\frac{1}{2\hat{s}}\left[\frac{1}{6}\frac{\hat{t}^2+\hat{u}^2}{\hat{t}\hat{u}}-\frac{3}{8}\frac{\hat{t}^2+\hat{u}^2}{\hat{s}^2}\right]$
$gq \to gq$	$\frac{1}{2\hat{s}}\left[-\frac{4}{9}\frac{\hat{s}^2+\hat{u}^2}{\hat{s}\hat{u}}+\frac{\hat{u}^2+\hat{s}^2}{\hat{t}^2}\right]$
$gg \to gg$	$\frac{1}{2}\frac{1}{2\hat{s}}\frac{9}{2}\left(3-\frac{\hat{t}\hat{u}}{\hat{s}^2}-\frac{\hat{s}\hat{u}}{\hat{t}^2}-\frac{\hat{s}\hat{t}}{\hat{u}^2}\right)$

Figure 23: Left plot: a representative subset of the Feynman diagrams that contribute to the hadroproduction jet cross-section at the Born level. Right plot: the result for the partonic cross-sections for different scattering channels.

where the rapidities $y_{1,2}$ are measured in the detector (laboratory) reference frame. From momentum conservation, we see that the values of the Bjorken-x that jet production is probing is given by

$$x_1 = \frac{p_T}{\sqrt{s}}\left(e^{y_1}+e^{y_2}\right), \qquad x_2 = \frac{p_T}{\sqrt{s}}\left(e^{-y_1}+e^{-y_2}\right). \tag{160}$$

Therefore, to reconstruct the kinematics of the underlying partonic collision one needs to measure the kinematics of the two jets.

Q: How is the *inclusive jet cross-section* defined? Can we determine the underlying partonic kinematics? Count variables and constraints.

It is possible to show, using the above kinematics, that for a given $\sqrt{s}$ and pseudo-rapidity η, the kinematically maximum available p_T is

$$p_T^{\rm max} \simeq \sqrt{s}e^{-y}/2\,. \tag{161}$$

Assume that parton masses can be neglected here, so we have that $y = \eta$. The $\eta = 0$ case is trivial: all the energy of the proton-proton collision goes into the p_T of the final state particles. For $\eta \neq 0$, one sees from Eq. (160) that the highest p_T will be produced when $\eta_1 = -\eta_2$, which corresponds to $x_1 = x_2$, and leads to Eq. (160).

The calculation of the matrix elements is simplified in the partonic center of mass frame, defined by the following condition for a $2 \to 2$ scattering:

$$y_1^* = -y_2^* \quad \to \quad y_1^* = \frac{1}{2}\left(y_1 - y_2\right) = -y_2^* \tag{162}$$

and we can show that the scattering angle with respect to the beam axis θ^* is determined by the difference of rapidities of the two jets

$$\cos\theta^* = \tanh y_1^* = \tanh\left(\frac{y_1-y_2}{2}\right). \tag{163}$$

Q: what is the boost required in this transformation? From

$$y \quad \to \quad y' = y + \frac{1}{2}\log\frac{1-\beta}{1+\beta}, \tag{164}$$

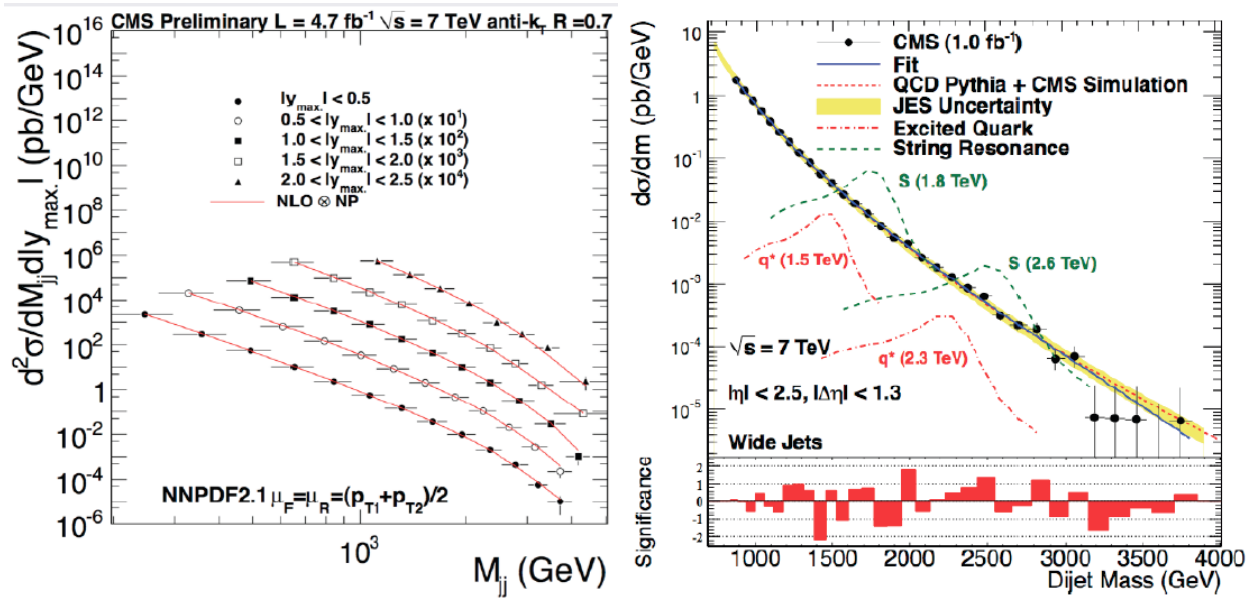

Figure 24: Left plot: the CMS measurement of the dijet cross-section at 7 TeV, compared with NLO QCD predictions with the NNPDF2.1 set. Right plot: the same observable, now used to search for New Physics that would appear as bumps in the otherwise smooth distribution due to new exotic particles being produced.

we see that

$$\frac{1}{2}\log\frac{1-\beta}{1+\beta} = -\frac{1}{2}(y_1+y_2)\,, \tag{165}$$

so the boost is determined by the PDFs in this particular event.

Another important kinematic variable is the invariant mass of the dijet system

$$M_{12}^2 = (p_1+p_2)^2 = 4\,p_T^2\,\cosh^2\,y^*\,, \quad M_{12} = 2\,p_T\,\cosh\,y^*\,. \tag{166}$$

which grows with the p_T of the jets and with their separation in rapidity (which is the same in the center-of-mass and laboratory reference frames). The fact that in dijet production we have a number of possible scales poses an important problem in our perturbative QCD calculations:

What should be the optimal scale in dijet production? We should use $\mu_F = \mu_R = M_{12}$, or perhaps $\mu_F = \mu_R = p_T$? There is no unambiguous answer for this in pQCD.

At hadron colliders, inclusive and dijet production are crucial properties to look for New Physics, as well as for the determination of fundamental strong coupling parameters such as $\alpha_S(M_Z)$ and the gluon PDF. In the case of QCD measurements, such as the M_{jj} invariant mass spectrum of dijets measured from CMS at 7 TeV, shown in Fig. 24, the comparison of the data with different PDFs provides direct information on the behavior of the gluon at large-x. The very same process can also be used for searches for BSM physics, for example, in Fig. 24 we show the dijet mass spectrum compared with the predictions for exotic scenarios like excited quarks or string resonances, that would show up as bumps in the otherwise smoothly falling distribution with M_{jj}. The absence of any noticeable bump allows them to place stringent limits in these scenarios for New Physics.

In the early 20-th century, the Rutherford experiment found evidence for the point like structure of the

nuclei in atoms from the scattering of energetic α particles off a gold foil. In the 70s, the same idea was used in the SLAC deep-inelastic scattering experiments to find evidence of point-like constituents within the protons, the quarks, as we showed in Fig. 2. It is thus reasonable to expect that maybe quarks could in turn exhibit another layer of complexity, that could be identified in the same way, by scattering energetic particles, in this case other quarks and gluons, against quarks, at hadron colliders such as the LHC.

To search for quark compositeness, the relevant scattering diagrams are those in the t-channel, for which the differential cross-section can be written as

$$\frac{d^2\sigma^{\rm jet}}{d\,M_{12} d\,\cos\theta^*} = \sum_{ij} \int_0^1 dx_1 dx_2 f_i(x_1) f_j(x_2) \delta(x_1 x_2\, s - M_{12}) \frac{d\hat{\sigma}}{d\cos\theta^*} \tag{167}$$

where the partonic cross-section is (in the center of mass frame) nothing but the Rutherford cross-section for the scattering of point like particles from a Coulomb-like potential

$$\frac{d\hat{\sigma}}{d\cos\theta^*} \sim \frac{1}{\sin^4(\theta^*/2)} \tag{168}$$

Q: why the Rutherford scattering formula is relevant here? Why the QCD interaction can be approximated by a Coulomb-like interaction? What would be the relevant underlying Feynman diagrams?

Defining the variable χ, to remove the Rutherford singularity, we find that if quarks are point like we should find a flat cross-section as a function of χ:

$$\chi \equiv \frac{1+\cos\theta^*}{1-\cos\theta^*} \qquad \frac{d\hat{\sigma}}{d\chi} \propto \text{constant} \tag{169}$$

where we have used that

$$d\chi = 2d\cos\theta^*/(1-\cos\theta^*)^2\,. \tag{170}$$

This naive picture is of course complicated by higher order QCD effects, but in any case it remains true that any structure in the measured χ would hit towards quark substructure. A recent ATLAS search in this channel can be seen in Fig. 25. The QCD predictions, for point-like quarks, are in good agreement with the data showing that if quarks have substructure, this should appear at energy scales larger than $\Lambda = 3$ TeV.

To summarize, in this section we have studied the predictions of QCD at hadron colliders, where the QCD factorization theorem ensures that the same PDFs that we measure in DIS can be used to make predictions at the LHC. We have studies two of the simplest, yet at the same time richest, process at hadron colliders: Drell-Yan and jet production, crucial both for BSM searches and for precision SM measurements. However, with fixed-order perturbative calculations we can describe only final states of low multiplicity, while real events involve hundreds or thousands of particles. Moreover, QCD calculations are done in terms of quarks and gluons, while real event are composed by hadrons. Providing a realistic simulation of the hadronic final state can be achieved by the so-called Monte Carlo parton shower event generators, which are discussed now.

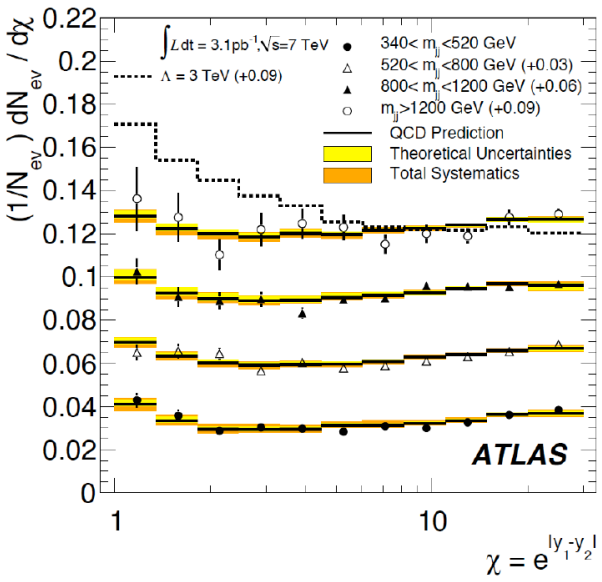

Figure 25: Measurement of the jet cross-section as a function of χ, where the QCD predictions are compared to a model with quark substructure, characterized by a scale $\Lambda = 3$ TeV.

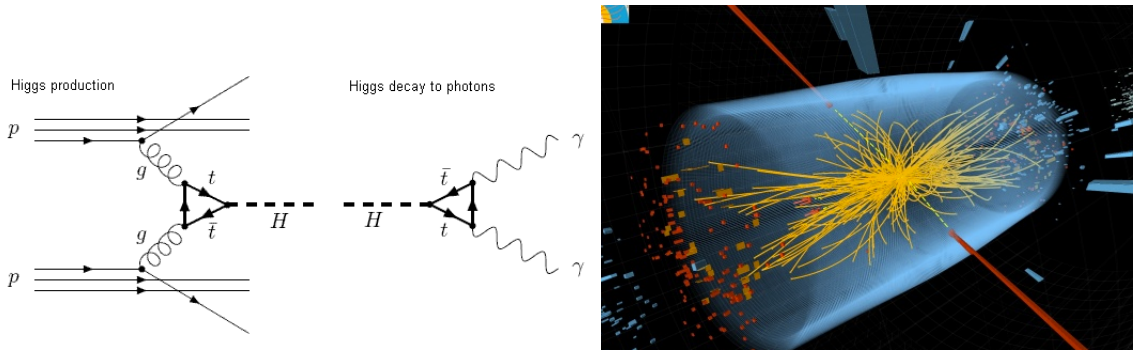

Figure 26: Left plot: Feynman diagram for the Higgs boson production in the gg channel, followed by a decay into di-photons. Right plot: a candidate CMS event for the same process.

Parton showers and Monte Carlo event generators

Up to now we have discussed fixed order perturbative QCD calculations, where the final state looks clean and well defined, see for example the Feynman diagram for Higgs production in gluon channel followed by a decay to di-photons in Fig. 26. However, real events look much more messy, as the CMS display for a Higgs candidate event, for the same underlying partonic process, shows. The connection between the fixed-order QCD calculations in various processes, from e^+e^- annihilation to hadron collisions, and a realistic simulation of the hadronic final state, is achieved by the Monte Carlo parton shower event generators.

The key idea of Monte Carlo event generators is the following:

- The starting point is the partonic configuration after the hard scattering, when all particles have virtualities $Q \gg \Lambda_{\rm qcd}$
- Then a *parton shower* follows, where quarks an gluons radiate more quarks and gluons via soft and collinear splittings (which are dominant in the matrix elements, and resummed to all orders) until virtualities of all partons in the event is $Q_0 \simeq \Lambda_{\rm qcd}$
- The hadronization of colored hadrons into color singlet hadrons is performed using models
- Finally, soft and semi-hard components of the process such as underlying event or multiple parton scattering are also modeled

ending up with a realistic description of the final state in hadronic collisions. Monte Carlo generators are based on a number of models, with parameters that need to be adjusted to experimental data.

Let's illustrate how the parton branching process is performed. A splitting of parton a into partons b and c, all of them massless, is depicted in Fig. 27. We will work under the assumption that the parton branching procedure is ordered in virtually

$$p_b^2 \, , p_c^2 \ll p_a^2 \equiv t \tag{171}$$

which makes sense since the (time-like) branching process moves from large virtualities (result of the hard scattering) to small virtualities (where non-perturbative QCD kicks in). Moreover, we will work in the small angle limit, where QCD matrix elements are enhanced due to infrared singularities.[5] In this limit the

[5]This is the same *collinear* limit that we have studied in the case of DIS and e^+e^- annihilation processes.

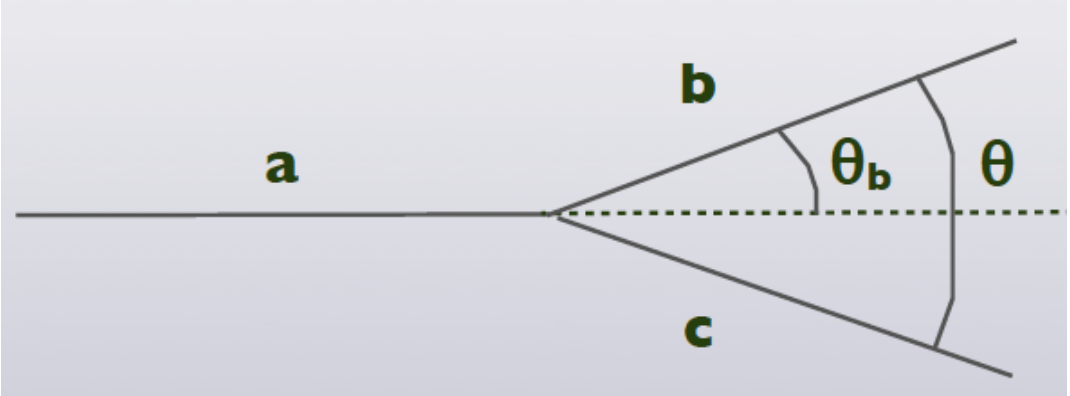

Figure 27: The collinear branching of a *mother* parton a into two *daughter* partons b and c.

virtuality t reads

$$t = 2\,E_b\,E_c\,(1-\cos\theta) \;\simeq\; z(1-z)\,E_a\,\theta^2\,, \qquad z \equiv \frac{E_b}{E_a} \;=\; 1 - \frac{E_c}{E_a} \tag{172}$$

in terms of the energy fraction z and the branching angle θ. In this approximation, using also the conservation of transverse momentum in the splitting, we find the following useful relation:

$$\theta = \frac{\theta_b}{1-z} = \frac{\theta_c}{z}\,. \tag{173}$$

It is an interesting exercise to compute the splitting amplitudes for various possible combinations of quarks and gluons. In the case of the $g \to gg$ splitting, using the QCD Feynman rules, summarized in Fig. 7, we find that the vertex term can be written as

$$V_{ggg} \;=\; ig_s f^{def}\;\left[g^{\mu\nu}\,(p_a+p_c)^\rho + g^{\nu\rho}\,(p_c-p_b)^\mu - g^{\rho\mu}\,(p_a+p_b)^\nu\right] \tag{174}$$

Squaring the matrix element, we end up with a *factorized* expression for the matrix elements with $n+1$ particles $|\mathcal{M}_{n+1}|^2$

$$|\mathcal{M}_{n+1}|^2 \sim \frac{4\,g^2}{t} C_A\,F(z;\epsilon_a,\epsilon_b,\epsilon_c)|\mathcal{M}_n|^2 \tag{175}$$

in terms of the matrix element with n particles $|\mathcal{M}_n|^2$ (computed before the splitting) and a universal factor F which depends only on the details of the splitting, but *not* of the hard scattering n-body matrix element.[6] Summing over polarizations, we find that the structure of infrared divergences of the soft and collinear branchings are the same regardless of the hard scattering process: this is a consequence of the universality of soft and collinear singularities in QCD. We can write the $(n+1)$-particle squared matrix element $|\mathcal{M}_{n+1}|^2$ after the splitting as follows

$$\sum_{\rm pol} |\mathcal{M}_{n+1}|^2 \sim \frac{4\,g^2}{t}\,C_A\,\left[\frac{1-z}{z} + \frac{z}{1-z} + z(1-z)\right]\,|\mathcal{M}_n|^2 \tag{176}$$

We again observe this important property of QCD, namely that

[6] See Ellis-Stirling-Webber for a more in-depth calculation of the factors F.

The cross-section for $n+1$ particles, when any pair has arisen from a soft or collinear splitting, can be factorized into the n particle cross-section times a universal factor, a splitting function, which is process independent.

This property of course should be more than familiar to us, since we have derived it explicitly already in a number of different contexts, including e^+e^- annihilation and DIS.

From Eq. (176) we can observe the characteristic infrared divergences of the branching

- Soft singularities when $z \to 1$ or $z \to 0$: one of the partons becomes soft.
- Collinear singularity when $t \to 0$, see Eq. (172), when the two partons become collinear.

Finally, we can compute the cross-section for the $(n+1)$-particles final state in terms of the n-particle final state supplemented by a collinear branching, obtaining the following result,

$$d\sigma_{n+1} \, = \, d\sigma_n \, \frac{dt}{t} \, dz \, \frac{\alpha_s}{2\pi} \, \hat{P}_{ab}(z) \tag{177}$$

where $\hat{P}_{ab}(z)$ is the *unregularized splitting function*, a very close sibling of the DIS splitting functions from Eq. (110), and is given, in particular case of a final-state $g \to gg$ splitting, by

$$\hat{P}_{gg}(z) = C_A \left[\frac{1-z}{z} + \frac{z}{1-z} + z(1-z) \right] , \tag{178}$$

and analogous expressions exist for other possible QCD branchings, such as $g \to q\bar{q}$ or $q \to qg$.

By including the contribution of more and more sequential branchings, we can compute the multiple emission of small-angle partons to all orders in the QCD perturbative expansions. This is what is done by the Monte Carlo parton showers such as `Pythia`,`Herwig` or `Sherpa`, hence we say that these showers have LL accuracy (meaning Leading Log). Therefore, parton showers are not only a method to simulate realistically the final state of high energy collisions, they also allow to improve the perturbative accuracy of fixed order computations.

The parton shower MC branching equations

Let us now derive the Monte Carlo equations for a generic parton shower, starting from the hard scattering configuration. For simplicity, we will consider a *space-like shower*, corresponding the process schematically represented in Fig. 28: starting from a parton with low virtuality t_0 (since it is found in the proton, thus $t_0 \simeq \Lambda_{\rm QCD}$), it emits soft and collinear radiation under reaching the hard scattering virtuality $t = q^2$. The initial parton carries momentum fraction x_0, and the parton that enters the hard-scattering carries momentum fraction x_n.

The branching process depicted in Fig. 28 can be better represented by a path followed in the (t, x) plane, shown in Fig. 29. The way to compute the equations that govern the multiple soft and collinear branchings in a QCD parton shower is based on determining the number of paths that lead to a given region in the (t, x) plane and the number of paths that leave this same region and reach the hard scattering virtuality Q.

Using the schematic diagram in Fig. 29, the variation of the PDF due to all paths that enter into the (t, x) region is, using the result that we have derived in Eq. (177) for a soft or collinear branching, is the

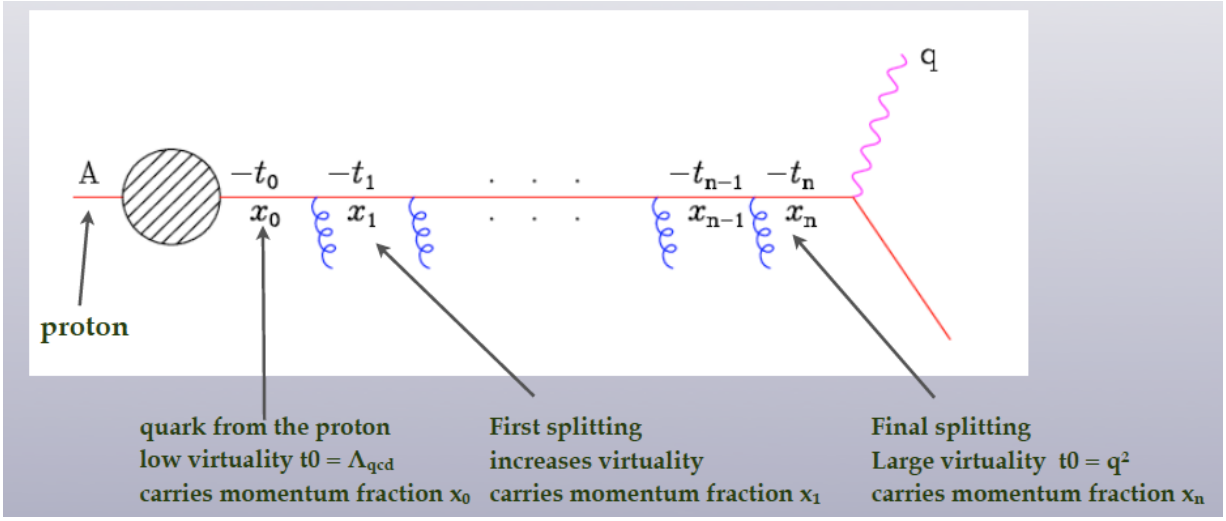

Figure 28: Schematic representation of a time-like parton shower branching, starting from a parton with low virtuality t_0, which emits soft and collinear radiation under reaching the hard scattering virtuality.

following:

$$\delta f_{\rm in}(x,t) = \frac{\delta t}{t} \int_x^1 dx' dz \frac{\alpha_s}{2\pi} \hat{P}_{qq}(z) f(x',t) \delta(x - x' z) , \tag{179}$$

where the PDF $f(x',t)$ is now inside the integral, while the contribution from the paths that leave this same region is given by

$$\delta f_{\rm out}(x,t) = \frac{\delta t}{t} f(x,t) \int_0^x dx' dz \frac{\alpha_s}{2\pi} \hat{P}_{qq}(z) \delta(x - x' z) , \tag{180}$$

where now the starting point of the PDF is fixed and thus is appears outside the integral. Therefore, putting them together, we obtain that due to the soft and collinear branchings, the PDF should satisfy an LL evolution equation:

$$t \frac{\partial}{\partial t} f(x,t) = \int_x^1 \frac{dz}{z} \frac{\alpha_s}{2\pi} P_{qq}(z) f\left(\frac{x}{z},t\right) \tag{181}$$

which is nothing but the same splitting functions that we encountered in DIS. Indeed, the parton branching description is an alternative way of deriving the QCD evolution equations.[7]

Now we can introduce an important concept for Monte Carlo event generators, known as the *Sudakov form factor*. This quantity is defined as

$$\Delta(t) \equiv \exp\left(- \int_{t_0}^t \frac{dt'}{t'} \int dz \frac{\alpha_s}{2\pi} \hat{P}_{qq}(z) \right) . \tag{182}$$

Using the Sudakov form factor, it is easy to derive the following modified evolution equations:

$$t \frac{\partial}{\partial t} \left(\frac{f(x,t)}{\Delta(t)} \right) = \frac{1}{\Delta(t)} \int \frac{dz}{z} \frac{\alpha_s}{2\pi} \hat{P}_{qq}(z) f\left(\frac{x}{z},t\right) \tag{183}$$

[7]The splitting functions are the same for time-like and space-like showers at LO, but differ starting from NLO onwards. The parton branching description outlined above can only be used at LO accuracy though.

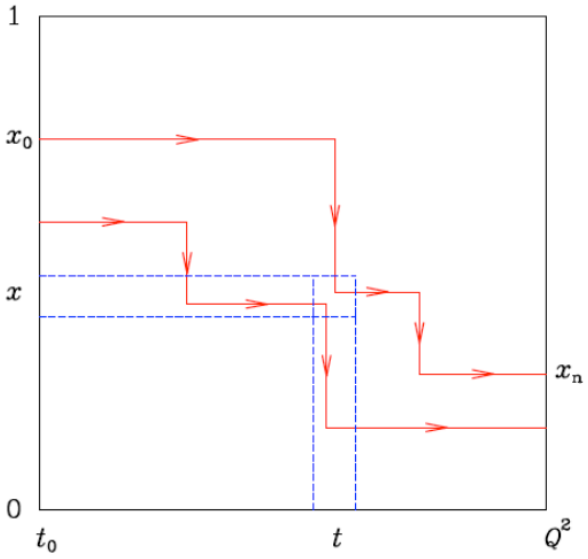

Figure 29: Path in the virtuality/momentum fraction plane for a initial state parton in a *space-like shower* from a low virtuality $t_0 \simeq \Lambda^2_{\rm QCD}$ to the hard scattering virtuality $t \simeq Q^2$. to high virtuality. See text for more details.

which can be easily integrated to give the following result:

$$f(x,t) \,=\, \Delta(t)\, f(x,t_0) \,+\, \int_{t_0}^{t} \frac{dt'}{t'}\, \frac{\Delta(t)}{\Delta(t')} \int \frac{dz}{z}\, \frac{\alpha_s}{2\pi}\, \hat{P}_{qq}(z)\, f\left(\frac{x}{z}, t'\right) \tag{184}$$

Let's take a closer look to this equation

- The first term of the contribution to all paths where virtuality changes from t_0 to t without any branching
- The second term is the contribution from all paths that have a branching at t' and then evolve without branching up to a virtuality t

So the Sudakov form factor, Eq. (182) has a clean theoretical interpretation as

The probability that, in a parton shower, a given parton evolves from t_0 to t without any branching (and then a branching takes place at t).

Eq. (182) is the basis of a Monte Carlo branching algorithm. The numerical implementation proceeds as follows

(a) At some point in the branching chain, we have a parton with virtuality t_1 and momentum fraction x_1,

(b) The MC algorithm generates, probabilistically, the values of t_2 using the equation

$$\frac{\Delta(t_2)}{\Delta(t_1)} \,=\, \mathcal{R} \tag{185}$$

where $\mathcal{R}$ is a flat random number between 0 and 1.

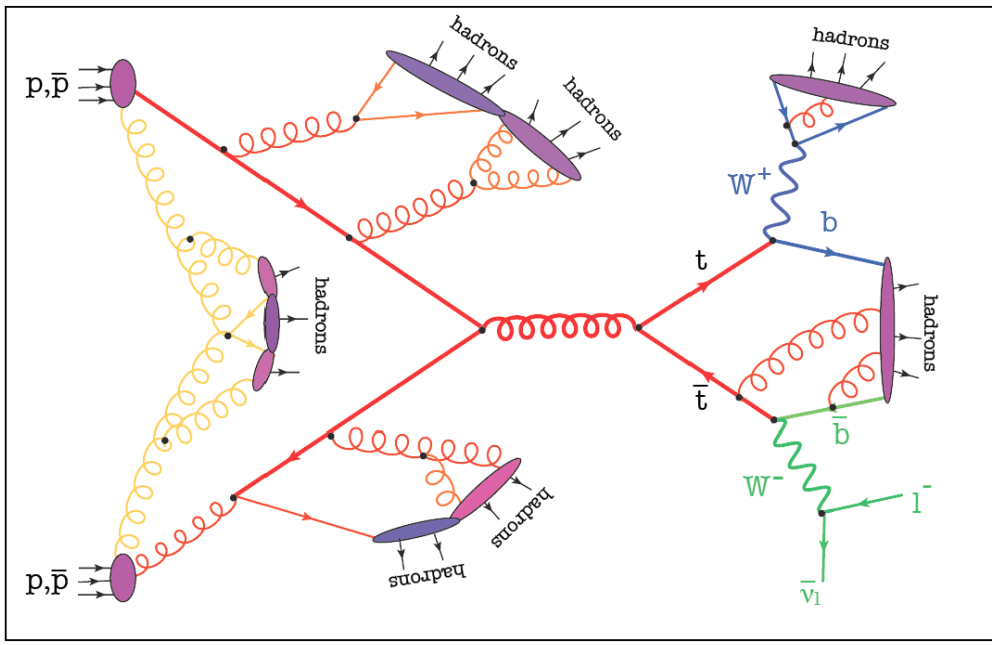

Figure 30: Schematic representation of the various ingredients that enter an hadronic collision, from the initial state (parton distributions) to the hard scattering cross-section to the final state (parton shower, hadronization), and then supplemented by non-perturbative soft physics for the underlying event and multiple parton interactions (Drawing by K. Hamilton).

(c) Next the algorithm determines the value of x_2 of this splitting, using the condition

$$\int_{\epsilon}^{x_2/x_1} dz \, \frac{\alpha_s}{2\pi} \hat{P}_{qq}(z) \, = \, \mathcal{R}' \int_{\epsilon}^{1-\epsilon} dz \, \frac{\alpha_s}{2\pi} \hat{P}_{qq}(z) \tag{186}$$

where $\mathcal{R}'$ is another flat random number between 0 and 1, and the integral is performed only over *resolvable branchings*.

Using this procedure, starting from a relatively simple hard-scattering event, we can provide a realistic simulation of the final state particles using perturbative QCD. In Fig. 30 we show the schematic representation of the various ingredients that enter an hadronic collision, from the initial state (parton distributions) to the hard scattering cross-section to the final state (parton shower, hadronization), and then supplemented by non-perturbative soft physics for the underlying event and multiple parton interactions.

Once all partons in the shower have low virtualities, $t \sim \Lambda^2_{\rm QCD}$, perturbative QCD breaks down, and it is non-perturbative, long-distance dynamics that determine how these low-virtuality quarks and gluons are confined into the hadrons that are observed in the detector.

Since perturbative QCD cannot be used to compute hadronization process, we need to resort to a variety of different models. The difference between models is often taken as a systematic uncertainty in any measurement that involves the use of parton showers.

The basic hypothesis is that of local quark-hadron duality: *the flow of momenta and quantum numbers at hadron level follows that of the parton level.* With this assumption, and taken into account the fundamental symmetries of QCD, various hadronization models have been proposed, and are implemented in different

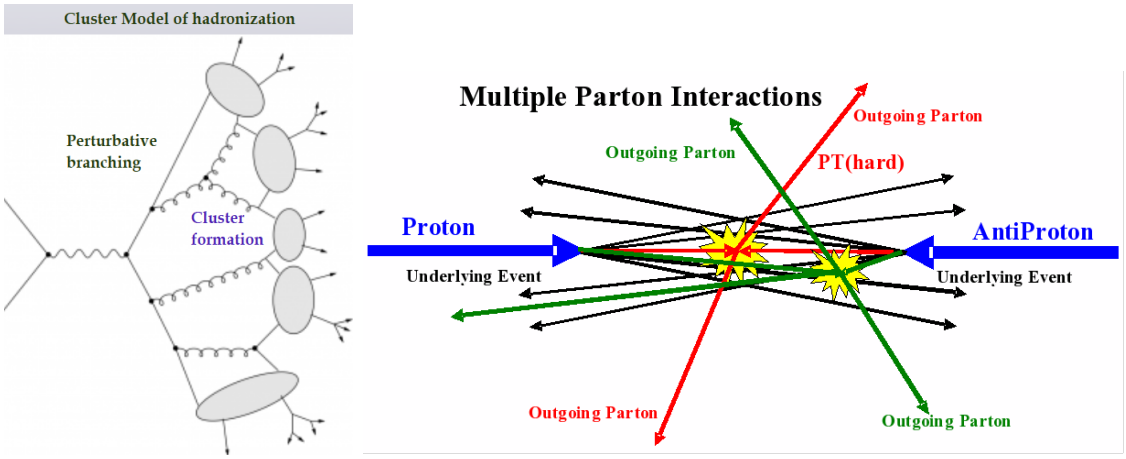

Figure 31: Left plot: schematic representation of the cluster model of hadronization, where a cluster formation step follows the perturbative parton branching process. Right plot: schematic representation of multiple parton interactions at an hadron collider.

shower MC programs. For example, the cluster model exploits an important property of the pre-confinement of color in parton branching: color singlet clusters of partons form after perturbative branching and then decay into the observed hadrons. This model is illustrated in Fig. 31, and the basic idea is to cluster the low-virtuality partons into color-singlet clusters that are then hadronized.

Finally, let us mention that real hadron-collider events need to deal not only with a single hard scattering, but actually in each event there can be multiple soft, semi-hard and hard collisions on top of the main one. If these collisions arise from the same basic hadron-hadron collision, they are known as *Multiple Parton Interactions*, and they are represented in Fig. 31. When collisions arise from different pp collisions within the same bunch-crossing, as happens when the collider luminosity is high, then they are denoted as *pile-up*. Taming the large pile-up present at the relatively large luminosities of the LHC is a major concern in experimental analysis.

Jet reconstruction and jet substructure

When discussing e^+e^- annihilation we found that exclusive observables exhibited infrared divergences, that could only be canceled in inclusive enough observables by means of a jet definition. At the LHC, jets are omnipresent, and jet reconstruction a crucial topic. In this lecture first we provide a general introduction to the topic of jet reconstruction, with emphasis on hadron colliders, and then we explore jet substructure, which is essential at the LHC specially in searches for massive new particles.

Jet reconstruction

As we have seen in e^+e^-, jets are fundamentally ambiguous concept. A sensible jet definition needs to be introduced, that can be equally well applied to partons, hadrons and calorimeter cells. The conditions for a robust jet algorithm were defined in 1990 in the Snowmass accord:

Several important properties that should be met by a jet definition are [3]:

1. Simple to implement in an experimental analysis;
2. Simple to implement in the theoretical calculation;
3. Defined at any order of perturbation theory;
4. Yields finite cross sections at any order of perturbation theory;
5. Yields a cross section that is relatively insensitive to hadronisation.

A crucial property of a jet definition is that it should be *infrared and collinear safe*, that is, provide sensible results to all orders in the QCD perturbative expansion. As we saw in the case of the Sterman-Weinberg jets, infrared safety can be formulated by requiring that

A cross-section, computed in pQCD, should be unchanged if any of the particles undergoes a soft or a collinear splitting

.

An example of a IRC unsafe definition would be the following:

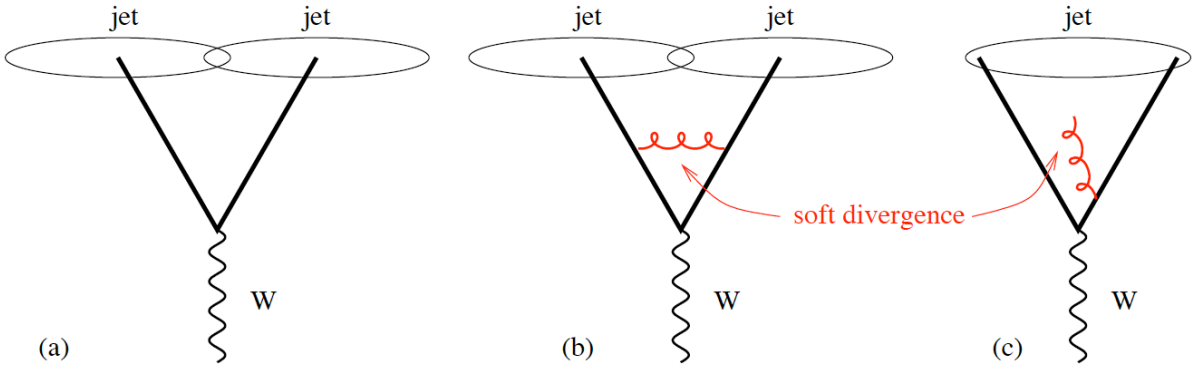

since we see the emission or an arbitrarily soft parton merges the two jets that would otherwise be separated, spoiling the cancellation of real and virtual soft divergences and producing an infinite result. The most popular jet reconstruction algorithm at the LHC is known as the *anti-k_T algorithm*. The is to cluster pairs of partons sequentially following some measure of their *distance*. The algorithm works as follows

(a) Make a list of all final-state particles in your collision (can be partons, hadrons, calorimeter cells)

(b) Now compute the following distance between a pair of particles

$$d_{ij} = \min\left(p_{T,i}^{-2}, p_{T,i}^{-2}\right) \frac{(y_i - y_j)^2 + (\phi_i - \phi_j)^2}{R^2} \,. \tag{187}$$

where R is the jet radius, the fundamental parameter of the algorithm. We also compute the distance of particle i with the beam

$$d_{iB} = p_{T,i}^2 \,. \tag{188}$$

(c) Find the minimum distance. If it is a d_{ij}, recombine the two particles by adding their four-momentum. Else, declare particle i to be a jet and remove it from the list of particles.

(d) Continue the algorithm until the list of particles is empty

An important property of the anti-k_T algorithm is that its *catchment area* (the area in which each each picks up soft particles) is relatively regular, and this is a very beneficial property for jet energy calibration as well as for the subtraction of underlying event and pileup. In Fig. 32 we show the catchment area of two jet algorithms, with $R = 1$: the k_T algorithm and the anti-k_T algorithm. It is clear that the second produces much more regular jets than the first of the algorithms. The k_T algorithm is defined in exactly the same way as the anti-k_T algorithm but with a modified distance

$$d_{ij} = \min\left(p_{T,i}^2, p_{T,i}^2\right) \frac{(y_i - y_j)^2 + (\phi_i - \phi_j)^2}{R^2} \,. \tag{189}$$

Another widely used sequential recombination algorithm is know as the Cambridge/Aachen algorithm, where the distance is based purely on angular variables

$$d_{ij} = \frac{(y_i - y_j)^2 + (\phi_i - \phi_j)^2}{R^2} \,, \tag{190}$$

and which is specially useful in the context of jet substructure, as we discuss now.

Jet substructure

A closely related topic that has seen an impressive development recently is that of jet substructure. The motivation to look closer to the internal structure of jets is provided by the following observation. Consider the decays of a resonance with a mass at the electroweak scale. Typically due to the limited phase space it will be produced with a small boost, and thus, if decays to QCD partons, the resulting jets will be well separated. However, at the LHC a new kinematical regime becomes available: that where the EW-scale resonance is produced with a very large boost, $p_T \gg m$. In these conditions, the subsequent hadronic decays of the resonance end up being collimated into a single jet, becoming thus indistinguishable from the overwhelming QCD background - unless jet substructure tools are used.

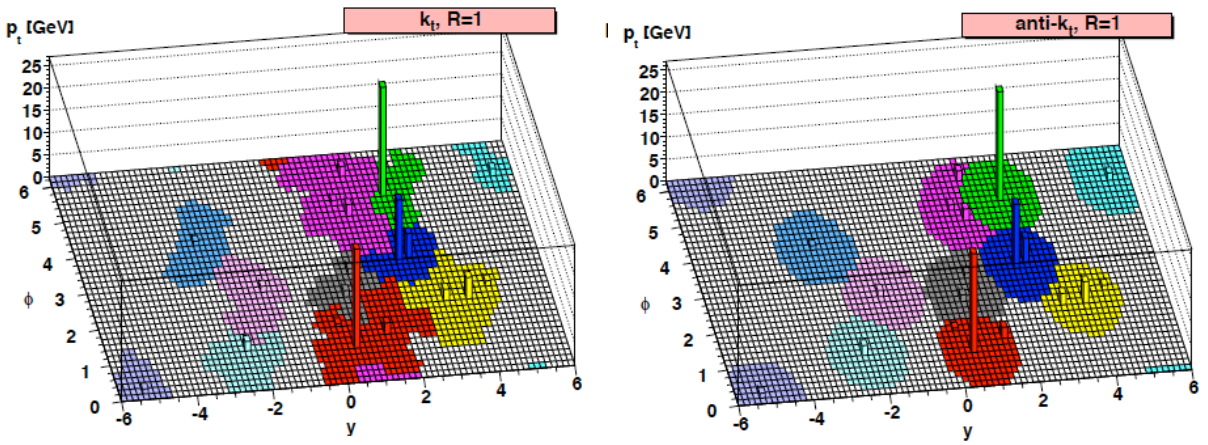

Figure 32: The catchment area of two jet algorithms, with $R = 1$: the k_T algorithm and the anti-k_T algorithm. It is clear that the second produces much more regular jets than the first of the algorithms.

The situation is illustrated in Fig. 35. A heavy resonance, such as a W boson or a top quark, produced with a large enough boost, $p_T \gg m$, when decaying hadronically the final state becomes indistinguishable from than of QCD jets. This seems a major problem, since it seems one would be missing many events of important electroweak processes because of the dominance of the QCD jet backgrounds. Given that many BSM scenarios involve the production of boosted heavy resonances, a major limitation to the LHC program might be feared. Fortunately, we can use our understanding of QCD radiation to distinguish background from interesting signals even in the boosted regime.

To understand which is the kinematic regime relevant for jet substructure let's consider one of the most paradigmatic examples, namely the decay of a boosted Higgs boson into a $b\bar{b}$ pair. The processes is illustrated schematically in Fig. 34. For simplicity, we assume that the Higgs has been produced centrally, and take the azimuthal angle to be $\phi = 0$.

Using the parametrisation which is more suitable for hadronic collisions, we can write the four-momentum of the Higgs boson as follows:

$$p_H = \left(\sqrt{m_H^2 + p_{T,H}^2}\,, p_{T,H}\,, 0\,, 0\right) \tag{191}$$

and that of the decay bottom quarks

$$p_b = \left(z\sqrt{m_H^2 + p_{T,H}^2}\,, p_{x,b}\,, 0\,, p_{z,b}\right) \tag{192}$$

$$p_{\bar{b}} = \left((1-z)\sqrt{m_H^2 + p_{T,H}^2}\,, p_{x,\bar{b}}\,, 0\,, -p_{z,b}\right) \tag{193}$$

where z is the fraction of the Higgs boson original energy that is being carried by the b quarks.

Now using four-momentum conservation and neglecting the small masses of the bottom quarks, we find that the kinematics of the process is uniquely defined in terms of three variables:

- The Higgs boson mass, m_H,
- The Higgs transverse momentum, $p_{T,H}$,
- and the fraction of energy carried by the bottom quark z (which determines the asymmetry of the

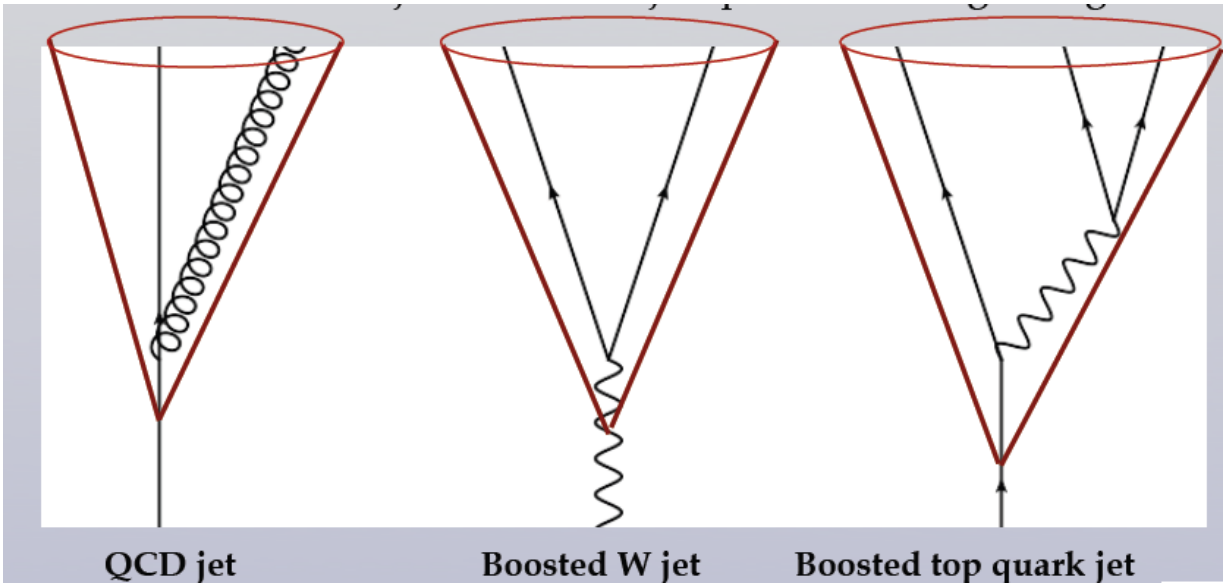

Figure 33: If a heavy resonance is produced with a large enough boost, $p_T \gg m$, then when decaying hadronically the final state becomes indistinguishable from than of QCD jets - unless one looks at the jet substructure.

decay)

It is an easy computation to show that

$$p_{x,b} = \frac{p_{T,H}}{2} + (2z-1)\frac{p_{T,H}^2 + m_H^2}{2\,p_{T,H}} \tag{194}$$

$$p_{x,\bar{b}} = \frac{p_{T,H}}{2} - (2z-1)\frac{p_{T,H}^2 + m_H^2}{2\,p_{T,H}} \tag{195}$$

$$p_{z,b} = \left[(p_{T,H}^2 + m_H^2)\left(z^2 - z + \frac{1}{2}\right) - \frac{p_{T,H}^2}{4} - (2z-1)^2\frac{(p_{T,H}^2 + m_H^2)^2}{4\,p_{T,H}^2}\right]^{1/2} \tag{196}$$

The above formulae are valid in all generality. Now let us consider the boosted regime, $p_{T,H} \gg m_H$, and then we obtain a substantial simplification to end up with

$$p_{x,b} = z\,p_{T,H} \tag{197}$$

$$p_{x,\bar{b}} = (1-z)\,p_{T,H} \tag{198}$$

$$p_{z,b} = \sqrt{z\,(1-z)}\,m_H \tag{199}$$

Therefore, in the boosted regime, the angular separation between the bottom and anti-bottom quarks will be given by

$$R_{b\bar{b}} = \frac{p_{z,b}}{p_{x,b}} - \frac{p_{z,\bar{b}}}{p_{x,\bar{b}}} = \frac{1}{\sqrt{z\,(1-z)}}\frac{m_H}{p_{T,H}} \tag{200}$$

Eq. (200) allows to determine when the boosted regime kicks in at the level of final state topology. If we have a jet definition with jet radius R, them, if the transverse momentum of the Higgs boson is such that $R \geq R_{b\bar{b}}$, the two b quarks will end up collimated into a single jet, and there traditional Higgs reconstruction, based on two separate b-tagged jets, becomes impossible. For $R = 0.5$ and $z = 1/2$, we find that in the case

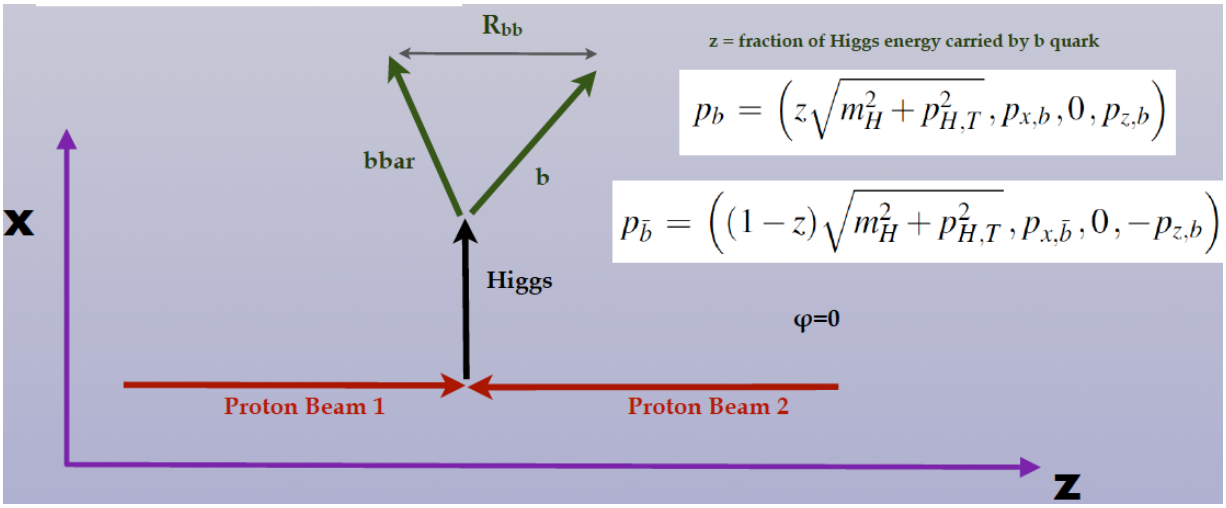

Figure 34: Scheme for the central production of a Higgs boson in a hadronic collision, followed by the decay into a $b\bar{b}$ pairs.

of $H \to b\bar{b}$ the boosted regime is relevant when $p_{T,H} \geq 500$ GeV. This of course is a reason of concern, since these high $p_{T,H}$ events are very important for Higgs characterization studies.

To be able to find a way out, a number of jet substructure techniques have been developed in order to efficiently distinguish jets with non-trivial substructure from QCD jets. The basic ideas are common for all methods:

- QCD jets arise from soft and collinear splittings, while in the decay of heavy resonances all prongs share a similar amount of energy
- QCD jets do not show structure in the jet mass distribution, while for heavy resonances the jet mass is peaked around the resonance mass.
- Removing soft radiation in a jet should leave signal events unchanged, while decreasing the contamination from QCD events

A plethora of jet substructure techniques have been developed in the recent years. Here we will discuss one of the most important substructure taggers, known as the BDRS mass-drop tagger.[8] This tagger is based on the Cambridge/Aachen algorithm, and it works as follows:

(a) Recluster a given jet with the C/A algorithm with a large value of R, say $R = 1.0$ The jet can have been originally clustered with any other algorithm, like anti-k_T, and other values of R, but before we can use BDRS we need to recluster with C/A

(b) Recall that in the Cambridge/Aachen algorithm, particles are clustered according to their angular distances:

$$\Delta R_{ij}^2 = (y_i - y_j)^2 + (\phi_i - \phi_j)^2 \, . \tag{201}$$

[8] From the 2008 paper from Butterworth, Davidson, Rubin and Salam, who showed that using jet substructure on can use $H \to b\bar{b}$ event at the LHC.

(c) First of all undo the last step of the C/A clustering, and take a look at the properties of the resulting *subjets*. If this last splitting had been a soft/collinear QCD emission, we expect that the invariant mass of the leading subjet to be not to different from the jet mass m_j. Therefore, to be tagged as a *fat jet*, BDRS require a substantial mass drop, so that the subjet masses are much smaller that the original jet mass

$$m_{j1} \,\leq\, \mu\, m_j\,, \tag{202}$$

with m_{j1} the invariant mass of the hardest subjet, and the threshold μ is a parameter of the algorithm. To see the motivation of this cut, note that in the case of a soft-collinear splitting we have

$$m_j^2 \,=\, m_{j1}^2 \,+\, m_{j2}^2 \,+\, 2\, z(1-z)\, E_j^2\, \theta_{j1,j2}^2 \tag{203}$$

and therefore neglecting the mass of the softer subjet we find

$$m_{j1}^2 \,\simeq\, m_j^2 \left(1 - \frac{2\, z(1-z)\, E_j^2}{m_j^2}\, \theta_{j1,j2}^2\right) \,\leq\, \mu\, m_j^2 \tag{204}$$

so the cut in μ effectively discards soft and collinear splittings.

(d) A QCD splitting will be mostly collinear, so BDRS also requires that this last splitting should be relatively symmetric, as would be the case in the decay of a heavy resonance. This is achieved by requiring that

$$y_{\rm mdt} \,\equiv\, \frac{\min(p_{T,j1}^2, p_{T,j2}^2)}{m_j^2} \Delta\, R_{j1,j2j}^2 \,\geq\, y_{\rm cut} \tag{205}$$

with $y_{\rm cut}$ another parameter of the algorithm. To understand where this cut comes from, we note that in the QCD soft limit we can write:

$$y_{\rm mdt} \,\equiv\, \frac{\min(p_{T,j1}, p_{T,j2})}{m_j^2} \Delta\, R_{j1,j2j}^2 \,\simeq\, \frac{\min\left(z_{j1}^2, z_{j2}^2\right)}{z_{j1}\, z_{j2}} \,=\, \frac{\min\left(z_{j1}, z_{j2}\right)}{\max\left(z_{j1}\,, z_{j2}\right)} \,\geq\, y_{\rm cut} \tag{206}$$

So therefore, this cut discards kinematic configurations where the branching is too asymmetric.

(e) If the two conditions Eq. are satisfied, we can tag the fat jet as arising from the decay of a boosted heavy resonance, rather that being a standard QCD jet. Else, we discard the softest subjet, and repeat the procedure for the hardest subjet until the BDRS condition is satisfied or until we reach the end of the clustering history, at which point the jet is classified as a QCD jet.

Other jet substructure tools are based on similar ideas: identify the substructure variables for which QCD jets differ more from fat jets arising from decays of boosted resonance, and cutting on those to increase the signal significance. These tools have been implemented by ATLAS and CMS in many of the Run I analysis, and this technology will become even more important at Run II. In Fig. 35 we show two examples of boosted resonance reconstruction. First of all, in top quark pair decays, in a large fraction of events the W bosons decay hadronically. If the p_T is large enough, the hadronic decays of the W will be collimated into a single jet, which can then be reconstructed with substructure techniques, resulting in a nice peak around the W mass for the the jet invariant mass. ATLAS has managed to reconstruct the $Z \to b\bar{b}$ decays in events where the Z boson carries large transverse momentum, and where jet substructure techniques allow to identify this

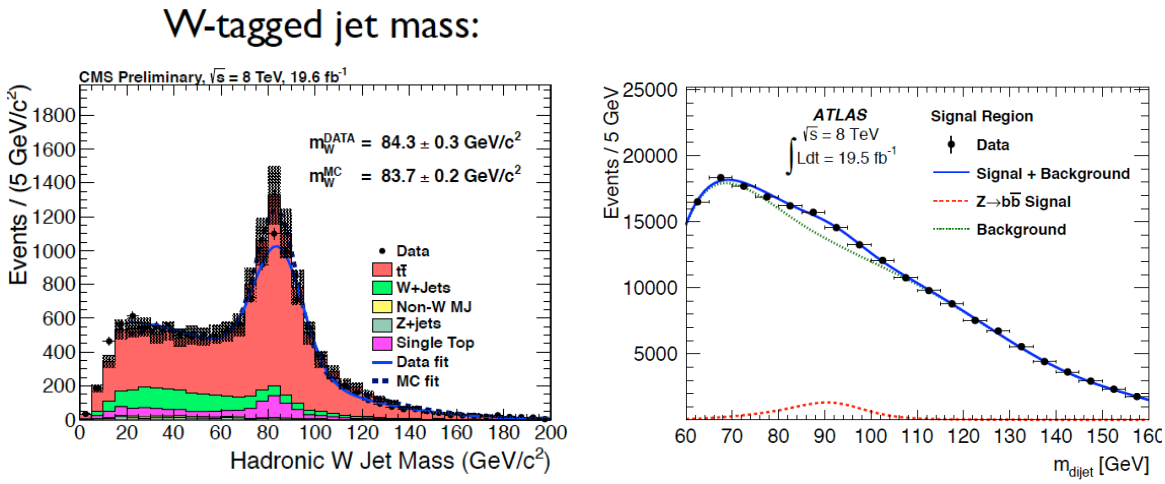

Figure 35: Left plot: in top quark pair decays, in a large fraction of events the W bosons decay hadronically. If the p_T is large enough, the hadronic decays of the W will be collimated into a single jet, which can then be reconstructed with substructure techniques, resulting in a nice peak around the W mass for the the jet invariant mass. Right plot: ATLAS has managed to reconstruct the $Z \to b\bar{b}$ decays in events where the Z boson carries large transverse momentum, and where jet substructure techniques allow to identify this decay channel over the overwhelming QCD background.

decay channel over the overwhelming QCD background.

Of course, the ultimate hope is to be able to discover new physics in boosted final states using jet substructure technique. in Fig. 36 we show the Feynman diagram which correspond to the pair production of fermionic top partners (that would arise for example in models where the Higgs boson is a composite particle) and that might contain a number of *fat jets* in the final state, in particular from the hadronic decays of W bosons. In the right part of the plot we show an event display corresponding to this search, where the C/A algorithm has been used o identify a *fat jet* from the decay of a boosted top quark.

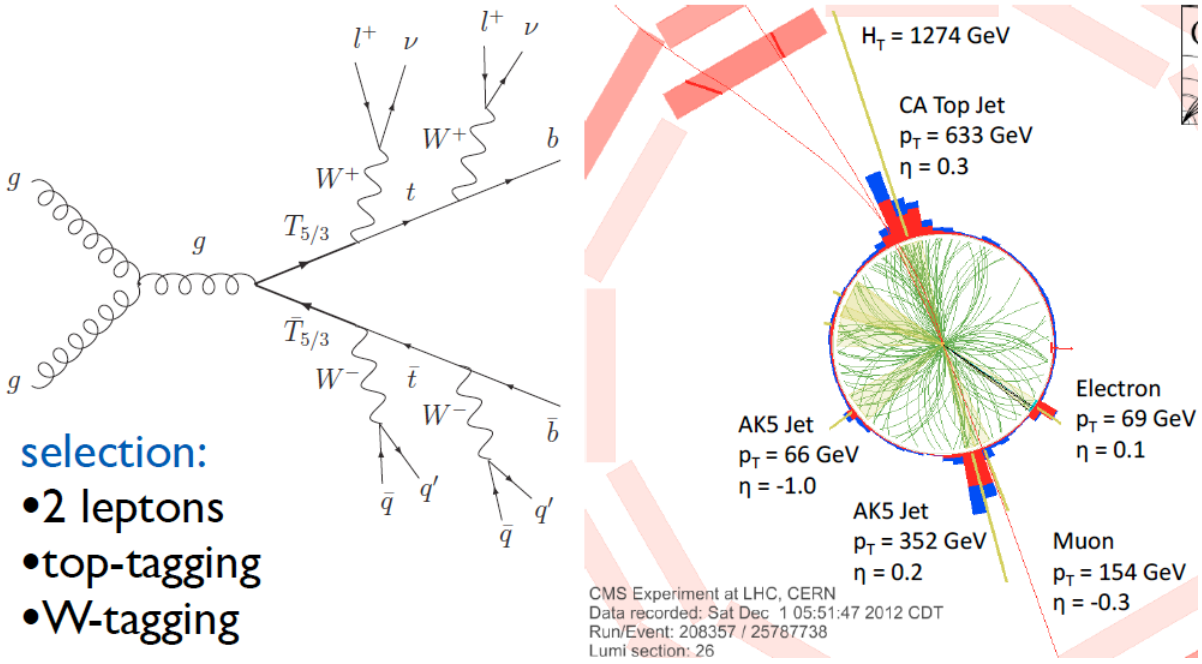

Figure 36: Feynman diagram which correspond to the pair production of fermionic top partners (that would arise for example in models where the Higgs boson is a composite particle) and that might contain a number of *fast jets* in the final state, in particular from the hadronic decays of W bosons.

Electroweak interactions

After this detailed study of the strong interaction, we move to discuss the other main building block of the Standard Model, namely the electroweak interactions and the Higgs sector. As in the case of QED and QCD, electroweak interactions can be described by a renormalizable QFT with a Lagrangian which is invariant under a specific type of gauge transformations. In particular, electroweak interactions are invariant under the $SU_L(2) \otimes U(1)$ gauge group.

In $SU_L(2) \otimes U(1)$ group, the first subgroup corresponds to the *weak isospin* quantum number and the second subgroup to the *weak hypercharge*.

Let us start by assuming that we have a purely bosonic theory, and write down a Lagrangian which exhibits this specific gauge invariance, in analogy with QED and QCD. Our Lagrangian will now have three massless bosons W_i, associated to the weak isospin subgroup, and one more boson, B, charged under the weak hypercharge group. As for the photon and gluon, these bosons are massless due to gauge invariance constraints. The resulting Lagrangian will be

$$\mathcal{L} = -\frac{1}{4} W^{i,\mu\nu} W^i_{\mu\nu} - \frac{1}{4} B^{\mu\nu} B_{\mu\nu} \,, \tag{207}$$

with $i = 1, 2, 3$, and where the corresponding field strength tensors have the familiar expressions

$$W^i_{\mu\nu} = \partial_\mu W^i_\nu - \partial_\nu W^i_\mu - g_W \epsilon^{ijk} W^j_\mu W^k_\nu \,, \tag{208}$$

$$B_{\mu\nu} = \partial_\mu B_\nu - \partial_\nu B_\mu \,, \tag{209}$$

with g_W the coupling associated to the weak isospin interaction, and where we have used that the structure constants of $SU_L(2)$ are the totally antisymmetric tensor ϵ^{ijk}. The fact that $SU(2)$ is non abelian leads to the self-interactions of the W^i_μ bosons, as was the case for the gluons in QCD.

The Lagrangian Eq. (207) cannot describe the weak interaction, which is short-ranged because of the large mass of the force carriers. One needs to introduce a mass term without spoiling gauge symmetry. The way to achieve this is by means of *spontaneous symmetry breaking*.

The coupling of the gauge fields to matter, as usual, will be through the covariant derivative, which for the case of the $SU_L(2) \otimes U(1)$ gauge group reads

$$D^\mu = \delta_{ij} \partial^\mu + i g_W \left(T \cdot W^\mu \right)_{ij} + i Y \delta_{ij} g'_W B^\mu \,, \tag{210}$$

where g'_W is the weak hypercharge coupling and Y is the value of the so-called *weak hypercharge* of a given matter particle. The matrices T are a suitable representation of the $SU(2)$ algebra. The $SU(2)$ algebra is defined by

$$\left[T^i, T^j \right] = i \epsilon^{ijk} T^k \,, \tag{211}$$

and typically one defines the combination

$$T^\pm = T^1 \pm i T^2 \,. \tag{212}$$

The Higgs mechanism and EW symmetry breaking

In the Standard Model, the electroweak $SU(2) \otimes U(1)$ gauge symmetry group is spontaneously broken by the *Higgs mechanism*. This requires to add a new complex doublet of scalar fields,

$$\phi = \left(\begin{array}{c} \phi^+ \\ \phi^0 \end{array} \right) , \tag{213}$$

which transform as a doublet of $SU_L(2)$ and have weak hypercharge value of $Y = 1/2$. It is possible to couple the Higgs field ϕ to the massless electroweak Lagrangian while preserving gauge symmetry by means of the same covariant derivative that was introduced in Eq. (210), namely

$$\begin{aligned} \mathcal{L} &= \left(\partial^\mu \phi^\dagger + i g_W \left(T \cdot W^\mu \right) \phi^\dagger + i \frac{1}{2} \delta_{ij} g'_W B^\mu \phi^\dagger \right) \cdot \\ &\quad \left(\partial_\mu \phi - i g_W \left(T \cdot W_\mu \right) \phi - i \frac{1}{2} \delta_{ij} g'_W B^\mu \phi \right) - \mathcal{V} \left(\phi^\dagger \phi \right) \end{aligned} \tag{214}$$

where for simplicity the isospin indices have been left implicit. It is easy to check explicitly that the above Lagrangian is invariant under $SU_L(2) \otimes U(1)$ transformations.

A remarkable feature of Eq. (214) is the presence of a potential term for the scalar field. Other than the fact that it can depend only on the product $\phi^\dagger \phi$, to enforce gauge symmetry, there is no other restriction on its form. In the Standard Model, the Higgs potential takes the following value

$$\mathcal{V} \left(\phi^\dagger \phi \right) = \lambda \left(\phi^\dagger \phi \right)^2 - \mu^2 \left(\phi^\dagger \phi \right) . \tag{215}$$

The Higgs potential Eq. 215 is the only *ad-hoc* component of the Standard Model, whose shape is not determined by any symmetry. Other than minimality, there is no principle that selects Eq. 215 as compared to other potentials that can also break EW symmetry.

There are some interesting feature of this potential:

- the sign of the mass term is different as the one that would be used for example in the $\lambda \phi^4$ scalar theory. This causes the field to have a *vacuum expectation value* $\langle \phi \rangle \neq 0$ at the minimum.
- the λ accounts for the self-interactions of the scalar field ϕ with itself.

Therefore $\lambda, \mu^2 > 0$, this potential exhibits degenerate minima for values of the field ϕ which are different from zero, as shown in Fig. 37: this is the famous *Mexican hat* potential of the Higgs field. Remarkably, as we will show, single Higgs measurements only probe the region of the Higgs potential close to the minimum. To reconstruct the full potential, measuring double Higgs production is necessary, this situation is represented in Fig. 38.

In order to better represent the phenomenon of electroweak symmetry breaking, it useful to make explicit the four real components of the Higgs doublet as follows:

$$\left(\begin{array}{c} \phi^+ \\ \phi^0 \end{array} \right) = \left(\begin{array}{c} \phi_1 + i \phi_2 \\ \phi_3 + i \phi_4 \end{array} \right) \tag{216}$$

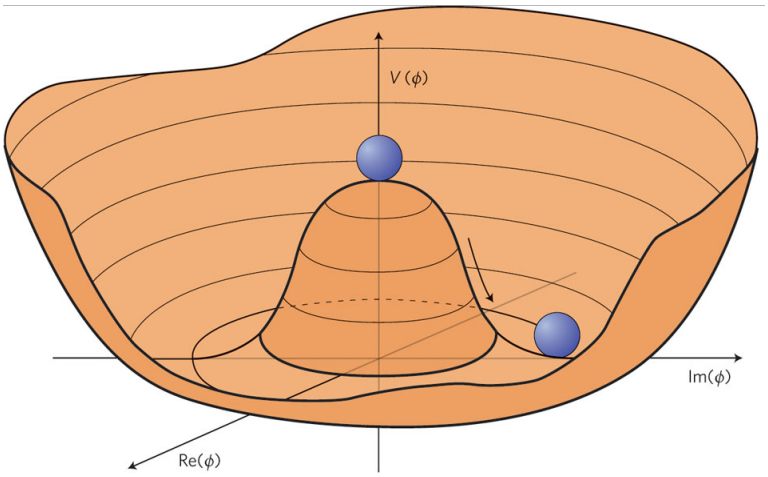

Figure 37: The Higgs field potential for a choice of parameters so that $\lambda, \mu^2 > 0$.

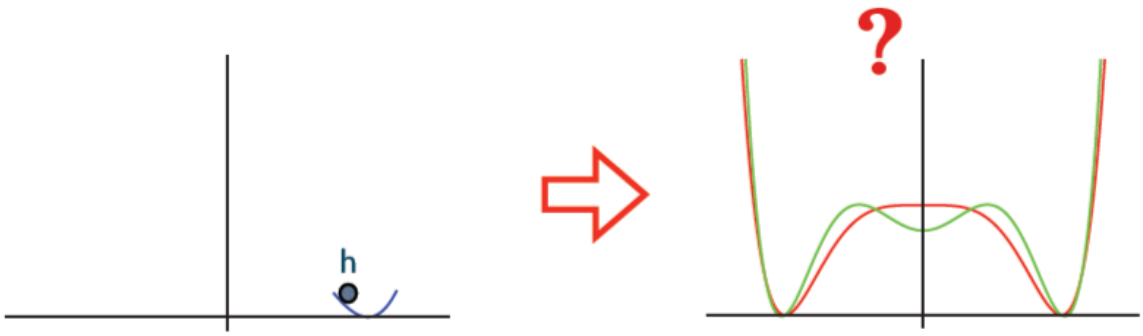

Figure 38: Single Higgs measurements only probe the region of the Higgs potential close to the minimum (the vacuum expectation value). To reconstruct the full potential, measuring double Higgs production is necessary [3].

so that the inner product of Higgs fields reads

$$\phi^\dagger \phi = \sum_{i=1}^{4} \phi_i^2 \,, \tag{217}$$

which is of course invariant under four dimensional rotations. By minimizing the classical potential, we find that the space of minima is degenerate, and defined by the condition

$$|\phi| = \sqrt{\frac{\mu^2}{2\lambda}} \equiv \frac{v}{\sqrt{2}} \,, \tag{218}$$

and transformation of the Higgs field that satisfy this condition therefore have no energy costs associated.

Since all minima that satisfy the above equation are equivalent, it is possible to select as a particular choice

$$\langle \phi \rangle = \frac{1}{\sqrt{2}} \begin{pmatrix} 0 \\ v \end{pmatrix} \tag{219}$$

This is called a vacuum expectation value, or vev. While this choice is arbitrary, we should ensure that it is invariant under residual $U(1)$ hypercharge transformations. We realize that with this choice, transformations generated by the specific combination $T^3 + Y$ leave the vacuum expectation value invariant, that is

$$\left(T^3 + Y\right) \langle \phi \rangle = 0 \tag{220}$$

This combination is the single unbroken generator that is associated with the *electric charge*

$$Q \equiv T^3 + Y = \begin{pmatrix} 1 & 0 \\ 0 & 0 \end{pmatrix} , \tag{221}$$

which arises because

$$T^3 = \begin{pmatrix} 1/2 & 0 \\ 0 & 1/2 \end{pmatrix} , \quad Y = \frac{1}{2} \begin{pmatrix} 1 & 0 \\ 0 & 1 \end{pmatrix} , \tag{222}$$

since the Higgs boson has $Y = 1/2$ weak hypercharge.

The specific choice of vacuum expectation value (vev) that we have adopted breaks the $SU_L(2) \otimes U(1)$ symmetry, since we have identified a preferred direction in the internal space. This can be easily seen: under a generic $SU(2)$ transformation, the vev Eq. (219) would be transformed into a different vacuum expectation value.

The Higgs mechanism is the paradigmatic example of *spontaneous symmetry breaking*: the underlying theory respects the symmetry but the ground state does not. As we now show, this allows to generate a mass for the massive weak bosons without breaking gauge symmetry.

At this point we need to reparametrize the scalar field in order to be able to represent the fluctuations with respect to the vacuum expectation value of the Higgs field. We can introduce the following parametrization

$$\phi = U^{-1}(\xi) \begin{pmatrix} 0 \\ (h+v)/\sqrt{2} \end{pmatrix} \tag{223}$$

where we have introduced the following unitary matrix

$$U(\xi) \equiv \exp\left(-i \frac{T \cdot \xi}{v}\right) . \tag{224}$$

Now we have four degrees of freedom, three in ξ and one in h, corresponding to the four original degrees of freedom of the complex scalar doublet. Is clear that if now we set to zero these field fluctuations we reproduce the original vev value. Note also that Eq. (224) has the same form as a $SU(2)$ gauge transformation. But since our theory is gauge invariant, we are free to perform arbitrary gauge transformations without modifying the physics of our theory. So therefore let's us perform the following $SU(2)$ gauge transformation of the Higgs field

$$\begin{aligned} \phi &\rightarrow U(\xi)\phi \\ T \cdot W^\mu &\rightarrow U T \cdot W^\mu U^{-1} + \frac{i}{g_W} \left(\partial^\mu U\right) U^{-1} , \end{aligned} \tag{225}$$

the second equation has of course a closely related expression as the gluon gauge transformation under the color group $SU(3)$. Upon this gauge transformation, the ξ_i degrees of freedom no longer appear in the Higgs Lagrangian, since we cancel them from ϕ and the rest of the electroweak Lagrangian is invariant under gauge transformations. They will re-appear latter as the longitudinal models of the massive gauge bosons. This gauge is known as the *unitary gauge*.

Following the Higgs field redefinition, and in the unitary gauge, the Higgs Lagrangian now reads

$$\begin{aligned}\mathcal{L} &= \frac{1}{2}\partial_\mu h \partial^\mu h - \mathcal{V}\left((v+h)^2/2\right) \\ &+ \frac{(v+h)^2}{8}\chi^\dagger \left(2g_W \left(T\cdot W_\mu\right) + g'_W B_\mu\right)\left(2g_W \left(T\cdot W^\mu\right) + g'_W B^\mu\right)\chi\,, \end{aligned} \tag{226}$$

where we have defined $\chi \equiv (0,1)$, a unit vector in the direction of the vev. In addition to Eq. (226), we also have in the theory the kinematic massless gauge boson term, Eq. (207), which are left unaffected by either adding the Higgs filed to the theory or by the gauge transformation.

Let us take a closer look at the consequences of spontaneous symmetry breaking. In the Higgs Lagrangian, we can consider only the terms that are quadratic in the vector boson fields. Using the expressions for the generators of $SU(2)$,

$$T_1 = \begin{pmatrix} 0 & 1/2 \\ 1/2 & 0 \end{pmatrix}, \qquad T_2 = \begin{pmatrix} 0 & -i/2 \\ i/2 & 0 \end{pmatrix}, \qquad T_3 = \begin{pmatrix} 1/2 & 1 \\ 0 & -1/2 \end{pmatrix}, \tag{227}$$

we obtain the following result

$$\mathcal{L} \subset \frac{v^2}{8}\left[\left(g_W W^3_\mu - g'_W B_\mu\right)\left(g_W W^{\mu,3} - g'_W B^\mu\right)\right] + 2g_W^2 W^-_\mu W^{\mu,+}\,, \tag{228}$$

where we have defined the following combination of the W gauge boson fields:

$$W^\pm_\mu \equiv \frac{W^1_\mu \mp i W^2_\mu}{\sqrt{2}}\,. \tag{229}$$

Now, we want to express the quadratic terms of the Lagrangian so they they are diagonal in the fields, since physical fields propagate independently. Note also that the two fields B and W^3 are electrically neutral, since they vanish under the action of the electric charge operator Q. Therefore, it is possible to rotate the electrically neutral fields into new fields which are diagonal in the Lagrangian, and thus that propagate independently, using the following condition:

$$\begin{pmatrix} W^3_\mu \\ B_\mu \end{pmatrix} = \begin{pmatrix} \cos\theta_W & \sin\theta_W \\ -\sin\theta_W & \cos\theta_W \end{pmatrix}\begin{pmatrix} Z_\mu \\ A_\mu \end{pmatrix}, \tag{230}$$

where the degree of mixing of the two fields is determined by the ratio of the coupling constants of the $SU(2)$ weak isospin and $U(1)$ weak hypercharge:

$$\sin^2\theta_W \equiv \frac{g'^2_W}{g'^2_W + g^2_W}\,. \tag{231}$$

It is now easy to see how the quadratic terms of the Lagrangian transform under the rotation Eq. (230) and

we get that the term quadratic in vector boson fields reads now

$$\mathcal{L} = \frac{v^2 g_W^2}{4} W_\mu^- W^{\mu,+} + \frac{\left(g_W'^2 + g_W^2\right)^2 v^2}{8} Z_\mu Z^\mu \,, \tag{232}$$

and there is no mass term for the photon A_μ as expected since we want to recover QED. Therefore, the Higgs mechanism allows to give masses to the physical W and Z fields

$$M_W = \frac{1}{2} v g_W \,, \quad M_Z = \frac{1}{2} v \sqrt{g_W^2 + (g_W')^2} \,. \tag{233}$$

The result is the net effect of electroweak symmetry breaking, which we summarize now:

- We start with a QFT of gauge fields invariant under $SU(2) \otimes U(1)$. Gauge fields are massless due to gauge invariance.
- We have added a complex scalar doublet ϕ, which couples to the W, B fields though the covariant derivative as requested by gauge invariance.
- This field ϕ has a potential which exhibits degenerate minima for $\phi \neq 0$. Choosing a particular direction in the space of minima, and expanding the field around it, we obtain terms which are quadratic in the W, B fields.
- Diagonalizing the propagators, we find that of the two rotated fields, one, the photon A_μ is massless and the other, the Z boson, acquires a mass $M_Z = v\sqrt{g_W^2 + g_W'^2}/2$.

Of the initial four components of the complex doublet scalar ϕ, one one is physical, the Higgs boson h, while the other three are substituted by the longitudinal modes of the now massive gauge bosons. If we take the Lagrangian, consider only the Higgs sector, and expand the potential, we find the following terms

$$\mathcal{L} = \frac{1}{2} \partial_\mu h \partial^\mu h - \mu^2 h^2 - \lambda v h^3 - \frac{1}{4} \lambda h^4 \,, \tag{234}$$

and therefore the mass of the Higgs boson is $M_h = \sqrt{2}\mu = \sqrt{2\lambda} v$, as can be read from the kinetic term. Since the mass of the W and Z bosons is known, v has been known for a long time, and the only other free parameter related to the Higgs sector is μ, its mass. Once the Higgs mass is measured, there are no other free parameters in the electroweak Lagrangian.[9]. Note also that at the LHC we have only probed the first two terms in Eq. (234). In order to measure the coefficient of the third term, and thus to really reconstruct the shape of the Higgs potential, we need to measure double Higgs production.

For the various components of the electroweak Lagrangian Eq. one can extract the Feynman rules for the interactions of massive gauge fields among themselves, between gauge bosons and the Higgs boson, and the self interactions of Higgs bosons. As an example, in Fig. 39 we show the Feynman rules for some of the possible triple and quartic interactions between different combinations of electroweak gauge bosons. The complete set of Feynman rules of the weak sector of the SM can be found in standard textbooks.

[9] We are not considering the interactions with fermionic matter for the time being.

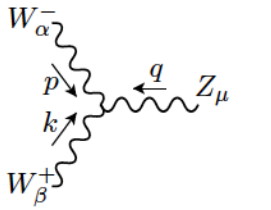

$$ig \cos\theta_W \left[g_{\alpha\beta}(p-k)_\mu + g_{\beta\mu}(k-q)_\alpha + g_{\mu\alpha}(q-p)_\beta\right]$$

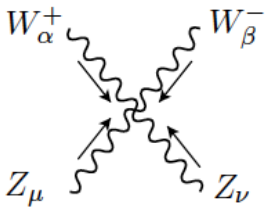

$$-ig^2 \cos^2\theta_W \left[2g_{\alpha\beta}g_{\mu\nu} - g_{\alpha\mu}g_{\beta\nu} - g_{\alpha\nu}g_{\beta\mu}\right]$$

Figure 39: Representative Feynman diagrams for the self-interactions between electroweak gauge bosons, with the corresponding Feynman rules.

Fermion	T_L^3	Y_L	T_R^3	Y_R	Q_f
up quark	1/2	1/6	0	2/3	2/3
down quark	1/2	1/6	0	2/3	2/3
electron neutrino	1/2	-1/2	-	-	0
electron	-1/2	-1/2	-	-1	-1

Table 1: The weak isospin and weak hypercharge for the first family of right- and left-handed fermions in the Standard Model. The same assignments hold for the second and third families.

Mass generation for fermions and the Yukawa coupling

The discussion in the previous section was restricted to the purely electroweak sector of the Standard Model Lagrangian. We now discuss how the same Higgs mechanism provides the mass for the fermionic fields, and what this implies for the Yukawa coupling between the Higgs boson and all massive fermions. The key requirement is that the complete Standard Model Lagrangian must be invariant under $SU_L(2) \otimes U(1)$. As we will show now, this implies that any explicit mass term in the Lagrangian is forbidden, and thus one needs to generate a mass through spontaneous symmetry breaking as well.

In order to satisfy gauge invariance, bosonic fields must couple to the matter (fermion) fields using the covariant derivative. Before electroweak symmetry breaking, the electroweak Lagrangian with fermions contains

$$\mathcal{L} \subset \bar{\psi}_R \left(\gamma^\mu \partial_\mu + i g'_W Y_R \gamma^\mu B_\mu\right) \psi_R + \bar{\psi}_R \left(\gamma^\mu \partial_\mu + i g_W \gamma^\mu T \cdot W_\mu + i g'_W Y_L \gamma^\mu B_\mu\right) \psi_R \,, \tag{235}$$

where we have used the fact that $SU_L(2)$ rotations only affect left handed fermions, and that weak hypercharge is different for left handed and right handed fermions. The values of the weak hypercharge of right and left-handed fermions are fixed by their electric charge, $Q = T^3 + Y$, and for the SM matter particles their values are summarized in Table 1.

Before electroweak symmetry breaking, all the SM fermions are massless, since a explicit mass term would violate $SU_L(2) \otimes U(1)$ symmetry. This allows to treat separately left-handed and right-handed fermions in terms of their weak charges.

As we see in Table 1, left-handed fermions correspond to a $SU_L(2)$ doublet, while right-handed quarks are singlets, and there are no right-handed neutrinos (at least in the SM).

Let us now show how the Higgs mechanism, which gave mass to W, Z bosons, can also give mass to the fermions. Let us now add to the weak Lagrangian the so-called *Yukawa interaction* terms, of the form

$$\mathcal{L} \subset \sum_f g_f \bar{\psi}_f \psi_f \phi \,, \tag{236}$$

where the sum runs over all the massive fermions in the SM. This term is gauge invariant, and after electroweak symmetry breaking, when we have

$$\phi = \frac{1}{\sqrt{2}} \begin{pmatrix} 0 \\ h + v \end{pmatrix} \tag{237}$$

we find that fermions acquire a mass $m_f = g_f v/\sqrt{2}$. In addition, the Yukawa interaction term Eq. (236) also

dictates the strength of the interaction between the Higgs boson and the fermions, since now the Lagrangian contains

$$\mathcal{L} \subset \sum_f \left(\frac{\sqrt{2} m_f}{v} \right) \bar{\psi}_f \psi_f h \,, \tag{238}$$

so therefore the interaction between the Higgs boson and the SM fermions is proportional to the fermion mass.

In the SM, the values of the Yukawa couplings g_f are not fixed by any principle, but are free parameters of the theory that need to be determined experimentally.

Concerning the interactions between the fermions and the weak bosons, we can start from the Lagrangian Eq. (235) and perform the transformation into the physical weak bosons, $W^\pm$ and Z^0, as well as the photon, as done before. When this is performed, we find that the weak Lagrangian contains the following interaction terms:

$$\begin{aligned} \mathcal{L} \quad \subset \quad & \sum_f \bar{\psi}_f \left(i\gamma^\mu - m_f - g_W \frac{m_f h}{2 m_W} \right) \psi_f \\ - \quad & \frac{g_W}{2\sqrt{2}} \sum_f \bar{\psi}_f \left(\gamma^\mu (1-\gamma_5) T^+ W^+_\mu + \gamma^\mu (1-\gamma^5) T^- W^-_\mu \right) \psi_f \\ - \quad & e \sum_f q_f \bar{\psi}_f \gamma^\mu A_\mu \psi_f - \frac{g_W}{2\cos\theta_W} \sum_f \bar{\psi}_f \gamma^\mu \left(V_f - A_f \gamma_5 \right) \psi_f Z_\mu \,. \end{aligned} \tag{239}$$

From this Lagrangian, we can read the values of the coupling constants between the SM fermions and the W, Z bosons. In the case of the Z boson, the specific values of the coupling depend on the fermion, while for W the coupling is the same for all (left-handed) fermions. For the Z boson, we have that the vector (V_i) and axial-vector (A_i) couplings are given by

$$V_f = T^3_f - 2 Q_f \sin^2 \theta^2_W \,, \quad A_f = T^3_f \,, . \tag{240}$$

The purely electromagnetic interaction is also reproduced. While at very high energies the weak and electromagnetic coupling are of the same order, at low energies the effective weak coupling appears to be much smaller, since it is suppressed by the large masses of the weak gauge bosons. In Fig. 40 we show the Feynman rules that allow to compute scattering amplitudes involving the interaction of fermions and weak gauge bosons.

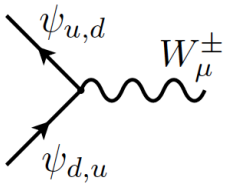

$$i\frac{g}{\sqrt{2}}\gamma_\mu\frac{1-\gamma_5}{2}$$

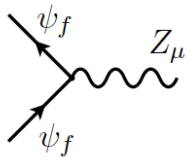

$$i\frac{g}{\cos\theta_W}\gamma_\mu\left(g_V^f-g_A^f\gamma_5\right)$$

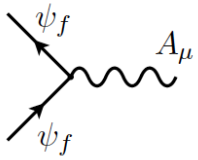

$$-ieQ_f\gamma_\mu$$

$$g_V^f=\frac{1}{2}T_f^3-Q_f\sin^2\theta_W,\quad g_A^f=\frac{1}{2}T_f^3\ .$$

Figure 40: Feynman diagrams for the interactions between fermions and weak gauge bosons.

Higgs phenomenology at hadron colliders

In this last lecture of the course we discuss the phenomenology of Higgs production at the LHC. Following the discovery, the detailed characterization of the properties of the Higgs boson is now one of the cornerstones of the LHC physics program for the next 20 years.

References

[1] D. J. Gross and F. Wilczek, Phys. Rev. Lett. **30**, 1343 (1973). doi:10.1103/PhysRevLett.30.1343

[2] H. D. Politzer, Phys. Rev. Lett. **30**, 1346 (1973). doi:10.1103/PhysRevLett.30.1346

[3] N. Arkani-Hamed, T. Han, M. Mangano and L. T. Wang, arXiv:1511.06495 [hep-ph].